New Optical Sensor Suite for Ultrahigh Temperature Fossil Fuel Applications

Semiannual Technical Progress Report

DOE Award Number: DE-FC26-03NT41922

Reporting Start Date:

Reporting Period End Date: 30 September 2005

Principal Authors: Russell G. May (Prime Research, LC)
Tony Peng (Prime Research, LC)
Gary Pickrell (Virginia Tech)

Date Report Issued: 31 October 2005

Submitting Organization: Prime Research, LC
1750 Kraft Dr Ste 1000
Blacksburg, VA 24060

Virginia Polytechnic Institute and State University
Blacksburg, VA 24061

DISCLAIMER

This report was prepared as an account of work sponsored by an agency of the United States Government. Neither the United States Government nor in the agency thereof, nor any of their employees, makes any warranty, express or implied, or assumes any legal liability or responsibility for the accuracy, completeness, or usefulness of the information, apparatus, product, or process disclosed, or represents that its use would not infringe privately owned rights. Reference herein to any specific commercial product, process, or service by trade name, trademark, manufacturer, or otherwise does not necessarily constitute or imply its endorsement, recommendation, or favoring by the United States Government were in the agency thereof. The views lists opinions of authors expressed herein do not necessarily state or reflect those of United States Government or any agency thereof.

ABSTRACT

Development of practical, high-temperature optical claddings for improved waveguiding in sapphire fibers continued during the reporting period. A set of designed experiments using the Taguchi method was undertaken to efficiently determine the optimal set of processing variables to yield clad fibers with good optical and mechanical properties. Eighteen samples of sapphire fibers were prepared with spinel claddings, each with a unique set of variables. Statistical analyses of the results were then used to predict the set of factors that would result in a spinel cladding with the optimal geometrical, mechanical, and optical properties. To confirm the predictions of the Taguchi analysis, sapphire fibers were clad with the magnesium aluminate spinel coating using the predicted optimal set of factors. In general, the clad fibers demonstrated high quality, exceeding the best results obtained during the Phase I effort. Tests of the high-temperature stability of the clad fibers were also conducted. The results indicated that the clad fibers were stable at temperatures up to 1300°C for the duration of the three day test. At the higher temperatures, some changes in the geometry of the fibers were observed.

The design, fabrication, and testing of a sapphire sensor for measurement of temperature was undertaken. The specific sensor configuration uses a polished sapphire wafer as the temperature-sensitive element. The wafer is attached to a sapphire fiber (clad or unclad), and interrogated as a Fabry-Perot sensor. Methods for assembling the sensor were investigated. A prototype sensor was fabricated and tested at room temperature and elevated temperatures. Results were difficult to interpret, due to the presence of modal noise which was found to result from the use of a spectrometer that was not designed for use with multimode fibers. A spectrometer optimized for use of multimode fiber has been obtained, and further evaluation of the sapphire temperature sensor is continuing.

TABLE OF CONTENTS

1 INTRODUCTION

The goal of this project is the research and development of advanced, robust photonic sensors based on improved sapphire optical waveguides, and the identification and demonstration of applications of the new sensors in advanced fossil fuel powerplants, where the new technology will contribute to improvements in process control and monitoring.

The advantages of fiber optic sensors over electronic sensors, particularly in environments where the electronic sensing materials can not withstand the rigors of the harsh conditions, are well known. Typically, advanced power generation systems operate at higher temperatures and pressures than traditional power plants. Traditional sensor technology for measuring temperature, pressure, flow and strain will not survive the harsh conditions anticipated in these plants. Furthermore, these plants will require more extensive process monitoring and condition assessment to maintain optimum performance and minimize maintenance costs. An effective means is required to reduce the complexity and cost of connecting the larger number of sensors to a central data acquisition platform. Therefore, one of the goals of the program is the identification of all potential applications in supercritical boiler plans where photonic sensors can be used for process control and monitoring.

For the ultrahigh-temperature environment found in current and future power generation facilities, new materials for the optical sensors will be required. Previous efforts to utilize sapphire fiber sensors that can theoretically operate above 1650° C (3000° F) have been limited because the fiber itself does not lend itself to incorporation in the known sensor techniques, due to its unclad and multimode construction. Another goal of this program is the development of high-temperature, ceramic claddings for sapphire fibers to improve the waveguiding properties of sapphire fibers and facilitate their use in photonic sensor systems.

Current efforts towards improvement of sapphire fibers focus on creating claddings on sapphire (aluminum oxide single crystal, Al_2O_3) fibers by dip-coating the fibers in a mixture of magnesium oxide (MgO) powders and magnesium aluminate spinel ($MgAl_2O_4$) powders to form a coating on the sapphire fibers. The technique involves dip coating a sapphire fiber in a suspension of MgO and spinel powders, drying the coating, then firing at elevated temperatures to react the MgO powder with the sapphire fiber, and to densify the coating. The overall reaction for the process is given by the chemical equation:

$$MgO + Al_2O_3 = MgAl_2O_4$$

which proceeds rapidly at 1750°C (3182° F).

The coated fibers are then fired at high temperatures to facilitate the reaction between the MgO in the coating and the Al_2O_3 in the fibers by ion diffusion, and create a cladding consisting of $MgAl_2O_4$ surrounding the sapphire core. As a result, the diameters of the sapphire fibers are reduced and the number of modes propagating in the sapphire fibers is also reduced.

2 EXECUTIVE SUMMARY

The overall goal for this project is to explore the potential of optical sensors based on modified sapphire fibers for use and advanced fossil fuel power generation systems. Specific program objectives include (1) development of methods to produce high-temperature optical cladding for sapphire fibers to improve their waveguide properties and enable new classes of high temperature sensors; (2) development of new techniques to produce sensor elements within sapphire fibers, including fiber Bragg gratings and/or intrinsic Fabry-Perot interferometers; and (3) demonstration of new, ultrahigh-temperature optical sensors for specific measurements required for advanced powerplant control systems, as identified by powerplant manufacturers/integrators/operators.

The project is organized into two consecutive phases. This report documents the accomplishments during the first year of Phase II. The objectives for this phase include (1) development of a suite of optimized sensor designs for the targeted applications and for testing in targeted applications in coal-fired boilers; and (2) demonstration of the feasibility and performance of the sensors for both laboratory and full scale testing, such that they are easily integrated into powerplant control systems.

Development of a practical, high-temperature optical cladding for improved waveguiding in sapphire fibers continued during the reporting period. Research conducted during Phase I on solid-state methods for the coating of magnesium aluminate spinel claddings onto sapphire fibers demonstrated that there are several variables that influence the optical and mechanical quality of the resulting clad fibers. The results indicated that these variables, which include chemical composition of the coating, processing steps for preparation of the coating slurry, and firing profiles for binder burn-out and sintering of the coatings, often interact, making determination of an optimal set of variables difficult. Therefore, a set of designed experiments was undertaken to efficiently determine the optimal set of processing variables to yield clad fibers with good optical and mechanical properties.

To guide the design of the experiments for expediency and efficiency, the Taguchi methodology was employed. First, a set of 13 desired responses for the experiments was determined. These responses fall into three general categories relating to good optical quality, good mechanical quality, and acceptable fiber geometry. Leveraging the extensive experience gained in the solid-state processing of spinel coatings during Phase I, a list of variables (or "factors" in Taguchi terminology) was identified for study during the designed experiments. Finally, an array of 18 experiments was derived using standard Taguchi methodology.

Experimental set-ups were designed and constructed to measure the properties of the resulting clad fibers according to the desired responses. Then, 18 samples of 125 μm diameter sapphire fibers were prepared with spinel claddings, each with a unique set of factors according to the dictates of the Taguchi array. Each sample was then measured, and a numerical value was assigned for each response.

The measured results of the 18 experiments were statistically analyzed using Qualitek-4 software to determine the significance of each factor in contributing to the desired responses. The output of these statistical analyses were then used to predict the set of factors that would result in a spinel cladding with the optimal geometrical, mechanical, and optical properties.

To confirm the predictions of the Taguchi analysis, a set of four 125 μm diameter sapphire fibers were clad with the magnesium aluminate spinel coating using the predicted optimal set of factors. In addition, three 75 μm diameter sapphire fibers were clad using the same optimal factors. In general, the 125 μm diameter clad fibers demonstrated high quality, exceeding the best results obtained during the Phase I effort. The results from the 75 μm diameter clad fibers were not as good, suggesting that the optimal factors derived from designed experiments on 125 μm fibers are specific for that fiber diameter.

Tests of the high-temperature stability of the clad fibers were also conducted. Four samples of clad fibers were fabricated according to the optimal factors. Samples of these fibers were then heated in a furnace at temperatures of 1000°C, 1100°C, 1200°C, 1300°C, 1400°C, and 1500°C, for three days at each temperature. Following heat treatment at each temperature step, each fiber was polished, and its cross-section was analyzed under an optical microscope. Specifically, the fibers were examined to determine if changes in the core diameter or cladding thickness had occurred, which would indicate continued reaction of the magnesium aluminate spinel cladding with the sapphire core. The results indicated that the clad fibers were stable at temperatures up to 1300°C for three days. At the higher temperatures, some changes in the geometry of the fibers were observed, with more dramatic changes occurring upon exposure to 1500°C for three days, including the formation of cracks, the growth of the cladding thickness, and a reduction in the fiber core diameter. A strategy for stabilizing the cladding, involving an improved composition of the spinel slurry during coating, is proposed.

Also during the reporting period, the design, fabrication, and testing of a sapphire sensor for measurement of temperature was researched. The design investigated was based on a Fabry-Perot interferometer originally developed at the Virginia Tech Center for Photonics Technology; Prime Research is negotiating a license for this design from Virginia Tech. The specific sensor configuration uses a polished sapphire wafer as the temperature-sensitive element. The wafer is attached to a sapphire fiber (clad or unclad), and interrogated as a Fabry-Perot sensor. Changes in the temperature of the wafer cause a change in the optical path length of the Fabry-Perot cavity, which can be related to the change in temperature through the known coefficient of thermal expansion. The high degree of parallelism of the two sides of the wafer (and thus the Fabry-Perot cavity) permits the achievement of reasonable fringe visibility, even with multimode fibers.

Methods for assembling the sensor were investigated. The use of materials that can withstand the harsh environments of boiler plants was a priority in determining the assembly process.

A prototype sensor was fabricated and tested at room temperature and elevated temperatures. A commercial optical spectrum analyzer was used to obtain the interference spectrum in the telecommunications C-band. Results were difficult to interpret, due to the presence of additional undesired fringes in the output spectrum. Further investigation revealed that modal noise was most likely responsible for the undesired modulation of the sensor output. If the output of a multimode fiber (such as a sapphire fiber) is restricted by an aperture of smaller spatial area than the core of the multimode fiber, the aperture will act as a spatial filter, passing a limited subset of the modes that propagate in the multimode fiber. When the number of propagating modes is filtered, intermodal interference will result. This spurious modal noise is particularly sensitive to the movement of the multimode fiber.

Further investigation indicated that the optical spectrum analyzer used for the experiments was one of the sources of the modal noise. This spectrum analyzer was designed specifically for use with single-mode fibers, and has an entrance pupil with a spatial extent less than that of the multimode fiber core.

The influence of the modal noise can be greatly minimized, if not completely eliminated, through the use of multimode fibers exclusively in the sensor system, in addition to the use of a spectrometer designed for use with multimode fibers. Towards this end, a spectrometer optimized for use of multimode fiber has been obtained, and further evaluation of the sapphire temperature sensor is continuing.

3 EXPERIMENTAL PROGRESS

3.1 Development of Sapphire Fiber Cladding

Progress was made in the development of materials and methods to apply high-temperature optical claddings to sapphire fibers, in order to improve their optical waveguiding properties and reduce their mode volume. Single crystal sapphire fibers are highly multimoded due to the large diameter of the fiber and the large difference in refractive indices between the fiber and the surrounding air. Achieving high fringe visibility in Fabry-Perot interferometers assembled from these fibers is not easy. The fringes are highly sensitive to the flatness, the smoothness, and especially the parallelism of the two surfaces forming the Fabry-Perot cavity. Sapphire fibers clad with spinel coatings support fewer electromagnetic modes due to the reduced core diameter and the reduced difference in refractive indices between core and cladding. Since the refractive index of spinel cladding is about 3% smaller than that of the sapphire core, spinel-clad fibers also have smaller numerical apertures then unclad fibers, improving the fringe visibility of Fabry-Perot interferometer.

Spinel-clad sapphire fibers were prepared during this program by a dip coating technique, in which the fiber was to several times in a slurry containing ceramic powders consisting of mostly magnesium oxide. In each dipping, a thin layer of slurry is coated on the surface of a sapphire fiber. Repeated dipping increases the thickness of the accumulated coating. During firing of the coating at high temperature, magnesium oxide diffuses into the sapphire fiber. A spinel cladding is formed as a result of the reaction between sapphire and the diffusing magnesium oxide.

To achieve lightwave guiding with minimum scattering, the interface between the sapphire core and spinel cladding must be optically smooth. Several conditions have to be met to achieve this. First, the magnesium oxide coating needs to have uniform packing density along the sapphire fiber, so that a concentric interface can be formed along the fiber. Second, the packing density needs to be high with the least amount of voids. Otherwise, a microstructure with many voids may be generated at the core/cladding interface after high temperature diffusion, resulting in a rough core/cladding interface. Third, the firing conditions have to be carefully controlled such that, after the spinel cladding is completely formed, the spinel grains at the interface do not grow further in size. The hexagonally symmetrical spinel grains intruding into the sapphire core can cause scattering at the interface.

To permit easy handling without fracturing the fiber, the cladding must be free of cracks. Since the thermal expansion coefficient of the spinel cladding is slightly larger than that of the sapphire core, the degree of contraction of the cladding is greater than that of the core after cooling from firing, thus subjecting the cladding to tensile stresses. If the cladding is not strong enough to sustain these residual stresses, cracks could occur in the cladding. The mechanical properties such as bending strength and flexibility of clad fibers can suffer tremendously if there are cracks in the cladding. To avoid crack

formation in the cladding, the firing profile, including maximum firing temperature, dwell time, and cooling rate must be carefully planned and controlled.

Another important requirement is the thermodynamic stability of the cladding in the desired industrial environment at temperatures up to 1500°C. There should be no further reactions between the spinel cladding and sapphire core and no microstructural changes during sensor operation.

In the dip coating process, a thin coating of wet ceramic slurry adheres to the surface of the sapphire fiber after each dipping. The solvents in the wet ceramic slurry then evaporate, leaving a dried coating of ceramic powders held together, most often by a polymeric binder. The binder will later be burned out in the firing stage.

How closely the ceramic powders pack during this process depends on several factors. The most important factor is the degree of ceramic powder dispersion in the slurry. If the powders are very finely dispersed, a high packing density can be achieved after the evaporation of solvent from the fine interstitials among the ceramic particles. On the contrary, if the ceramic powders stick together and form large agglomerates, the resulting large voids among the agglomerates can reduce the packing density. Another important factor is the type and amount of binder used. If too much binder is used, excessive voids can be formed during binder burn out, thus reducing the powder packing density. Furthermore, packing density can be increased by mixing powders with different sizes. Smaller size powders can fit into the voids formed by larger particles, thus increasing the powder packing density.

Another factor in creating uniform coating thickness and packing density along the whole length of a fiber is the "skinning effect." In this context, "skinning" refers to the formation of a dry "skin" on the surface of the wet slurry; an increase of slurry viscosity due to solvents evaporation at the surface of slurry is responsible for the formation of the skin. In the dip coating process, the thickness of the wet ceramic coating on fiber is proportional to the viscosity of slurry at the surface adjacent to the fiber. As the fiber being withdrawn from the slurry, the viscosity of slurry at the surface adjacent to the fiber could decrease drastically along the way if the original powder concentration at the surface is close to saturation, resulting in a dipped fiber with a "carrot" shape. That is, the coating is thick at the top, and the thickness gradually deceases towards the bottom of a fiber. To avoid this kind of "carrot" shape fibers, the types and amounts of solvents have to be carefully chosen to minimize solvent evaporation. Other measures such as enclosing the container holding the slurry mixture can also help.

3.1.1 Application of designed experiments using the Taguchi method to optimize sapphire cladding

Research directed towards development of the magnesium aluminate spinel cladding during the first year (Phase I) of this program showed that the mechanical and optical qualities of the cladding depends on several factors, some of which may be

interdependent. In order to efficiently determine the slurry composition and processing procedure that leads to the optimal spinel cladding, we undertook a series of designed experiments during the reporting period, using the Taguchi method.

The Taguchi method is a technique for designing and performing experiments. The goal is to investigate processes where the output depends on many factors without tediously and uneconomically running the process using all possible combinations of values of those factors. By systematically choosing certain combinations of variables, it is possible to separate their individual effects.

Successful implementation of designed experiments using the Taguchi Method requires that the objects of interest be carefully studied. Questions such as "What are the goals?", "What are the factors important in achieving the goals?", "How do you decide the levels in each important factor?", "What do you measure and how do you measure?" should be carefully answered before starting the experiments.

3.1.1.1 Establishing goals for designed experiments

The three major goals in implementing the designed experiments are (1) to create spinel-clad sapphire fibers with optically smooth cladding/core interface, (2) to create mechanically strong spinel cladding without cracks, and (3) to achieve uniform cladding thickness along the whole length of the fiber.

3.1.1.2 Determining factors for designed experiments

Based on the experience obtained during cladding development during Phase I of the program, a list of factors that appeared to contribute to the quality of the sapphire cladding was tabulated. Potentially important factors include:

1. Smoothness of the sapphire fiber surface used for dipping
2. Procedures for cleaning of sapphire fibers before dipping
3. Type and amount of dispersant
4. Solid loading of ceramic powders
5. Weight ratio between MgO and spinel powders
6. Percentage of nano-MgO powders in all MgO powders
7. Types and amount of binder
8. Fiber dipping speed and the mechanical stability of the dipping apparatus
9. Number of dips
10. Dispersion milling session time and speed
11. Binder burnout heating profile and atmosphere
12. High temperature firing temperature, time, and atmosphere

The number of factors chosen for the Taguchi experiments also depends on the array selected. It was decided according to the time constrain of the project that an L18 array

was most suitable. The L18 array is shown in Table 3-1 below. The L18 array consists of 7 three levels factors and 1 two level factor, and a total of 18 samples need to be fabricated. Each of the eighteen rows represents one coated sapphire fiber sample prepared using the corresponding factor and level in each column.

Table 3-1: L18 array (2^1x3^7) orthogonal array

	Columns (Factors)							
Sample #	1	2	3	4	5	6	7	8
1	1	1	1	1	1	1	1	1
2	1	1	2	2	2	2	2	2
3	1	1	3	3	3	3	3	3
4	1	2	1	1	2	2	3	3
5	1	2	2	2	3	3	1	1
6	1	2	3	3	1	1	2	2
7	1	3	1	2	1	3	2	3
8	1	3	2	3	2	1	3	1
9	1	3	3	1	3	2	1	2
10	2	1	1	3	3	2	2	1
11	2	1	2	1	1	3	3	2
12	2	1	3	2	2	1	1	3
13	2	2	1	2	3	1	3	2
14	2	2	2	3	1	2	1	3
15	2	2	3	1	2	3	2	1
16	2	3	1	3	2	3	1	2
17	2	3	2	1	3	1	2	3
18	2	3	3	2	1	2	3	1

The task now is to pick the most important 8 factors out of the list above and determine their levels. Experience gained from previous experiments helped to narrow down the list of potentially important factors. For example, since a fiber cleaning procedure using 2-propanol has been proved effective in producing samples with smooth core/cladding interface, Factor 2 above was removed from the candidate list. As to the smoothness of the sapphire fiber surface, since no defects or scratches are discernable using optical microscopes, Factor 1 was also removed from the list. According to the results from previous experiments, it was decided that the solid loading, i.e., the weight ratio of ceramic powders, is to be fixed at 16% and the number of dips at 150 dips. Since the binder burnout profile seems to have less effect on the clad fiber properties than the high temperature firing profile, the former also will be removed from the list.

One of the most important factors is the type and amount of dispersant. Extensive research and study was performed during Phase I to determine the best dispersant for the current slurry system. The dispersants studied include Darvan 811 (dispersant agent from R.T. Vanderbilt Company, Inc), Triton QS-44 (surfactant from The Dow Chemical Company), Coatosil 1211 (coating additive from GE Silicones), and manhaden fish oil from (Sigma-Aldrich Inc.). The dispersants were studied using techniques such as particle size analysis and sedimentation tests. The most important observation on which the final decision was based was from the sedimentation tests. According to Stokes' Law, the terminal settling velocity of a smooth, rigid sphere in a viscous fluid is

proportional to the square of the sphere radius. Therefore, in general, a fine ceramic particle would settle much slower than a course ceramic particle of the same kind. Figure 3-1 below shows the results of the sedimentation tests using either fish oil (Batch 1) or Darvan (Batch 3) as the dispersant, or without using any dispersant at all (Batch 2). As shown in the figure, the spinel powders settle the slowest in Batch 1, where fish oil was added as dispersant, with no clear-cut interface between sediment and the liquid above. In Batch 2, without any dispersant, the powders settle faster than in Batch 1 with a lower sediment/clear liquid interface. In Batch 3, where Darvan is added as the dispersant, the powders settle even faster. Most likely the powders agglomerate together in Batch 3 and form even larger agglomerates that increase the settling rate.

Other dispersant candidates such as Triton and Coatosil behave in a very similar manner as Darvan. It was therefore determined that fish oil is most capable of keeping the ceramic powders in a finely dispersed state. It seems that the dispersion capability of fish oil is enhanced by the presence of PVP. An observation supporting the beneficial role of PVP in dispersion is that the slurry viscosity always drops when PVP is added to the slurry containing fish oil as the dispersant.

Figure 3-1: Sedimentation test results of spinel powders from Baikowski International after 106 days. The solid loading of each batch is 15.7 weight % and the solvent are 18.66 g of 2-propanol and 2.12 g of 1-methoxy-2-propanol. In Batch 1, 50 µL of fish oil and 0.2 g of PVP are added. In Batch 2, no dispersant is added. In batch 3, 50 µL of Darvan 811 is added. All batches are ball milled for 21.5 hours.

The final 8 factors chosen are listed in Table 3-2 below.

Table 3-2: Final chosen factors and their levels

	Factors	Level 1	Level 2	Level 3
1	Nano MgO weight % in all MgO powders	10	20	----------
2	Dipping speed (mm/sec)	2.5	2.7	2.9
3	Maximum firing temperature (°C)	1550	1575	1600
4	MgO/Spinel ratio	6:1	9:1	12:1
5	Dispersion milling session time (hr)	3	6	12
6	Fish oil amount (μL)	25	50	75
7	10K PVP weight ratio (%)	100	90	80
8	PVP amount (both 10K and 55K)(g)	0.4	0.5	0.6

3.1.1.2.1 Determining levels for factors

The proper choice of levels for each factor is extremely important in the execution of the Taguchi Method. Usually it entails a series of trial-and-error experiments with some scientific judgment and luck. In practice, the determination of optimal levels starts with one set of current conditions showing the most promise. In this set of most promising conditions, only the levels of one factor are altered while keeping all other factors fixed. Then the resulting responses are analyzed to determine whether the levels just changed are feasible and practical for the experiment. For example, it was observed in previous Phase I experiments that the slurry viscosity increases dramatically when the nano-MgO weight % (Factor 1) reaches about 25% in a certain set of experimental conditions. Since a set of full factorial experiments with the factors and levels shown in Table 1 consists of more than 4000 ($3^7 \times 2$) different sets of experiments, it is impossible to know for sure whether this huge increase in viscosity is also true in other sets of experimental conditions without extensive study, which is very time consuming. To keep it on the safe side, Level 2 in Factor 1 is set to 20% to prevent this huge increase in viscosity. On the other hand, if the levels are chosen too conservatively, it runs a risk that they make no difference at all to the results. So, some degree of scientific judgment is required in making the final decision. The levels for other factors are determined in a similar manner through a series of designed experiments.

3.1.1.3 Measurement of experimental response

To evaluate the design to experiment results, we measure responses appropriate for the goals we would like to achieve, namely, the smoothness of the cladding/core interface, the mechanical strength of the spinel cladding (and the presence or absence of cracks), and the uniformity of cladding thickness along the whole length of the fiber. There are in total 13 responses chosen, which may be grouped in three categories: geometrical responses, mechanical quality responses, and optical quality responses:

Geometrical Response:
- G1: core diameter
- G2: overall cladding thickness
- G3: outer cladding thickness
- G4: skin thickness
- G5: overall fiber diameter
- G6: concentricity

Mechanical Quality Response:
- M1: flexibility from 3-point bending test
- Crack parameters:
    - M2: total area of cracks
    - M3: length of the longest crack
    - M4: number of cracks

Optical Quality Response:
- O1: core/cladding interface roughness
- O2: Numerical Aperture (NA) measurement
- O3: attenuation measurement

3.1.1.3.1 Geometrical response

The definitions used for the geometrical responses can be best illustrated by Figure 3-2 below. The figure shows a polished cross section of a clad fiber. The core diameter (G1) is defined as the distance between points A and B. The core diameters along three other diagonally symmetric directions depicted by three red dotted lines are also measured. The reported value of G1 is the average of all four measured core diameters. The overall cladding thickness (G2) is defined as the distance between points B and D. As seen in Figure 3-2 and other cross-sectional pictures to be shown later, the cladding in fact consists of two distinctive parts: the bulk part of cladding located between points B and C, and a thinner layer of "outer cladding" between points C and D, which is designated as the response G3, outer cladding thickness. Similarly, values for G2 and G3 at 7 other diagonally symmetric directions are also measured. The reported values of G2 and G3 are the average of eight "overall cladding thickness" and "outer cladding thickness" measurements, respectively, in all 8 locations. It is believed that both cladding parts are made of spinel. However, we believe that they are formed by different mechanisms. The bulk part of cladding, i.e., the spinel located between points B to C, is formed by the reaction due to the MgO diffusing from the coating "into" the sapphire core, while the thin outer layer of spinel, i.e., the spinel located between points C to D, is formed by the reaction between the aluminum oxide molecules diffusing "outward" from the core into the coating and the MgO molecules inside the coating. The region between points D and E in Figure 3-2 defines the "residual layer," G4. It is believed that this residual layer consists of materials not fully reacted in the coating after firing. The reported value of G4 is the average of all thickness measured at 8 symmetrical locations. The overall fiber

diameter G5 is defined as the distance between points E and F. The last geometrical response is "concentricity", G6. It is defined as the distance between the center of the core/cladding interface, i.e., the interface containing points A and B in Figure 3-2, and the center of the cladding/skin interface, i.e., the interface containing point D in Figure 3-2.

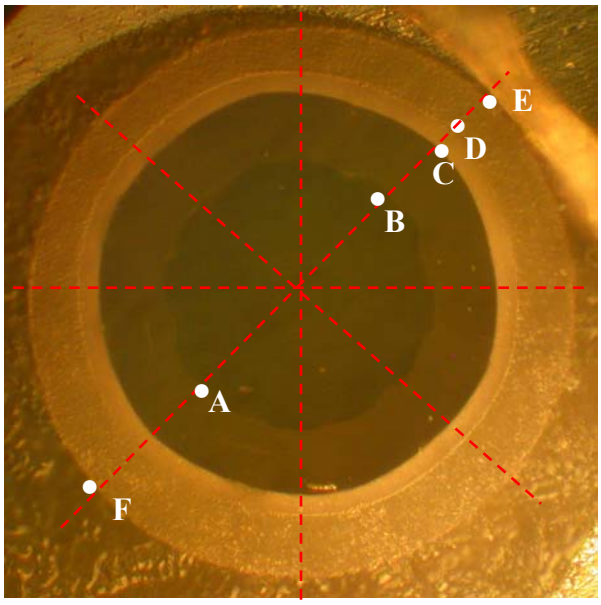

Figure 3-2: The polished cross section of a clad fiber.

3.1.1.3.2 Mechanical quality response

The first mechanical quality response is the "bending flexibility," M1, obtained from a 3-point bend test. The apparatus shown in Figure 3-3(a) was used to measure the radius of the induced bend in the clad fiber at the point at which the fiber fractured. As shown in the figure, the micrometer of an adjustable stage is coupled to a rotary motor which speed was controlled by a constant voltage source. A cylinder, i.e., cylinder C in Figure 3-3(b), is glued to the bottom of the adjustable stage. During the test, cylinder C descends in a constant rate of about 0.009 mm/sec (±0.001 mm/sec) until the test fiber breaks. Below the stage a cylinder, i.e., "cylinder A" in Figure 3-3(b), and a ceramic block, i.e., labeled "Stop" in the figure, are glued to a base plate. Another cylinder, cylinder B, positioned against the "stop" and is free to rotate leftward. The initial distance between cylinders A and B was 17 mm. During measurement, the reading (H1) on the micrometer when Cylinder C in Figure 3-3(b) first touches the test fiber is recorded. Then a constant voltage is supplied to the motor causing cylinder C to descend at a predetermined rate. The reading on the micrometer (H2) is once again recorded at the point of fiber breakage due to bending. The reported deflection is the difference between the two recorded readings, i.e., H2-H1, in millimeter, which in turn is reported as the value for response M1.

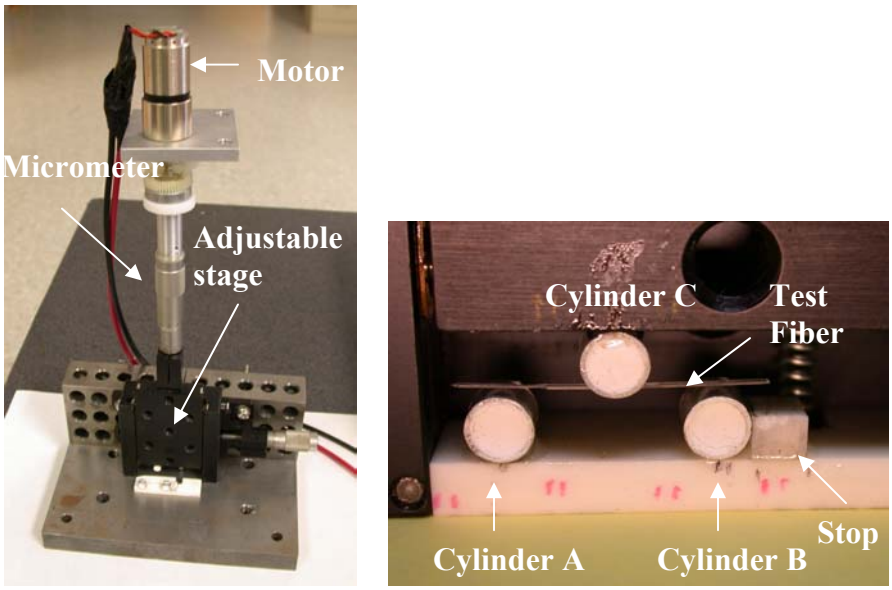

(a) (b)

Figure 3-3 (a) and (b): the apparatus used to perform the bending test

The mechanical response M2 represents the surface area of cracks in μm^2 in the cladding as depicted, for example, by the crack shown in Figure 3-1. The measure of the crack areas is obtained using a microscope with a video camera and image processing software. M3 is the length of the longest crack existing in the cladding, and M4 represents the number of individual cracks in the cladding.

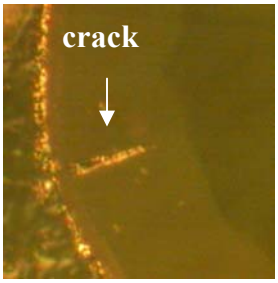

Figure 3-4: The portion of a polished cross section in the cladding of a clad fiber containing large cracks.

3.1.1.3.3 Optical quality response

The procedures for obtaining the core/cladding interface roughness (O1) can be illustrated by Figure 3-5. In this figure, a zig-zag core/cladding interface is clearly visible. In order to measure the degree of smoothness of the interface, a running average of the

interface, as shown in the figure as a smooth blue dotted curve, is drawn along the interface. The sum of the areas enclosed between the core/cladding interface and the running average curve, i.e., the sum of areas A1, A2, A3, ….. as shown in Figure 3-5, is calculated. This area is called the "roughness area (R.A.)". Furthermore, the area of the core enclosed by the running average curve is also calculated. This area is called the

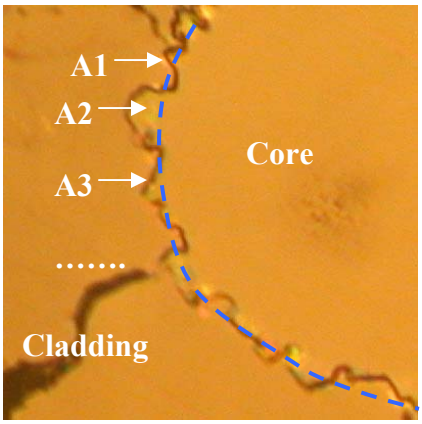

Figure 3-5: The calculation of core/cladding interface roughness

"core area (C.A.)". The core/cladding interface roughness is then defined as the ratio between the "roughness area" and the "core area", i.e., R.A/C.A.

The second optical quality response O2 is the numerical aperture (NA) of the clad fiber. The NA is measured using the experimental setup depicted in Figure 3-6 below. The clad fiber sample, about 3.0 inches long, is packaged into a ceramic tube with

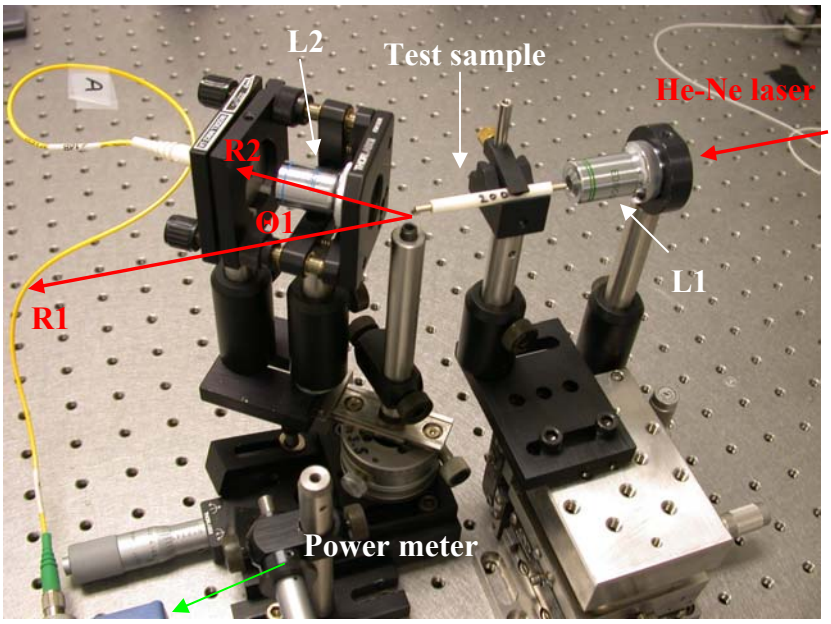

Figure 3-6: The N.A. measurement setup

stainless steel ferrules on both ends of the tube. The ends of the sapphire fiber are plotted into the ends of the steel ferrules using epoxy. The packaged fiber is polished on both ends using abrasive papers with sizes down to 0.5μm.

An objective lens used to launch light from a helium neon laser (633 nm) into the test sample, as shown in Figure 3-6 as "L1", has a magnification of 10 and a NA of 0.4, and the lens to collect and focus light into one end of a single-mode patch cord for intensity measurement, as shown in the figure as "L2", has a magnification of 10 and a NA of 0.25. The other end of the patch cord is connected to a handheld power meter.

At the beginning of measurement, the intensity of the light output by the test sample in the direction parallel to the axis of the sample, i.e., the direction depicted by ray "R1" in Figure 3-6, is measured. Then the fixture holding both the objective lens "L2" and one end of the patch cord is swung counterclockwise along an arc which center is aligned with one end of the test sample until the power reading drops to -13 dB of the value measured in the direction of ray "R1". The angle swung, i.e., θ1 in Figure 3-6, is recorded. The same procedure is repeated by swinging the fixture clockwise until the power drops to -13dB, and the angle, i.e., θ2 where this occurs is recorded. The reported NA (the response O2) is then calculated using the equation

$$N.A. = Sin\left(\frac{\theta_1 + \theta_2}{2}\right).$$

The last optical quality response is the attenuation of clad fibers, O3. The experimental set-up used to measure attenuation is shown in Figure 3-7 below. The light output from a superluminescent diode (SLD) at 1550 nm is first launched into one end of a three inch long sapphire fiber without any cladding, and the power collected at the other end of the test sample, i.e., P_0, is measured. Then the sample is replaced with a clad sapphire fiber

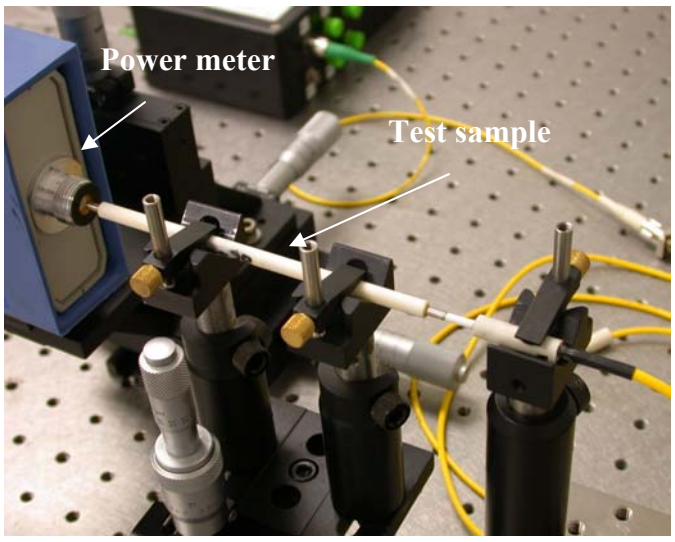

Figure 3-7: The attenuation measurement setup

of the same length and the same procedure is repeated. The measured power in this case is P. The reported attenuation O3 is calculated as

$$Attenuation = -10\log\left(\frac{P_0}{P}\right).$$

3.1.1.4 Procedure for application of coatings

The detailed steps for the preparation of clad fiber samples are listed below. The rationale or goal for each step is explained whenever possible. Some cautionary notes are also provided.

1. The ceramic powders are heated at 500°C for 4 to 5 hours before slurry preparation. The goal is to remove adsorbed water moisture on the powder surface. This step is especially important for nano-powders due to their extremely large specific surface areas. Two types of magnesium oxide powders were used. One is a type of nanopowder, and the other has particle size in the micrometer range. A small amount of spinel powders is also added as nucleation agent for newly formed spinel crystallites.

2. At the same time, the grinding media used in slurry ball milling is also heated at 300°C for 4 to 5 hours using a hot plate. The goal here is also to remove adsorbed water moisture. After the heating is completed, the grinding media is left to cool at room temperature for 15 to 20 minutes. A small fan is used to increase the cooling rate of the media.

3. The cooled grinding media is then put into a 4-oz wide-mouth polyethylene bottle with the desired amount of 2-propanol, the first of two solvents. Also added into the bottle is the dispersant, Menhaden fish oil. The bottle is then shaken by hand for 30 seconds. The choice of fish oil as the dispersant will be explained in one of the following sections.

4. Three types of ceramic powders, i.e., magnesium oxide nanopowders, magnesium aluminate spinel powders, and micron-size magnesium oxide powders, are added to the bottle sequentially. The bottle is shaken by hand for one minute after the addition of the first type of powder, another one minute after the addition of the second type of powder, and for two minutes after the last type of powder is added. The goal of hand shaking is to facilitate the dispersion of the powder in the slurry. Each type of powder is added to the bottle immediately after removal from the furnace at 500°C to minimize the adsorption of moisture from room atmosphere.

5. The bottle is then ball milled for a specified number of hours. The speed of rotation of the bottle influences the degree of size reduction of powders. It should be kept constant in each ball milling session. This milling session is called the “dispersion

milling session." Its goal is to disperse fully the powders without the possible interference of binder molecules in the dispersion performance.

6. After dispersion milling, two types of binder solutions are added to the slurry: both types are polyvinylpyrrolidone (PVP), one with 10K molecular weight, and the other with 55K molecular weight. The binder in powder form has been dissolved in 2-propanol in advance. Since binder has tendency to stick together, the goal here is to ensure that the binder dissolves thoroughly in the slurry. After each step adding binder, the bottle is shaken by hand for 30 seconds.

7. The last chemical added to the bottle is 1-methoxy-2-propanol, the second solvent. Compared to 2-propanol, 1-methoxy-2-propanol has a smaller rate of evaporation. The proper amount of 1-methoxy-2-propanol, together with other favorable conditions, can effectively prevent the occurrence of "carrot" shape fiber caused by the "skinning effect" discussed in Section 3.1.

8. The bottle is then put back onto the ball miller for the final stage of milling, called "binder milling" session, for 3 to 4 hours. Binder milling longer than 3 to 4 hours may have a detrimental effect on the slurry property.

9. Now the slurry is ready for dipping. The sapphire fiber is first cleansed with Kimwipes soaked with 2-propanol. The entire fiber is then soaked in 2-propanol for about 1 hour. The exact time of soaking does not seem to matter; it could be as short as 15 minutes. However, the type of chemical used is important. The surface properties of fibers soaked with chemicals other than 2-propanol may be undesirably altered. It was observed that the ceramic slurry had difficulty sticking to the fibers soaked in ethanol in advance.

10. To prevent solvent evaporation, the top of the graduated cylinder containing the slurry is covered by a piece of Parafilm with a small hole at the center. The size of the hole is a little larger than that of the fiber. The hole should not be too small for the fiber to pass through comfortably. On the other hand, it should not be so large that it can not effectively reduce the rate of solvent evaporation. Up to two fibers can be dipped simultaneously using an automated dipping machine. The dipping speed is an important factor which influences coating thickness. In general, a faster dipping speed creates a thicker coating. The number of dips is another obvious factor affecting coating thickness that needs to be determined.

11. The dipped fibers are then transferred to an oven for binder burnout. The heating profile consists of four stages. In the first stage, the fiber is heated for a room temperature to 340°C at a rate of 5°C/min. This is followed by a slow heating up from 340°C to 440°C at a rate of 1°C per minute. From a Differential Thermal Analysis (DTA) measurement performed at Virginia Tech, the PVP binder decomposes over a temperature range from 340°C to 440°C. A slow heating is designed to reduce the decomposition rate of PVP to avoid the formation of large voids in the coating. Following a slow heating, the third stage consists of heating the

fiber from 440°C to 600°C at a rate of 5°C/min. The fourth and final stage is a dwell period of one hour at 600°C. The goal is to make sure that the PVP burns out completely.

12. After binder burnout, the fibers are transferred to another high temperature furnace for the final firing in argon. The maximum firing temperature and time are the most critical elements in the heating profile. A 50°C increase in temperature may cause cracks to start forming in the cladding. A critical improvement regarding heating environment was made in the high temperature firing setup. It was realized that the samples need to be fired in very pure argon in order to have desirable overall properties. The argon gas was originally flowed into a 6"×6"×6" heating chamber from a small hole on the top of chamber as shown in Figure 3-8(a). To increase argon concentration, the samples are now enclosed in a ceramic tube housing which argon gas enters directly from an opening at the top as shown in Figure 3-8(b). The properties of clad fiber, especially their bending strength and flexibility, improved significantly after this modification.

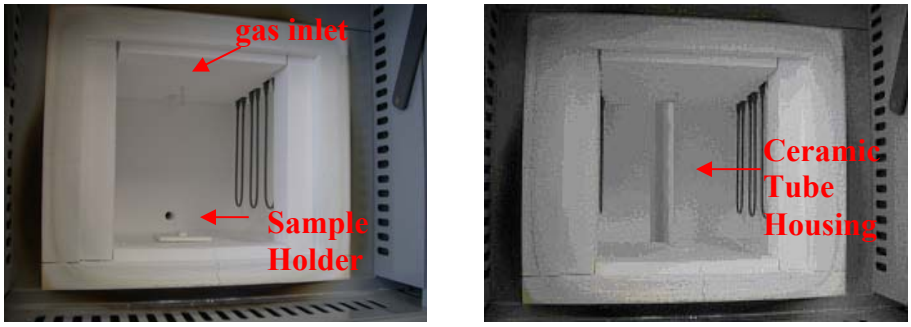

(a) (b)

Figure 3-8: The samples in (b) are fired in much purer argon than in (a).

3.1.1.5 Experimental results from designed experiments

Eighteen samples were fabricated according to the L18 array listed in Table 3-1 and the factors and levels listed in Table 3-2. Each sample was prepared using to the steps described in Section 3.1.1.4. For each three-inch long clad samples, the cross-sections in three different locations, i.e., the top, the bottom, and the middle of the sample length, were polished and analyzed.

The three polished cross sections for Sample 1 are shown in Figure 3-9. In each cross section, 10 out of the 13 responses are analyzed. The results of the analysis for sample 1 are listed in Table 3-3, Table 3-4, and Table 3-5 for the geometrical, mechanical, and optical responses, respectively. The value of each of the 10 responses used for the

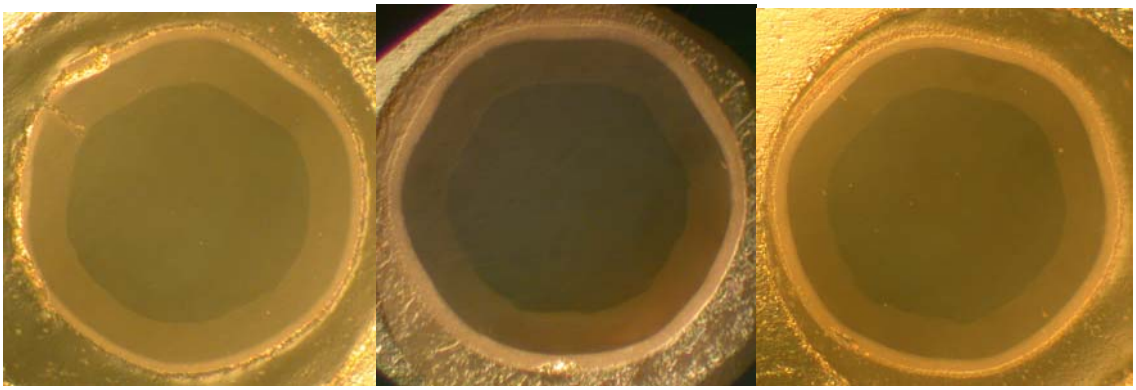

(a) cross-1 (top) (b) cross-3 (middle) (c) cross-2 (bottom)

Figure 3-9: the 3 cross sections polished and analyzed for sample 1

following Taguchi analysis is the average value calculated from the responses measured at all three cross-sections. There is only one data point each measured for the responses M1 (bending deflection), O2 (N.A.) and O3 (attenuation), which are not listed in the tables, due to the nature of measurement. The results for all 13 responses of sample 1 are listed in Table 3-6.

Table 3-3: All 6 geometrical response data for sample 1

6-1-05 Sample 1-1	mean core diameter (μm) (**G1**)	mean overall cladding thickness (μm) (**G2**)	mean outer cladding thickness (μm) (**G3**)	mean skin thickness (μm) (**G4**)	mean overall fiber diameter (μm) (**G5**)	interface center distance (μm) (**G6**)
cross 1	95.2	20.6	4.4	2.10	136.3	0.2
cross 2	95.2	21.4	5.5	2.60	138.1	0.7
cross 3	92.4	22.3	5.4	1.00	137.5	1.1
Average	**94.3**	**21.4**	**5.1**	**1.9**	**137.3**	**0.67**

Table 3-4: The mechanical response data M2, M3, and M4 of sample 1

6-1-05 Sample 1-1	crack parameter (μm^2) (**M2**)	crack length (μm) (**M3**)	number of cracks (**M4**)
cross 1	19.7	19.5	1
cross 2	0.0	0.0	0
cross 3	3.5	17.0	1
Average	**7.7**	**12.2**	**0.7**

Table 3-5: The core/cladding interface roughness data, O1, of sample 1

Sample Name	Core Area (C.A.) (pixel)	Roughness Area (R.A.) (pixel)	Roughness Factor (100*R.A/C.A.) (**O1**)
6-1-05 sample 1-1 cross-1	651190	2563	0.39
6-1-05 sample 1-1 cross-2	566041	2638	0.47
6-22-05 sample 1-1 cross-3	557439	3011	0.54
Average			**0.47**

Table 3-6: The results of all 13 responses of sample 1

	G1 (um)	**G2** (um)	**G3** (um)	**G4** (um)	**G5** (um)	**G6** (um)	**M1** (mm)	**M2** (um^2)	**M3** (um)	**M4** (no unit)	**O1** (no unit)	**O2** (no unit)	**O3** (dB)
1	94.3	21.4	5.1	1.9	137.3	0.67	0.75	7.7	12.2	0.67	0.47	0.041	3.3

(M1: bending deflection, O2: Numerical Aperture, and O3: attenuation)

The optical microscopic pictures of all three polished cross sections for each of the 17 samples from sample 2 to sample 18 are shown in Appendix A. Also included in the figures are the results of all 13 responses used for Taguchi analysis for that specific sample.

All the data of all 18 samples used for the following Taguchi analysis are listed in Table 3-7 below.

3.1.1.6Analysis of results

The list of factors was examined to ensure that they were independent and that the samples could be made within the timeframe required. It was decided that the timeframe available for the experiments did not permit interactions to be studied. Also, the decision was made that a larger screening array would be used initially to determine the significant factors; subsequent arrays could be used if deemed necessary. Some preliminary experiments were required to ensure that all of the factors and levels in the array could actually be used to produce meaningful samples. In some cases, the levels had to be adjusted to allow this.

Table 3-7. Data for all 18 samples

	G1 (μm)	G2 (μm)	G3 (μm)	G4 (μm)	G5 (μm)	G6 (μm)	M1 (mm)	M2 (μm^2)	M3 (μm)	M4	O1	O2	O3 (dB)
1	94.3	21.4	5.1	1.9	137.3	0.67	0.75	7.7	12.2	0.67	0.47	0.041	3.3
2	89.9	22.1	3.9	1.6	134.3	0.81	0.71	0.0	0.0	0.00	0.40	0.046	8.4
3	86.8	21.4	3.4	2.1	131.1	0.67	0.84	3.9	6.0	0.33	0.56	0.055	7.2
4	94.4	20.1	4.6	1.5	134.4	1.22	0.88	0.0	0.0	0.00	0.24	0.068	3.1
5 (R1)	79.4	24.7	5.8	33.0	194.1	0.76	0.73	0.0	0.0	0.00	0.59	0.059	4.5
6 (R1)	71.7	32.9	6.2	1.3	138.4	0.90	0.41	28.4	24.1	2.00	1.30	0.052	5.1
7	92.8	21.6	4.9	2.5	138.9	0.82	0.83	0.0	0.0	0.00	0.02	0.063	4.9
8 (R1)	84.7	27.4	5.8	150.3	442.1	1.18	0.78	0.0	0.0	0.00	1.13	0.096	24
9 (R1)	93.5	21.1	4.0	1.5	137.1	0.92	0.46	50.5	8.5	1.00	0.59	0.087	5.2
10	90.4	22.5	4.4	5.5	140.2	0.60	0.67	0.0	0.0	0.00	0.41	0.052	2.5
11 (R1)	89.3	25.2	5.5	2.1	141.1	0.50	0.59	17.6	6.7	0.67	0.44	0.061	7.2
12	97.6	19.2	2.6	2.4	135.7	0.61	0.73	35.6	18.9	1.67	0.70	0.089	10.5
13	92.4	22.6	4.9	2.6	137.8	0.93	1.08	9.3	7.1	0.33	0.65	0.152	5.3
14	87.2	25.8	4.6	1.4	138.6	0.72	0.65	108.3	25.9	1.33	0.73	0.107	12
15 (R1)	80.4	33.4	8.3	10.5	165.5	0.93	0.54	0.0	0.0	0.00	0.99	0.052	3.9
16	86.6	22.1	4.6	21.3	172.8	0.66	0.93	18.1	7.2	0.67	0.36	0.065	1.4
17	88.5	23.0	4.5	1.5	134.2	0.77	0.81	12.7	7.3	0.33	1.06	0.107	11.3
18 (R1)	67.5	31.1	6.3	37.8	206.1	0.59	0.64	0.0	0.0	0.00	1.88	0.044	5.3

Overall, a large amount of variation was observed in the responses measured, and a significant portion of this variation for certain responses remained in the error term (unexplained variation). Analysis of the data provided a number of useful insights which were incorporated into subsequent fibers made according to the optimum recommendations from the experimental array design analysis. Due to the short time available for the experiments, a rigorous confirmation experiment was not performed. However, results from the additional fibers seemed to indicate marked improvement in many of the critical responses, indicating that the relations determined in the analysis of data may indeed be appropriate. For the analysis of each response presented, only the pertinent data is included. Taguchi methods of experimental design and the associated methodology for analysis were used for selection of the experimental design array and for interpretation of the data which resulted.

The L18 array presents a very large number of responses to collect and analyze. For each response, three measurements were taken and the averages and standard deviations calculated. The average values were used as the measured value for input into the ANOVA analysis. In some of the responses measured, a high standard deviation was encountered, indicating that the measurement process could be contributing significantly to some of the variation that was seen. Average values were used in the ANOVA input

which should have mitigated this variation to some extent, although it was noted that the data indicated that the measurement process for many of the responses should be studied in more detail in the future. Below are listed some of the results of the analysis of the data for the responses measured.

3.1.1.6.1 Sapphire core diameter (G1)

The following is the analysis of the sapphire core diameter data generated in the 18 samples that were measured. The quality characteristic used was "smaller is better;" that is, it is desirable to have the core diameter as small as possible. The first column of Table 3-8 shows the factors considered, and the next three columns show the measured diameter response for the different levels of the factors. Since a total of 18 samples were prepared, each response value for factors 2 through 8 represents the average core diameter from six samples. As their only two levels for the first factor "Nano MgO amount", each value in the first 2 columns for that factor represents the average core diameter from the 9 samples.

Also listed in the last column of the Table is the difference between the averages of level 3 and level 1. For example, the average core diameter of the 6 samples with the factor "Dipping Speed" set to level 1 is 91.383 µm, and that to level 3 is 85.599 µm. So their difference, L3-L1, is -5.784. This difference gives some indication of the relative influence of the factors to the variation of results. More rigorous measures of the influence of each factor will be decided by the *F-Factor* and *Confidence Level* shown in the Analysis of Variance (ANOVA) Table 3-9 below. It should be noted that all of the data generated will not be shown. For example, only L3-L1 is shown here. There is similarly data for level 2 minus level 1 and level 3 minus level 2. These are not shown as information here because that they are already encoded into the other data presented.

Table 3-8

Column # / Factors	Level 1	Level 2	Level 3	L3 - L1
1 Nano MgO amount	87.5	86.655		n/a
2 Dipping Speed	91.383	84.249	85.599	-5.784
3 Firing Profile	91.816	86.5	82.916	-8.901
4 MgO/Spinel ratio	90.066	86.599	84.566	-5.5
5 First Stage Ball	83.799	88.933	88.5	4.7
6 Fish oil amount	88.199	87.149	85.883	-2.317
7 PVP type (K)	89.766	85.616	85.849	-3.918
8 PVP amount	82.783	87.233	91.216	8.432

Table 3-9 shows the ANOVA table for the analysis of the factor influences. The Qualitek-4 software tool for automated design and analysis of Taguchi experiments, available from Nutek, Inc., was used in the preparation of these results. The next four

tables show screen captures taken from the output of the software when applied to the analysis of our designed experiments.

The first column "DOF (*f*)" stands for "Degree of Freedom" and is equal to the number of levels minus 1. The second column "Sum of Sqrs (*S*)" stands for "Sums of Squares," which are used to determine the significance of factor. For factors with an equivalent number of degrees of freedom, the larger the "*S*" number, the more significant is the factor.

The value "*S*" is calculated according to the equation,

$$S = \sum_{i=1}^{L} \frac{A_i^2}{N_{Ai}} - C.F.$$

where

A_i is the sum of results that include Factor A at level i,
N_{Ai} is the total number of experiments in which level i of factor A is present,
L the total number of levels, and
C.F. the Correction Factor, which is defined as T^2/N, in which T is the sum of all results, and N is the total number of results.

The column "Variance (*V*)" is defined as *S/f*, and the column "F-Ratio (*F*)" as V/V_e, where V_e is the variance for the error terms (obtained by calculating the error sum of squares and dividing by the error degrees of freedom). In general, V_e increases as the degree of data scattering increases. Therefore, a large "F-Ratio (*F*)" number of a certain factor indicates that this factor possibly possesses a small degree of data scattering. This indicates that this factor is *significant* and has large influence on the results.

The column "Pure Sum (*S*')" is defined as $S-(V_e \times f)$. In this column, when a factor is found to have little or no influence and is excluded from any statistical control, the number "0" would be entered. As shown in Table 3-9, all the factors, except for "Firing Profile" and "PVP amount," have little or no effect on the results since their entries are 0's. The last column in the Table "Percent (P%)" shows *how sensitive the result is to the change of levels of the factors*. Here, the most influential factor is the "Firing Profile", which has a relatively small influence of 6.3%.

The ANOVA analysis is applied to the results in Table 3-9, and calculates a "Confidence Level" for each factor. This Confidence Level is then displayed in the column titled "Pure Sum" in Table 3-10. The term "POOLED" is listed in the column "F-Ratio (*F*)" for each factor in the table. When a factor is deemed unimportant, it can be factored out of the analysis by including (pooling) it into the error terms. The pooling is performed starting with the factors that show the least significance. In Table 3-10, all factors are pooled, which indicates that it was decided that none of the factors have significant influence on the results.

Table 3-9

Col # / Factor	DOF (f)	Sum of Sqrs. (S)	Variance (V)	F - Ratio (F)	Pure Sum (S')	Percent P(%)
1 Nano MgO amount	1	3.207	3.207	.037	0	0
2 Dipping Speed	2	172.294	86.147	.996	0	0
3 Firing Profile	2	240.62	120.31	1.391	67.683	6.301
4 MgO/Spinel ratio	2	92.807	46.403	.536	0	0
5 First Stage Ball	2	97.244	48.622	.562	0	0
6 Fish oil amount	2	16.126	8.063	.093	0	0
7 PVP type (K)	2	65.228	32.614	.377	0	0
8 PVP amount	2	213.583	106.791	1.235	40.646	3.784
Other/Error	2	172.936	86.468			89.915
Total:	17	1074.051				100.00%

The "Confidence Level (*C.L.*)" is listed in the "Pure Sum (*S'*)" column of the Table. The notation "NC" means "Not Calculated" for the factors with little or no influence. The value of "Confidence Level" is related directly to the magnitude of "F-Ratio (*F*)" in Table 3-9; i.e., the larger the *F* number, the higher would be the value of *C.L.* Here the confidence levels for the factors "Firing Profile" and "PVP amount" are 67.33% and 68.29% respectively. Therefore, based on the amount of scatter in the data, only "Firing Profile" and "PVP Amount" seem to have some degree of confident influence approaching 70% on the results. It is to be noted that 70% is a relatively small number for the Confidence Level. A desirable Confidence Level should approach about 95% to 100%. More data would be needed to improve the estimates of these effects.

Table 3-10

Col # / Factor	DOF (f)	Sum of Sqrs. (S)	Variance (V)	F - Ratio (F)	Pure Sum (S')	Percent P(%)
1 Nano MgO amount	(1)	(3.207)		POOLED	(CL= *NC*)	
2 Dipping Speed	(2)	(172.294)		POOLED	(CL= *NC*)	
3 Firing Profile	(2)	(240.62)		POOLED	(CL=67.33%	
4 MgO/Spinel ratio	(2)	(92.807)		POOLED	(CL= *NC*)	
5 First Stage Ball	(2)	(97.244)		POOLED	(CL= *NC*)	
6 Fish oil amount	(2)	(16.126)		POOLED	(CL= *NC*)	
7 PVP type (K)	(2)	(65.228)		POOLED	(CL= *NC*)	
8 PVP amount	(2)	(213.583)		POOLED	(CL=68.29%	
Other/Error	17	1074.045	63.179			100
Total:	17	1074.051				100.00%

Figure 3-10 graphically illustrates the effect of each level of six of the factors on the measured response (in this case, core diameter). In each plot, the x-access refers to the level, and the y-axis refers to the measured core diameter in micrometers. In general, only six of the graphical representations are shown as the data for these graphs is encoded into the other data presented.

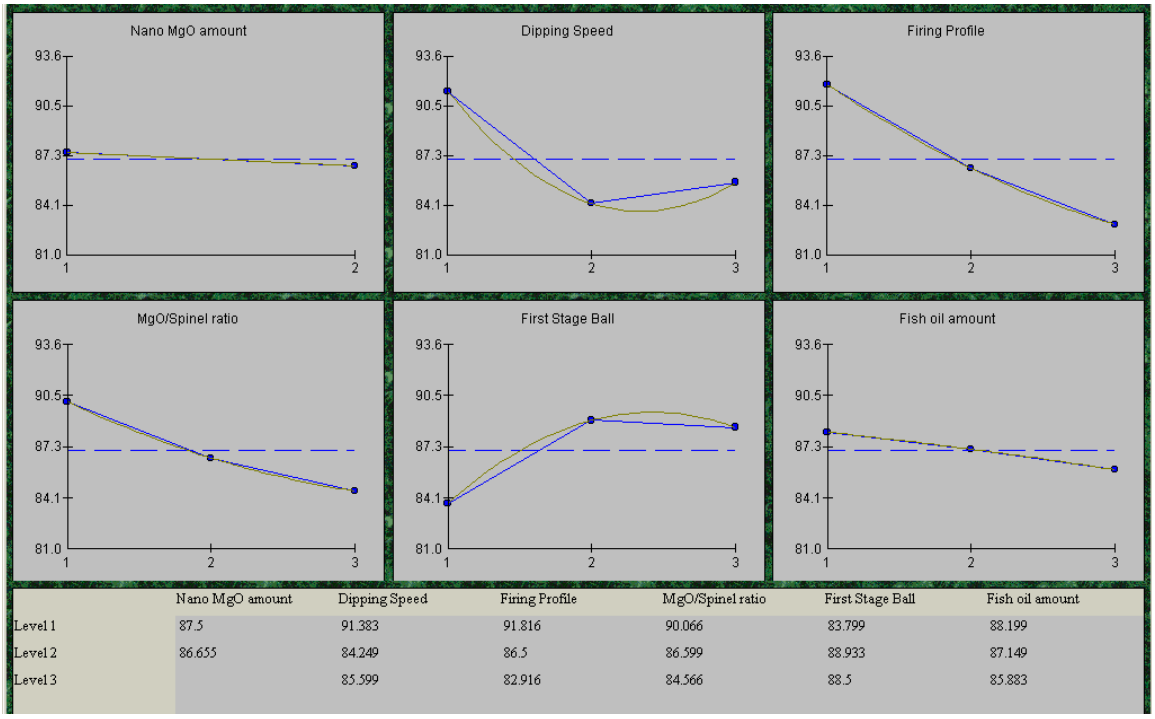

	Nano MgO amount	Dipping Speed	Firing Profile	MgO/Spinel ratio	First Stage Ball	Fish oil amount
Level 1	87.5	91.383	91.816	90.066	83.799	88.199
Level 2	86.655	84.249	86.5	86.599	88.933	87.149
Level 3		85.599	82.916	84.566	88.5	85.883

Figure 3-10

Table 3-11 shows the expected optimum performance for "Firing Profile" and "PVP amount" being determined as significant (with a confidence level less than 70% - so a very large amount of variation in the data relative to the factor level change). Based on the very large scatter in the data, the confidence interval around the predicted average (the "Expected Result at Optimum Condition" in Table 3-11) will be very large.

Table 3-11

Column # / Factor	Level Description	Level	Contribution
3 Firing Profile	1600	3	-4.162
8 PVP amount	0.4	1	-4.295

Total Contribution From All Factors...	-8.458
Current Grand Average Of Performance...	87.077
Expected Result At Optimum Condition...	78.62

If we assumed that all the factors were significant the optimal levels would be as those listed in Table 3-12.

Table 3-12

Column # / Factor	Level Description	Level	Contribution
1 Nano MgO amount	20	2	-.423
2 Dipping Speed	.105	2	-2.828
3 Firing Profile	1600	3	-4.162
4 MgO/Spinel ratio	12:1	3	-2.512
5 First Stage Ball	3	1	-3.278
6 Fish oil amount	75	3	-1.195
7 PVP type (K)	90% 10K	2	-1.462
8 PVP amount	0.4	1	-4.295

This gives the optimal levels as predicted by the data, but again due to the large scatter the factors mentioned above are not sufficiently high in significance to warrant inclusion in the optimal predictions.

The ANOVA results of the other 12 responses are listed in Appendix B.

3.1.1.7 The determination of overall optimal levels from ANOVA analysis

The factors determined to be significant and their optimal levels for each response are listed in Table 3-13 below. Unless otherwise noted, all levels in the table have confidence levels greater than 90%. Levels with confidence levels less than 89% are not listed except for Factor 1 and 2.

To determine the optimal overall levels, the relative importance of the responses measured is taken into account. A hierarchical structure was used for the optimal level selection, based on available time and the limited knowledge of the relative trade-offs between one response and the next.

The most important response was determined to be the "skin thickness" G4. One example of a "carrot shaped" dipped fiber with a thick and non-uniform skin is sample 18_{R1}, shown in Figure 3-11 below. In the background of this picture are grid lines 1.4 mm apart. The top of dipped fiber is on the left hand side of this figure. As can be seen, the overall fiber diameter is quite large at the top of fiber, and the diameter gradually decreases towards the bottom of fiber. This "carrot shape" indicates that the slurry has not been prepared using the optimized conditions. It may also create practical problems in fiber packaging in the future. So the first priority is to prevent this phenomenon from occurring. Therefore, according to row G4 in Table 3-13, Factor 7 and Factor 8 are set to be in Level 2 and Level 3 respectively. Factor 7 and 8 are related to the type and amount of PVP binder added to the slurry.

Table 3-13

	F1	F2	F3	F4	F5	F6	F7	F8
G1								
G2		1	1		3		1	3
G3				2	3	1	1	3
G4	2 (71%)	1 (87%)					2	3
G5								3
G6								
M1								
M2	1 (69%)						3	
M3	1	3	1	2	2	3	3	1
M4						3	3	1
O1	1 (75%)	1 (70%)	1					
O2	1 (68%)							
O3			1 (89%)					

The responses are:
G1: core diameter,
G2: overall cladding thickness,
G3: outer cladding thickness,
G4: skin thickness, G5: overall fiber diameter,
G6: concentricity (inter-center distance),
M1: flexibility from 3-point bending test,
M2: total area of cracks,
M3: length of the longest crack,
M4: number of cracks,
O1: core/cladding interface roughness,
O2: numerical aperture (N.A.) measurement,
O3: attenuation measurement,
F1: Nano MgO weight ratio,
F2: dipping speed,
F3: maximum firing temperature,
F4: MgO/Spinel ratio,
F5: dispersion milling time,
F6: fish oil amount,
F7: 10K PVP weight ratio,
F8: total PVP amount.

Level 2 in Factor 7 represents a 10% 55K PVP, i.e., 90% 10K PVP, and Level 3 in Factor 8 represents a 0.6 g total amount of PVP. In fact, eventually, G4 turns out to be the only factor in the "Geometrical Response" category that has been taken into account in the determination of final optimum conditions.

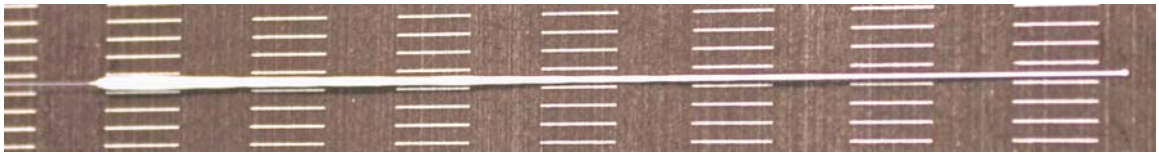

Figure 3-11: sample 18_{R1} after dipping

The second most important response was determined to be "core/cladding interface roughness", O1. According to row O1 in Table 3-13, Factor 3 (the maximum firing temperature) has to be set at Level 1 (1550°C) in order to have smooth core/cladding interface. The results from "attenuation test", O3, as listed in row O3 in Table 3-13, also support the same conclusion.

The next most important response is the "length of the longest crack", M3. In fact, from Table 3-13, the mechanical responses including "total area of cracks (M2)" and "number of cracks (M4)" predict similar results regarding the optimum levels for Factors 6, 7 and 8. The reason for picking the "length of the longest crack", M3, as one of the most important factors is that all 8 factors are considered significant for this response. To achieve minimal cracking in cladding, Factor 7 needs to be set in Level 3 and Factor 8 in Level 1, indicating that the percentage of 55K PVP needs to be increased to 20% and the total amount of PVP decreased to 0.4 g. However, since these levels are in conflict with the ones set to prevent "carrot" shape fibers, they are ignored.

Also from Row M3 in Table 3-13, Factor 3 (the maximum firing temperature) has to be set to Level 1 (1550°C) to prevent cracking. This level agrees with the one determined from the "core/cladding interface roughness" response, O1, to have a smooth interface. Finally, Factor 4 (MgO/Spinel ratio), Factor 5 (dispersion milling time), and Factor 6 (fish oil amount) are set to be in Level 2 (9:1), Level 2 (6 hours), and Level 3 (75μL) respectively according to Row M3 in Table 3-13.

The last two factors to be determined are Factor 1 (Nano MgO weight ratio) and Factor 2 (dipping speed). According to the results listed in column F1 and F2 in Table 3-13Table 3-13, it was decided to set Factor 1 at Level 1 (10% nano MgO powder) and Factor 2 at Level 2 (2.7 mm/second). The final optimal levels are listed in below.

3.1.1.8 Testing of optimized processing with 125 μm sapphire fibers

In order to assess the impact of the set of optimal processing parameters on the quality of the clad sapphire fiber, four pieces of clad fibers were fabricated using 125μm sapphire fibers and the final optimal conditions listed in Table 3-14.

	Factors	Level	Value
1	Nano MgO weight ratio in all MgO powders (%)	1	10
2	Dipping speed (mm/sec)	2	2.7
3	Maximum firing temperature (°C)	1	1550
4	MgO/Spinel ratio	2	9:1
5	Dispersion milling session time (hr)	2	6
6	Fish oil amount (μL)	3	75
7	10K PVP weight ratio (%)	2	90
8	PVP amount (both 10K and 55K)(g)	3	0.6

Table 3-14

Each piece of clad fiber has a length of 6.3 cm, except for the third sample, Sample 3, which is 4.9 cm long. Both ends of the clad fibers were polished and analyzed for geometrical, mechanical, and the core/cladding roughness (O1) responses. The optical microscopic pictures of each sample are shown in Figure 3-12 below. In general, all 4 samples have smooth core/cladding interfaces and claddings with very similar thicknesses.

The results of all the responses from the cross-sectional analysis are listed in Table 3-15 below. As can be seen in this table, the repeatability from sample to sample is quite good. For example, the average core diameters are 94.3, 95.5, 94.0, and 91.7μm for samples 1, 2, 3, and 4, respectively. The average of these 4 diameters is 93.9 μm with a standard deviation of 1.6 μm. Other responses have very similar values among all 4 samples, except for a single crack occurring in the cross sections for sample 3, while there are no cracks for samples 1, 2, and 4.

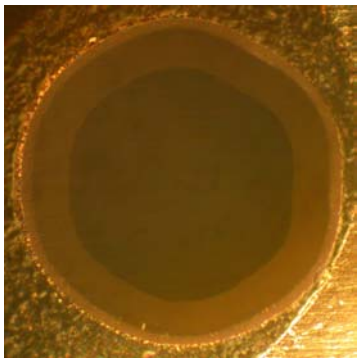
(a) Sample 1 – cross-section 1

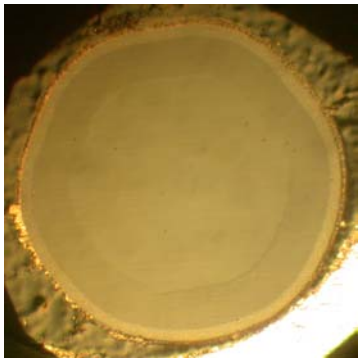
(b) Sample 1 – cross-section 2

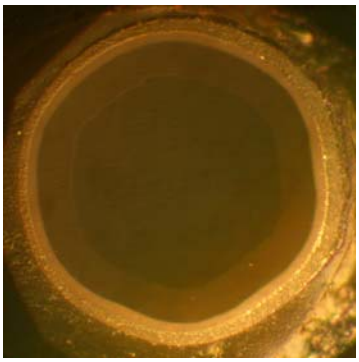
(c) Sample 2 – cross-section 1

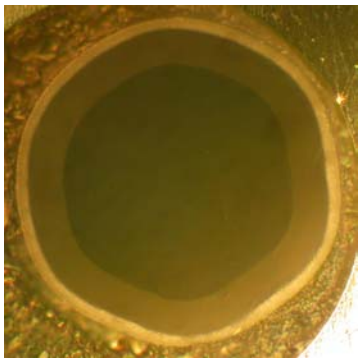
(d) Sample 2 – cross-section 2

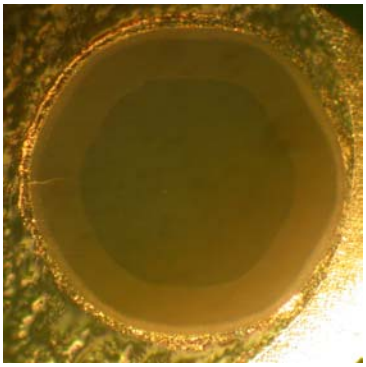
(e) Sample 3 – cross-section 1

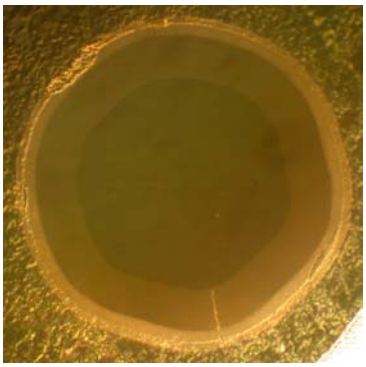
(f) Sample 3 – cross-section 2

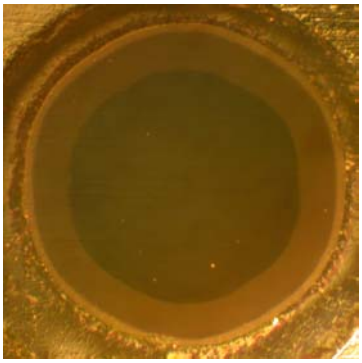
(g) Sample 4 – cross-section 1

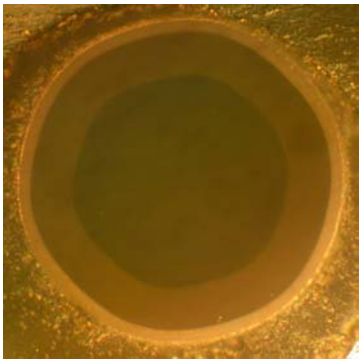
(h) Sample 4 – cross-section 2

Figure 3-12: Cross sections of 125 µm diameter confirmation clad fibers

Table 3-15

Sample	Cross	G1 (μm)	G2 (μm)	G3 (μm)	G4 (μm)	G5 (μm)	G6 (μm)	M2 (μm^2)	M3 (μm)	M4	O1
1	1	94.9	19.3	4.1	2.2	137.3	0.1	0	0	0	0.06
1	2	93.7	21.9	4.9	2.5	140.8	0.9	0	0	0	0.35
	Average	94.3	20.6	4.5	2.35	139.05	0.46	0	0	0	0.21
	St Dev	0.8	1.8	0.6	0.2	2.5	0.6	0	0	0	0.21
2	1	94.1	20.7	4.6	5.6	147.5	0.4	0	0	0	0.46
2	2	97	19.2	4.3	1	136.2	0.5	0	0	0	0.03
	Average	95.55	19.95	4.45	3.3	141.85	0.43	0	0	0	0.25
	St Dev	2.1	1.1	0.2	3.3	8.0	0.0	0	0	0	0.30
3	1	97.1	22.9	4.5	5.6	152.2	0.9	4.4	18.5	1	0.22
3	2	90.9	22.9	4.7	3.5	143.3	0.8	15.8	22.2	1	0.12
	Average	94	22.9	4.605	4.55	147.75	0.83	10.1	20.4	1	0.17
	St Dev	4.4	0.0	0.1	1.5	6.3	0.1	8.1	2.6	0	0.07
4	1	95.2	18.3	3.3	4.1	138.3	0.6	0.0	0.0	0	0.06
4	2	88.3	22.9	5.0	2.5	138.3	0.5	0.0	0.0	0	0.07
	Average	91.75	20.6	4.15	3.3	138.3	0.55	0	0	0	0.06
	St Dev	4.9	3.3	1.2	1.1	0.0	0.1	0	0	0	0.01

(G1: core diameter, G2: overall cladding thickness, G3: outer cladding thickness, G4: skin thickness, G5: overall fiber diameter, G6: concentricity (inter-center distance), M2: total area of cracks, M3: length of the longest crack, M4: number of cracks, O1: core/cladding interface roughness)

The 3-point bending test was performed on samples 1 and 3. For sample 1, three pieces of test samples, each of about 17 mm long, were cut from the original clad fiber. In the case of Sample 3, two pieces of test samples were prepared. The bending test results are listed in Table 3-16 below. As shown in the table, the average deflection for Sample 1 is 0.96 mm with a standard deviation of 0.05 mm. Compared to the values of deflection of all 18 samples in the results of Taguchi experiments listed in Table 3-7, a deflection of 0.96 mm is the second largest deflection in the table. The average deflection of Sample 3 drops to 0.78 mm, possibly due to the existence of a single crack in the cladding.

Table 3-16

Sample	Starting Height (mm) (H1)	Ending Height (mm) (H2)	Time Elapsed (s)	Change in Length (H2-H1) (mm)	Speed (mm/s)
Sample 1-1	9.52	10.48	79	0.96	0.0122
Sample 1-2	9.56	10.57	87	1.01	0.0116
Sample 1-3	9.53	10.44	83	0.91	0.011
(Sample 1-No crack)			Average	0.96	
			St Dev	0.05	
Sample 3-1	9.58	10.52	85	0.94	0.0111
Sample 3-2	9.56	10.18	60	0.62	0.0103
(Sample 3-One crack)			Average	0.78	
			St Dev	0.23	

3.1.1.9 Testing of optimized processing with 75 μm sapphire fibers

The sample preparation conditions listed in Table 3-14, from the Taguchi analysis were also implemented on 75μm diameter sapphire fibers. The fibers were dipped for either 100 times, 150 times, or 200 times in the slurry, in order to assess the effect of the number of dips on the final cladding diameter. It is to be noted that all fibers in the Taguchi experiments are dipped for 150 times. Each 75μm diameter sapphire fiber is about 5.0 cm long. The polished cross sections of clad 75μm diameter sapphire fibers are shown in Figure 3-13. Only one cross section from each sample is shown in the figure. The figure reveals that the cladding thickness increases as the number of dips increases. In the case of 200 dips, there is one crack forming in the cladding and the core/cladding interface is very rough. The results of cross sectional analysis of Figure 3-13 are listed in Table 3-17. Compared with the cross sectional pictures of the 125μm-diameter confirmation clad fibers illustrated in Figure 3-12, the core/cladding interface of the 150-dip fiber, as shown in Figure 3-13(b), seems rougher in its details, although this is not reflected in the value of roughness "O1" measurement listed in Table 3-17. It is quite obvious that the 200-dip sample shown in Figure 3-13(c) has a very rough interface.

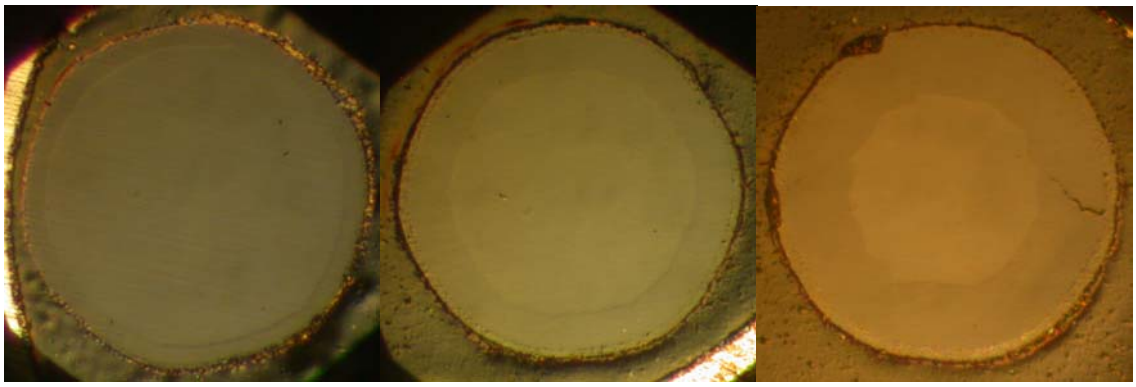

(a) 100 dips (b) 150 dips (c) 200 dips

Figure 3-13: Cross sections of 75μm diameter confirmation clad fibers

Table 3-17

# of dips	G1 (μm)	G2 (μm)	G3 (μm)	G4 (μm)	G5 (μm)	G6 (μm)	M2 (μm^2)	M3 (μm)	M4	O1
100	67.9	4.5	0	0	76.0	0.3	0	0	0	0.2
150	64.5	12.4	2.3	0	86.3	0.8	0	0	0	0.15
200	47.9	19.6	3.1	0	83.7	0.7	11.9	19.2	1	1.78

The sample with 100 dips was cut into 3 pieces, each 17mm long, for the 3-point bending test. The results are listed in Table 3-18 below. It can be seen in the table that the bending deflection of the 76 μm sapphire fiber clad with a 4.5 μm thick spinel cladding is very large (1.71 mm). The deflection here is about 1.7 times greater than that of a 125 μm clad fiber as shown in Table 3-16 above.

Table 3-18

Sample (100 dips)	Starting Height (mm) (H1)	Ending Height (mm) (H2)	Time Elapsed (s)	Change in Length (H2-H1) (mm)	Speed (mm/s)
Conf.-75 micron 1-1	9.62	11.6	185	1.93	0.0104
Conf.-75 micron 1-2	9.63	11.28	141	1.65	0.0117
Conf.-75 micron 1-3	9.62	11.13	138	1.55	0.0112
			Average	1.71	
			St Dev	0.20	

3.1.2 High-temperature stability tests of sapphire fiber cladding

Another important requirement for a practical high-temperature waveguide is its stability at high temperatures. From a microstructural point of view, it is important to understand, at elevated temperatures, whether further conversion from sapphire to spinel proceeds, or whether the core/cladding interface gets rougher due to spinel grain growth, and whether mechanical integrity degrades due to crack generation and propagation in the cladding.

3.1.2.1Testing of optimized processing with 125 μm sapphire fibers

In order to assess the impact of the set of optimal processing parameters on the quality of the clad sapphire fiber, four pieces of clad fiber were fabricated using the 125 μm sapphire fibers and the final optimal conditions listed in Table 3-14 to study the high temperature stability from 1000°C to 1500°C. One of the clad fibers was first heated to 1000°C for 3 days, followed by each of the other 3 pieces heated to 1100°C, 1200°C, and 1300°C sequentially. To study the stability at temperatures higher than 1300°C, the fiber heated at 1100°C was once again put into the furnace and heated to 1400°C for 3 days. Similarly, the fiber heated at 1200°C was once again put into the furnace and heated to 1500°C for 3 days. Each fiber was polished and its cross-section analyzed before and after the high temperature treatment.

The cross-sections of the clad fiber before and after the 1000°C treatment are shown in Figure 3-14 below. Figure 3-14 (a) shows the cross section of the as-fabricated clad fiber. Figure 3-14 (b) shows the same cross section after being heat treated at 1000°C for 3 days. Then the fiber was put into a mold and polished. Figure 3-14 (c) shows the cross section 1 to 2 mm below the surface shown in Figure 20 (b). As can be seen from these figures, there is little effect of the heat treatment on the fiber microstructure.

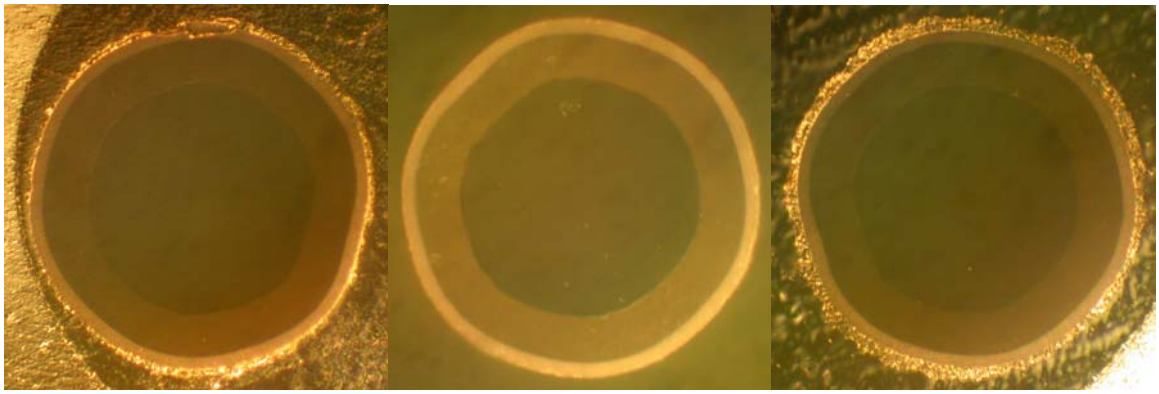

(a) (b) (c)

Figure 3-14: (a) The cross section of clad fiber before heat treatment, (b) the same cross section after heat treated at 1000°C for 3 days, and (c) the polished cross section 1 to 2 mm below the surface shown in (b).

The cross-sectional pictures of the sample heat-treated at 1100°C for 3 days are shown at Figure 3-15 below. In a similar fashion to the case of 1000°C heat treatment, there is overall little observable difference caused by the 1100°C treatment, except possibly a more distinctive core/cladding interface on the surface of the cross section as shown in Figure 3-15 (b).

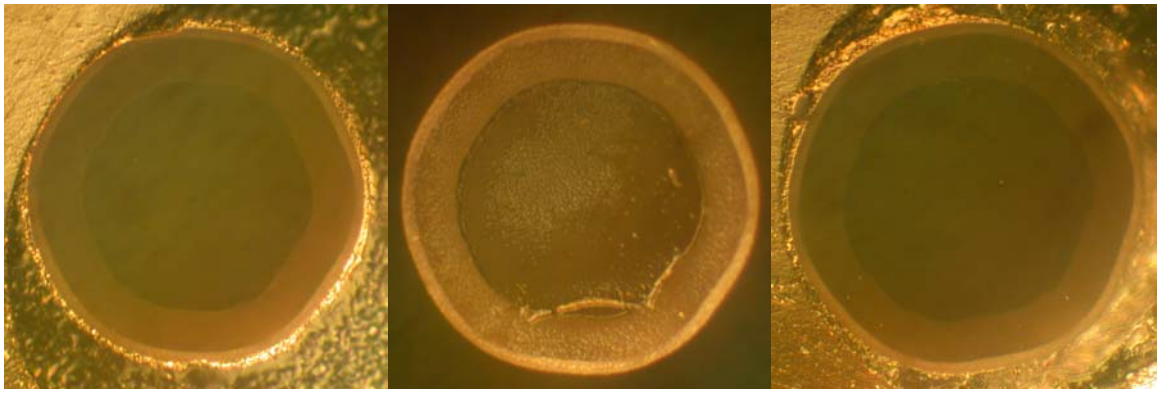

(a) (b) (c)

Figure 3-15: (a) The cross section of clad fiber before heat treatment, (b) the same cross section after heat treated at 1100°C for 3 days, and (c) the polished cross section 1 to 2 mm below the surface shown in (b).

The cross-sectional pictures of the sample heat treated at 1200°C for 3 days are shown at Figure 3-16 below. Similarly, there is no significant difference except possible thickening of the core/cladding interface on the surface of the cross section as shown in Figure 3-16 (b).

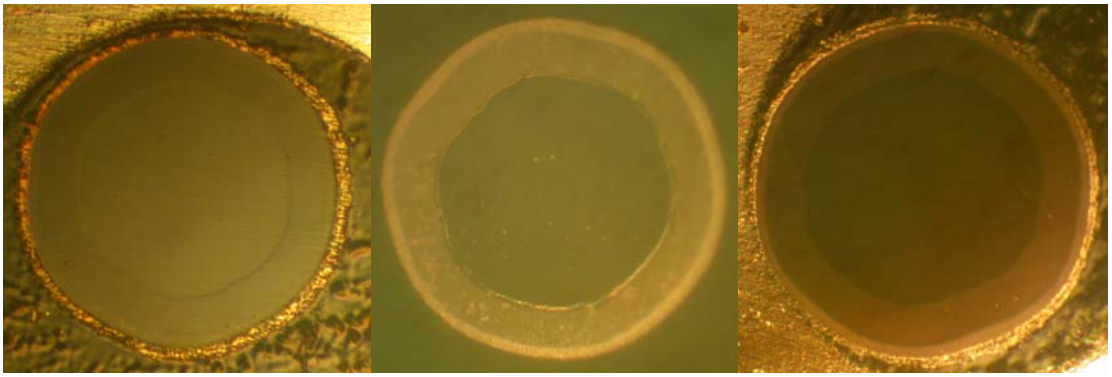

(a) (b) (c)

Figure 3-16: (a) The cross section of clad fiber before heat treatment, (b) the same cross section after heat treated at 1200°C for 3 days, and (c) the polished cross section 1 to 2 mm below the surface shown in (b).

The cross-sectional pictures of the sample heat-treated at 1300°C for 3 days are shown at Figure 3-17 below. More microstructural changes are discernable after heat treatment at 1300°C for 3 days. First, as shown in Figure 3-17 (b), the core/cladding interface at the surface after the heat treatment seems further thickening, and there seem to be surface cracks created in the cladding. However, as can be seen in Figure 3-17 (c), the polished cross section 1 to 2 mm below the surface shows no signs of cracks in the cladding. Yet again, as shown in Figure 3-17 (d), another polished cross section about 14 mm below the cross section in Figure 3-17 (c) does show signs of several cracks. Light was launched from the other end of the clad fiber and, as shown in Figure 3-17 (e), the light guiding property of the clad fiber does not seem to be greatly degraded due to the microstructural changes.

The sample heat treated at 1100°C for 3 days was put back into the furnace and heated to 1400°C for another 3 days. The cross-sectional pictures are shown at Figure 3-18 below. As shown in Figure 3-18 (b), at the core/cladding interface on the surface there is an even thicker layer of further converted material, presumably spinel. Also the cladding thickness in either Figure 3-18 (b) or (c) is visibly greater than that of Figure 3-18 (a).

The sample heat treated at 1200°C for 3 days was put back into the furnace and heated to 1500°C for another 3 days. The cross sectional pictures are shown at Figure 3-19 below. As shown in Figure 3-19 (b), the cladding thickness increases significantly at the expense of the sapphire core. There are also 4 cracks formed in the cladding, apparently due to this further conversion of sapphire into spinel.

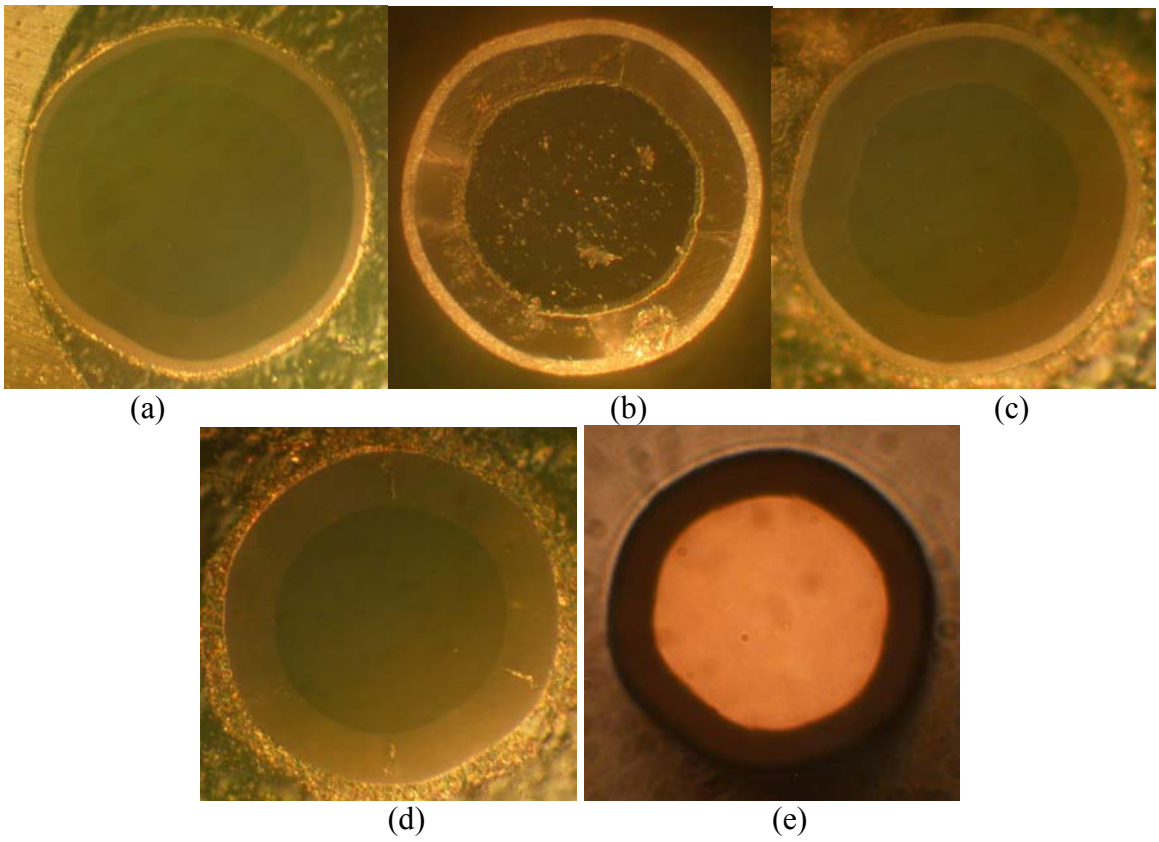

Figure 3-17: (a) The cross section of clad fiber before heat treatment, (b) the same cross section after heat treated at 1300°C for 3 days, (c) the polished cross section 1 to 2 mm below the surface shown in (b), (d) 14 mm below the surface shown in (c), and (e) the same surface as shown in (d) with light launched from the other end.

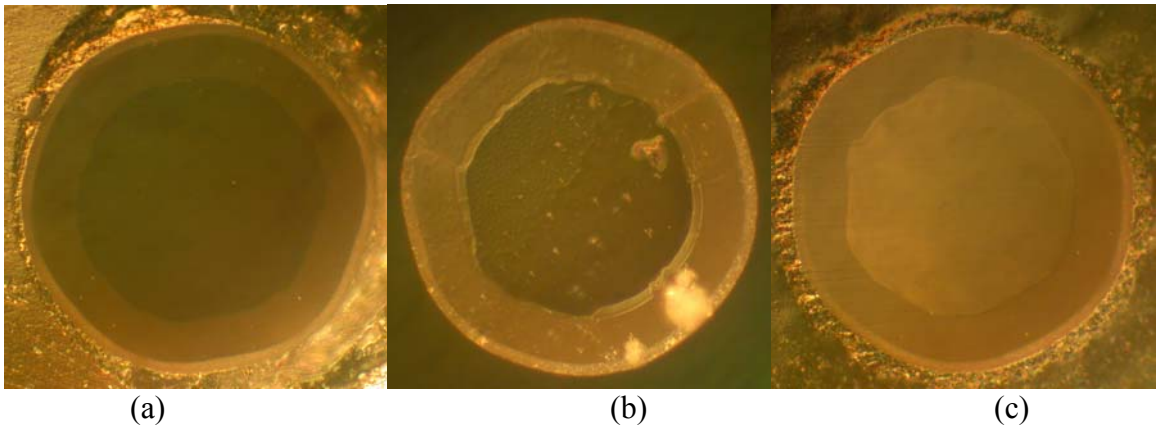

Figure 3-18: (a) The cross section of clad fiber before heat treatment, (b) the same cross section after heat treated at 1400°C for 3 days, and (c) the polished cross section 1 to 2 mm below the surface shown in (b).

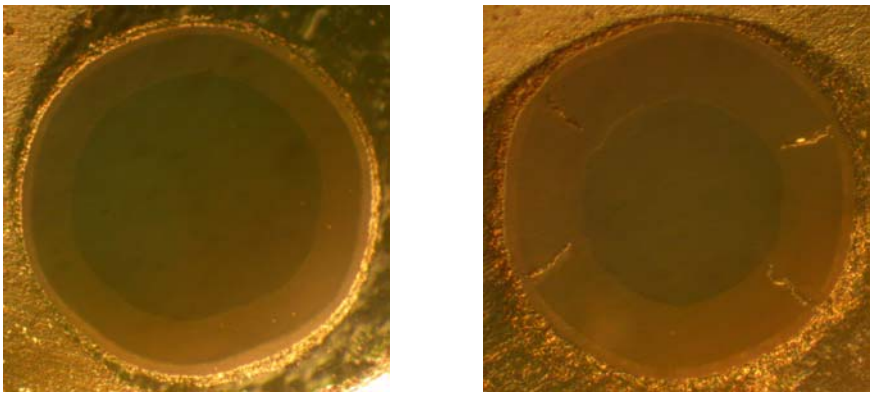

(a) (b)

Figure 3-19: (a) The cross section of clad fiber before heat treatment, (b) the polished cross section 1 to 2 mm below the surface shown in (b) after heat treated at 1500°C for 3 days.

The results of cross-sectional analysis, including core diameter, cladding thickness, ratio of cladding thickness and core diameter, overall fiber diameter, roughness, and crack parameter, for all the samples in the high temperature stability tests are listed in Table 3-19 below. Instead of comparing the cladding thickness of each cross section directly, the ratio of cladding thickness and core diameter of each individual sample is used to determine whether there is further increase in cladding thickness. The results are outlined as follows:

- The structures of spinel clad fibers show no signs of change after heating at 1000°C for 3 days.
- The same is true after heating at 1100°C for 3 days and at 1200°C for 3 days.
- After heating at 1300°C for 3 days:
  - The spinel cladding thickness and the core/cladding interface roughness show little sign of change.
  - Cracks may start to form in the cladding.
- After heating at 1400°C for 3 days:
  - The spinel cladding appears to start growing in thickness.
  - The core/cladding interface starts becoming rougher.
- After heating at 1500°C for 3 days:
  - The cladding starts to increase in thickness significantly at the expense of the sapphire core. The ratio between cladding thickness and core diameter increases 88% after firing.
  - Large cracks form.

Table 3-19: High temperature stability test results

		Core Diameter (A) (μm)	Cladding Thickness (B) (μm)	B/A (no unit)	Overall Fiber Diameter (μm)	Roughness (no unit)	Crack Parameter (μm^2)
1000°C	Original	89.9	21.7	0.241	132.3	1.03	0
	3 days	90.8	22.2	0.244 (+1.2%)	135.8	0.68	0
1100°C	Original	94.4	21.9	0.232	136.8	0.92	0
	3 days	91.4	20.2	0.221 (-4.7%)	131.9	0.57	0
1200°C	Original	93.2	20.4	0.219	134.4	0.96	0
	3 days	95.5	19.4	0.203 (-7.3%)	134.2	0.99	0
1300°C	Original	88.7	21.2	0.239	130.3	0.50	0
	3 days	90.5	22.7	0.251 (+5.0%)	135.9	0.76	0
	(14 mm below)	89.4	20.7	0.232	130.4	0.34	97.8
1300°C (1000°C)	Original	90.8	22.2	0.244	135.8	0.68	0
	3 days	88.5	22.8	0.258 (+5.7%)	134.2	0.38	0
1400°C (1100°C)	Original	91.4	20.2	0.221	131.9	0.57	0
	3 days	88.6	21.5	0.243 (+10 %)	131.0	1.54	0
1500°C (1200°C)	Original	95.5	19.4	0.203	134.2	0.99	0
	3 days	80.1	30.6	0.382 (+88 %)	140.9	0.89	128.8

3.1.2.2 Interpretation of stability test results

The results of the high-temperature stability tests warrant some concerns regarding the use of the spinel-clad fibers in the desired industrial environments at temperatures at or above 1300°C. These results suggest that they reaction that causes of sapphire to magnesium aluminate spinel has not reached an equilibrium when the final processing processing (sintering) of the cladding is concluded. Further reaction during in-service use is problematic: as the sapphire continues to dissolve, the core size will continue to shrink, and the refractive index of the cladding region will continue to change. Both of

these changes will affect the mode volume of the sapphire fiber, which may change the sensor signal, depending upon the sensor interrogation scheme used.

The lack of equilibrium suggests the existence of a thermodynamic driving force for continued reaction of the alumina (sapphire) and magnesium oxide and spinel. One strategy for minimizing this effect is to adjust the store geometry of the slurry mixture so that the resulting coating composition is chosen to correspond to the tow phase region of spinel and alumina on the spinel solid solution boundary (on the alumina-magnesia binary phase diagram). Under this condition, the driving force for the alumina to dissolve in the spinel would be reduced. Furthermore, the dwell time for the high temperature firing (sintering) should be lengthened to ensure that the cladding has fully reacted during the process. However, possible detrimental effects, such as core-cladding roughness or cracks, that may result from a modified firing profile should be investigated as well.

3.1.2.3 Suggestions for future work

The results of the experimental design and implementation have been documented above. Several areas of future work seem indicated. Understanding of the measurement process variation for each of the responses measured seems warranted based upon the observed variation. A very large amount of variation was observed in most of the responses measured. Some may be explained by the measurement process, but a significant portion is undoubtedly due to other sources. Identifying these sources of variation and eliminating them will allow more powerful conclusions from future experimentation.

Understanding of the stability of the clad fibers will be paramount to the successful operation of the sensors. The data appear to indicate that a portion of the system remains in a non-equilibrium state after the high temperature firing. This would seem to indicate that there could be further reaction if the fibers are held at elevated temperatures for long periods of time – which in general is the intended use environment of the fibers. Further study should be undertaken to improve the high-temperature stability of the cladding, possibly through the use of modified compositions.

3.2 Development of sapphire temperature sensors

During the reporting period, the design, fabrication, and testing, and testing of high-temperature sensors for the measurement of temperature using sapphire fibers was investigated. The design investigated was based on a Fabry-Perot interferometer originally developed at the Virginia Tech Center for Photonics Technology; Prime Research is negotiating a license for this design from Virginia Tech. The specific sensor configuration uses a polished sapphire wafer as the temperature-sensitive element. The wafer is attached to a sapphire fiber (clad or unclad), and interrogated as a Fabry-Perot sensor. Changes in the temperature of the wafer cause a change in the optical path length of the Fabry-Perot cavity, which can be related to the change in temperature through the known coefficient of thermal expansion. The high degree of parallelism of the two sides of the wafer (and thus the Fabry-Perot cavity) permits the achievement of reasonable fringe visibility, even with multimode fibers.

As mentioned earlier, due to their large diameters and large numerical apertures, unclad single-crystal sapphire fibers are highly multimoded. The fringe visibility of Fabry-Perot (FP) interferometers constructed using multimode fibers is generally poor. While fringe visibility can be rigorously defined, in essence it expresses the depth of intensity modulation of the interferometer output relative to the average intensity output. The fringe visibility is highly sensitive to the flatness, the smoothness, and especially the parallelism of the two surfaces forming the FP cavity. It was reported that the fringe visibility can be significantly reduced by an angle of the order of 10^{-2} degree between the two faces forming the FP cavity [1]. This strong dependence of fringe visibility in a multimode fiber on alignment angle has also been analyzed by Han, etal [2]. The very stringent requirement of end-face alignment poses a great challenge in the sensor design of FP interferometers based on multimode fibers, including sapphire fibers.

In most of the high-temperature interferometric sensors described in published literature, an air gap between two polished sapphire fiber ends, or between a polished fiber end and some kind of reflector, is constructed as the FP cavity. As mentioned in the previous paragraph, the precise parallel alignment between the two reflective surfaces is very critical in achieving fringes with acceptable visibility. On the other hand, this kind of precise alignment is most often very difficult to achieve. Therefore, a novel approach using a sapphire wafer instead of an air gap as the FP cavity was adopted. The sensor configuration is shown in Figure 3-20 below [3].

A sapphire wafer is fixed in front of an alumina tube with a very small inner diameter by a high-temperature alumina adhesive. A sapphire fiber is inserted into the tube until its polished end reaches the wafer. In this configuration, the parallelism requirement is

[1] F. Perennes, P.C. Beard, and T.N. Mills, Appl. Opt. 38, 7026 (1999).
[2] Ming Han and Anbo Wang, Applied Optics, 43, 4659 (2004).
[3] Yizheng Zhu, Zhengyu Huang, Ming Han, Fabin Shen, Gary Pickrell and Anbo Wang, Proc. of SPIE vol. 5590, p.19.

automatically satisfied by the very high degree of parallelism between the two surfaces of sapphire wafer, which can be readily achieved by the current workmanship of the wafer lapping-polishing industry. This approach to sapphire interferometer fabrication was originally demonstrated by the Center of Photonic Technology (CPT) at Virginia Tech. Negotiations to license this technology are currently underway.

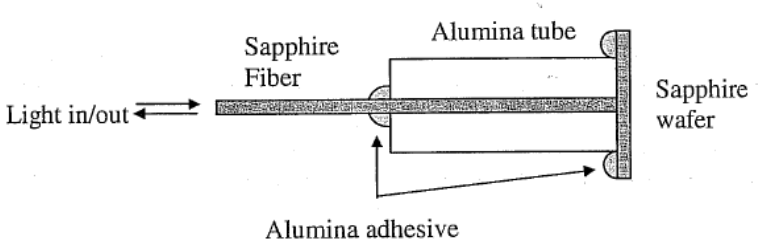

Figure 3-20: Sensor configuration using a sapphire wafer as the FP cavity [2]

3.3 Prototype sensor assembly process

The prototype high temperature sapphire sensors were fabricated using the following steps. Other options to couple the silica fiber to the sapphire fiber, such as fusion splicing, are currently under review. The current sensor head configuration and the technique used to affix the sapphire wafer to the end of the ceramic tube are also under review. The procedures described here use an unclad 75-μm sapphire fiber as the high temperature waveguide.

1. The first step was to prepare a polished silica fiber end to be coupled to the sapphire fiber. The end of a silica fiber was inserted into a ceramic ferrule and 5-minute epoxy was used to fix the fiber end inside the ferrule. Then the ferrule with the fiber inside was polished using polishing papers with abrasive sizes down to 0.5 μm. After completing this polishing step, the ferrule was fixed inside a ceramic tube using 5-mninute epoxy. The configuration of the silica fiber end after preparation is shown in Figure 3-21 below. (It is to be noted that the 5-minute epoxy at the ferrule tip shown in this Figure must be removed by polishing before coupling to the sapphire fiber).

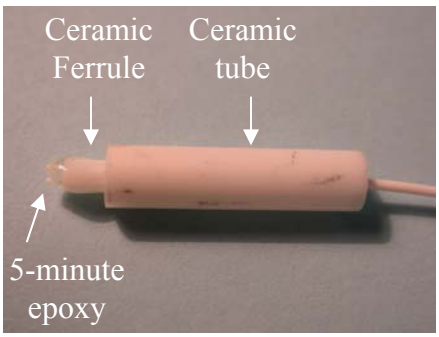

Figure 3-21: The preparation of the silica fiber for the coupling to sapphire fiber.

2. This step involves the preparation of the sapphire fiber end to be coupled to the silica fiber end. A 75-μm sapphire fiber (Micromaterials, Inc.) of about 10.8 cm long is inserted into a 2.5 cm long double-bore ceramic tube (McDaniel Advanced Ceramic, 0.13 mm bore diameter, and 0.79 mm outer tube diameter) until the end of sapphire fiber protrudes out of one end of the ceramic tube by about 1 mm. Next, 5-minute epoxy is applied at the protruded sapphire fiber at the end of ceramic tube. After the epoxy is cured, the end is polished using polishing papers with abrasive sizes down to 0.5 μm.
   The polished end of the double-bore ceramic tube prepared in Step 2 above and the silica fiber end prepared in Step 1 are coupled together using two micropositioners stages as shown in Figure 3-22 below. A power meter located at the other end of sapphire (not shown in this figure) fiber was used to monitor the power level and maximize power throughput during the coupling procedures. A very small drop of index matching gel was applied at the coupling junction . The silica fiber end could also be tilted to facilitate the coupling. At the moment the power throughput is maximized, UV-curable optical adhesive was applied surrounding the junction connecting the sapphire fiber end and the silica fiber end to fix the connection in place and it was cured using a UV lamp.

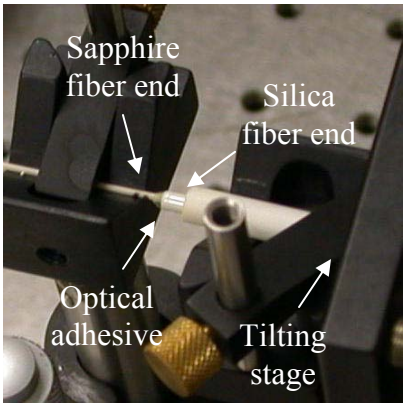

Figure 3-22: the coupling between silica and sapphire fibers.

3. At this stage of fabrication, we have a piece of 10.8 cm long sapphire fiber coupled to the silica fiber through a section of double-bore ceramic tube approximately 2.5 cm long. There is about 8.3 cm of bare sapphire fiber extending out from the 2.5 cm long double-bore ceramic tube. The sapphire fiber is then inserted into another piece of double-bore ceramic tube about 7.2 com long, as shown in Figure 3-23 below, until the polished end of the sapphire fiber is about 1 cm away from the end of the double-bore tube. Now it is ready to affix the sapphire wafer to the end of the double-bore ceramic tube.

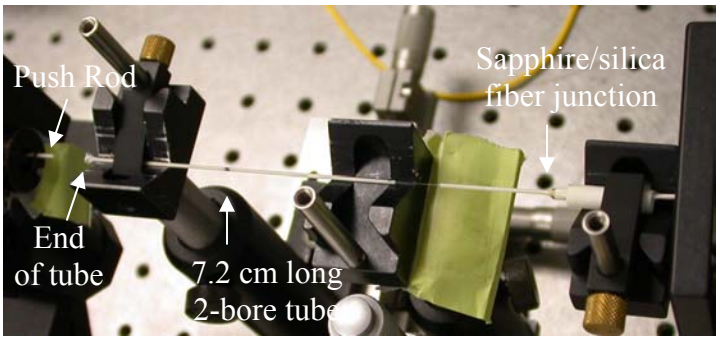

Figure 3-23: sapphire wafer assembly configuration

4. A small piece of sapphire wafer is pushed against the end of the double-bore ceramic tube using a push rod. High-temperature alumina adhesive is applied surrounding the area where the wafer and the double-bore tube are in contact. The wafer configuration after the push rod is removed is shown in Figure 3-24 below.

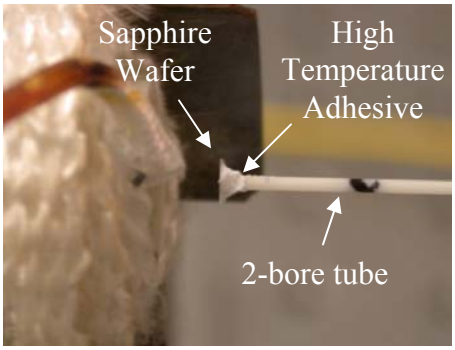

Figure 3-24: Sensor tip configuration

5. After the sapphire wafer is fixed to the end of the double-bore tube, the polished end of sapphire fiber, which is currently located about 1 cm away from the wafer, is pushed forward until it reaches the wafer. At this moment, there should be interference fringes, produced by the wafer, present on the optical spectrum analyzer.
6. Then the sapphire fiber inside the 7.2 cm long double-bore ceramic tube is fixed at the end of the ceramic tube opposite to the wafer, as shown in Figure 3-25, by a small drop of alumina adhesive. The wafer end of the double-bore ceramic rod is placed inside a coil heater. It is ready for temperature test now.

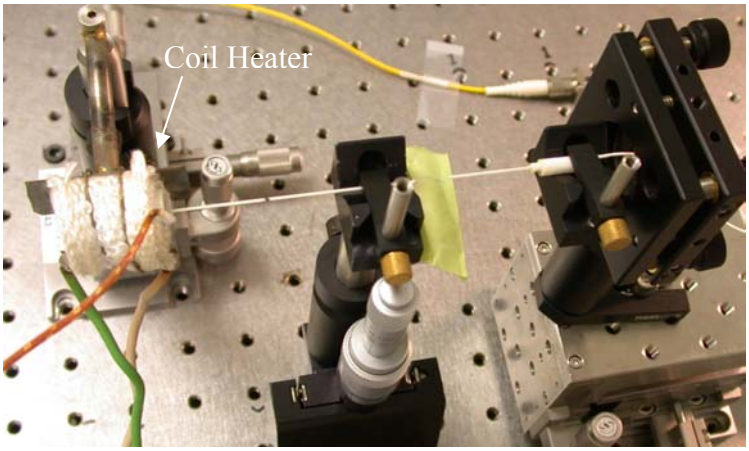

Figure 3-25: Sensor setup ready for temperature test.

3.4 Test and evaluation of temperature sensor

The experimental setup for the testing is shown in Figure 3-26 below. The broadband light at 1550nm from a Denselight superluminescent light emitting diode (SLED) with a single-mode fiber pigtail is fed into a single-mode 3dB 2x2 coupler. One of the two arms of the coupler opposite to the light source end is immersed in index matching gel to minimize back reflection. The other arm of the coupler is connected to a multimode patch cord before connecting to the sensor. The interference fringes are monitored using an Anritsu optical spectrum analyzer (OSA). This OSA is designed to be used specifically with a single mode fiber as the input. It was observed that with a multimode fiber input the power level was greatly reduced.

According to the original design, the ideal testing system should be an *all multimode* system consisting of a light source with multimode fiber output, a 2 by 2 coupler made of multimode fibers, a spectrometer or monitoring system compatible with multimode fiber input, and a multimode fiber patch cord. The construction of this all-multimode testing system is currently underway. The major advantage of using an all multimode system is the removal of modal noises originating from the implementation of both singlemode and multimode fibers in the experimental setup.

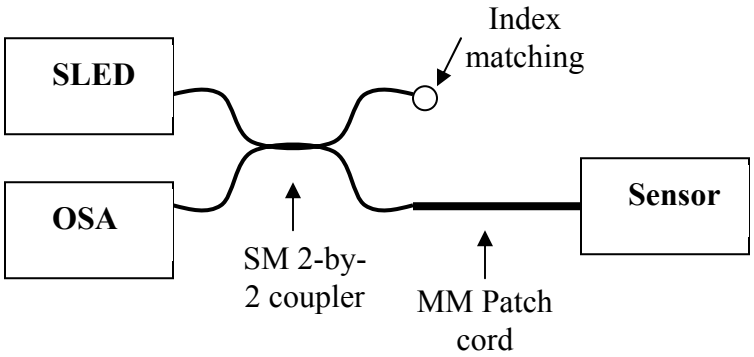

Figure 3-26: Experimental setup for evaluating temperature sensors

3.4.1 Room temperature testing using a clad sapphire fiber as the waveguide

This section describes the evaluation of a Fabry-Perot interferometric sensor using a clad sapphire fiber as the waveguide with a 0.005 inch thick (nominal thickness) sapphire wafer as the Fabry-Perot cavity at room temperature. The wafer had a measured thickness of 132 μm, and has a random crystallographic orientation (Meller Optics, Providence, RI). The clad fiber was fabricated using the procedures recommended by the Taguchi experimentation described in Section 3.1.1.7. A five inch long clad fiber was packaged in a ceramic tube with stainless steel ferrules at both ends. Both ends of the fiber package were polished using polishing papers with abrasive sizes down to 0.5 μm.

The optical bench setup for the testing is shown in Figure 3-27 (a) below. The clad fiber in the package was coupled to the silica fiber using positioning stages while a hand-held power meter (not shown in the figure) was used to maximize the power throughput at the other end of the clad sapphire fiber package. No index matching gel was applied at the coupling junction in this case. The power meter was then replaced with a push rod in order to affix the wafer to the end of clad fiber package as shown in Figure 3-27 (b). The interference patterns after the wafer was attached are shown in Figure 3-28 (a) and (b) below. The background with clad sapphire fiber in place but without the sapphire wafer is shown as the spectrum "A" in Figure 3-28 (a). It was observed that the shape of the background spectrum "A" could be easily altered by just moving the multimode fiber patch cord (see Figure 3-27 (a)) connected to the clad fiber. As the testing set-up consisted of both singlemode and multimode fibers, this change in output spectrum upon movement of the multimode fiber was attributed to modal noise, since the background spectrum "A" was sensitive to the shape of the multimode fiber patch cord. Therefore, steps were taken to ensure that the multimode fiber patch cord was not disturbed at any times during the experiments, in order to achieve a stable and constant background. The spectrum after the attachment of the sapphire wafer is shown as spectrum "B" in Figure 3-28 (a). The net spectrum obtained by subtracting spectrum "A" from spectrum "B" in Figure 3-28 (a) is shown in Figure 3-28 (b). The wafer thickness, *d*, can be calculated using the relation

$$nd = \frac{\lambda_1 \times \lambda_2}{2(\lambda_1 - \lambda_2)},$$

where *n* is the index of refraction of sapphire, which is 1.76, and λ_1 and λ_2 are two consecutive peak wavelengths as indicated by the two arrows shown in Figure 3-28 (b). This expression, the product *nd* is the optical path length attributed to the sapphire wafer thickness. The physical thickness of the wafer *d* calculated using the above equation and the two peaks in Figure 3-28 (b), i.e., 1521.8 nm and 1526.8 nm, is 132.0 μm, exactly the same as that of the measured wafer thickness.

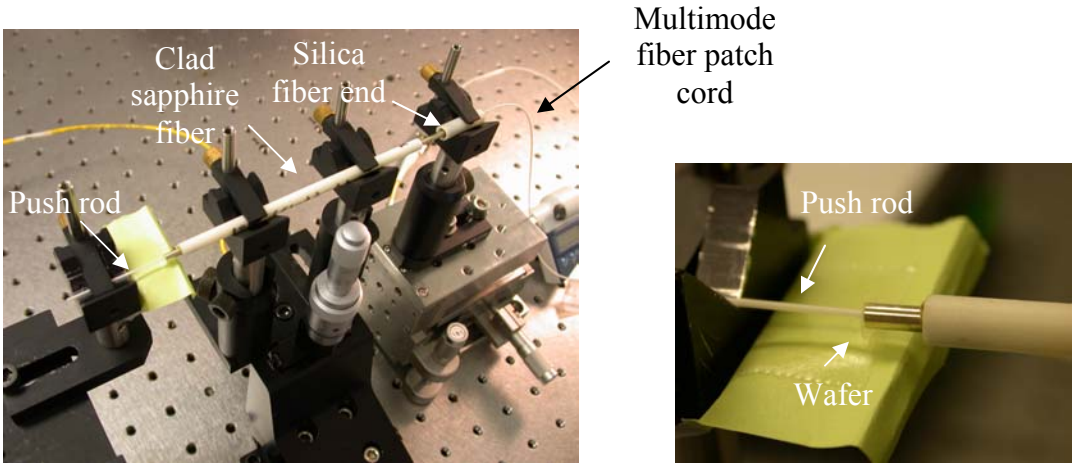

Figure 3-27: (a) Optical bench setup for the testing a clad sapphire fiber, and (b) the close up at the sapphire wafer (the wafer is sandwiched between the push rod and a stainless steel ferrule in this photo).

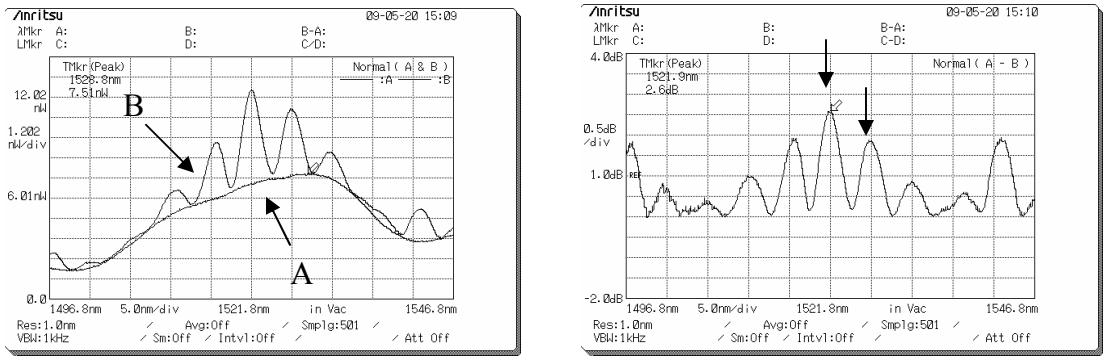

Figure 3-28: (a) The background before the attachment of the wafer (spectrum A), and the spectrum after the affix of wafer (spectrum B), (b) Spectrum B minus spectrum A. The sample is a clad sapphire fiber of 5-inch long.

3.4.2 Room temperature testing using an unclad sapphire fiber as the waveguide

In this test, the clad sapphire fiber was replaced with an unclad sapphire fiber of 75 μm diameter and 6 inch long. All other experimental details of the set-up were identical to those described in the previous section unless otherwise stated. In this case, the sapphire fiber was inserted into a 6-inch long double-bore ceramic tube (McDaniel Advanced Ceramic, 0.13 mm bore diameter, and 0.79 mm outer tube diameter), and the sapphire fiber extended out of both ends of the tube for about 1 mm. A small quantity of 5-minute epoxy was applied to either end of the ceramic tube to fix the sapphire fiber. After the epoxy is cured, both ends of the tube were polished using polishing papers with abrasive sizes down to 0.5 μm.

The sapphire-fiber/silica-fiber coupling and the sapphire wafer affix procedures were the same as those described in the previous section, with the exception here that an index mating adhesive was applied at the sapphire-fiber/silica-fiber junction. The interference patterns are shown in Figure 3-29 (a) and (b) below. Spectrum "A" in Figure 3-29 (a) represents the background before the attachment of sapphire wafer. It is apparent from this figure that the background here shows more signs of interference fringes than the background with a clad sapphire fiber as the waveguide as shown in the spectrum "A" in Figure 3-28 (a).

We believe that these interference effects present in the background spectrum are caused by modal noise, which in turn results from the combined use of multimode and single-mode fibers. The different electromagnetic modes propagating in a multimode fiber may interfere, if requirements for coherence are satisfied. However, if the active area of the photodetector used to monitor the multimode fiber output is large enough that all of the electromagnetic modes (and consequently there interference effects) are sampled simultaneously, then the interference effects are averaged out, and are not visible. However, if the photodetector active area is much smaller than the core diameter of the multimode fiber, or if a singlemode fiber is used to sample the multimode fiber output, then only the interference between a limited set of modes may be sampled, and the interference will not be averaged out. The smaller the photodetector (or core area of the sampling fiber), the stronger the observed interference effects will be. In the experimental set-up illustrated in Figure 3-26, the connection between the multimode fiber and the single-mode fiber of the 2x2 coupler is likely to be the source of the observed modal noise.

The net spectrum obtained by subtracting spectrum "A" from spectrum "B" in Figure 3-29 (a) is shown in Figure 3-29 (b). As can be seen in this Figure, the spacing between adjacent peaks varies a lot. For example, the spacing between peak 1 and 2 in Figure 3-29 (b) is only about 3.0 nm, while the spacing between peak 3 and 4 is about 6.7 nm. After taking into account the peak spacing of more adjacent peaks, the *average* peak spacing here is quite close to that in the case of clad fiber (see Figure 3-28 (b)), which is 5 nm. It is believed that this variation in spacing is caused by the modulation of the

desired Fabry-Perot cavity fringes by the undesired modal noise. The interference patterns (see Figure 3-28 (b)) obtained using a clad fiber as the waveguide seem to have more even peak spacing than the patterns obtained using an unclad sapphire fiber. This seems to indicate that the use of clad fiber, with its reduced modal volume, reduces the vulnerability to modal noise even in a system mixed with both SM and MM fibers.

For multimode interferometers, modal noise may be minimized by eliminating the use of single-mode fibers in the system, ensuring that connections or splices between fibers are well aligned, and ensuring that the active areas of photodetectors or the entrance pupils of spectrometers are larger than the multimode fiber core area. Therefore, for further testing, the experimental set-up of Figure 3-26 was modified by replacing the single-mode 2x2 coupler with a multimode 2x2 fiber, constructed using fiber with a 62.5 μm core diameter. In addition, a multimode fiber with a 62.5 μm core was used as the patch cord. However, modal noise was still observed in the background. Some investigation revealed that the Anritsu optical spectrum analyzer (OSA) used in the experiment was designed for use with single-mode fiber only, and had an entrance pupil small enough to pass only a limited set of mode from the multimode fiber, generating the observed modal noise. A spectrometer designed for use with multimode fibers has been ordered, and will be used for future interrogation of sapphire interferometric sensors.

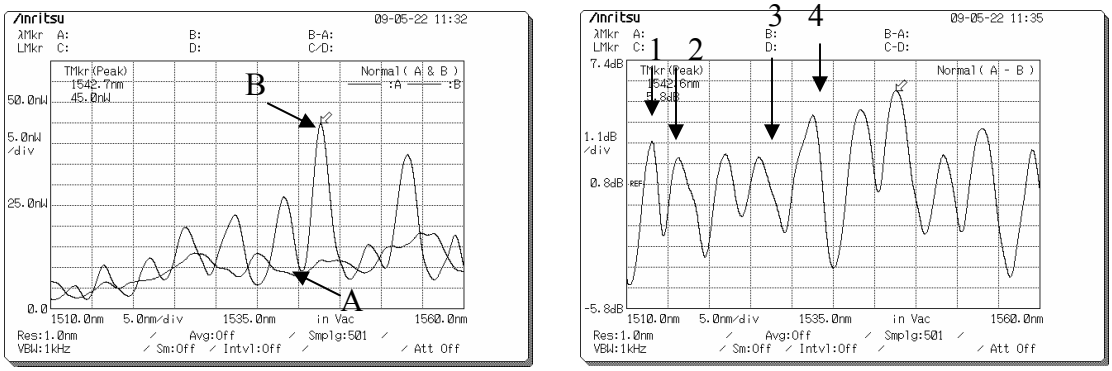

(a) (b)

Figure 3-29: (a) The background spectrum before the affix of wafer (spectrum "A"), and the spectrum after the affix of wafer (spectrum "B"), (b) Spectrum "B" minus spectrum "A". The sample is a clad sapphire fiber of 5-inch long.

3.4.3 Preliminary test results of prototype sensor at elevated temperatures

A prototype sensor was constructed following the procedures described in Section 3.3 using an unclad 75-μm sapphire fiber as the high temperature waveguide. The sensor configuration and experimental setup are exactly the same as those illustrated in Figure 3-24 and Figure 3-25, respectively, in Section 3.3. The sapphire wafer used here has a measured thickness of 136 μm with a c-axis orientation (Meller Optics, Providence, RI).

The interference patterns at room temperature are shown in Figure 3-30 below. The output was similar to the patterns discussed in the previous section, as the spacing between the adjacent peaks was not even. For example, the spacing between peak 1 and peak 2 in Figure 3-30 was 4.4 nm, and those between peak 2 and peak 3 and peak 3 and peak 4 were 4.9 nm and 5.7 nm, respectively. The average spacing is 5.0 nm. The variation in peak spacing was likely due to the modulation of the Fabry-Perot fringes by the modal noise resulting from the use of the Anritsu spectrometer optimized for use with single-mode fibers.

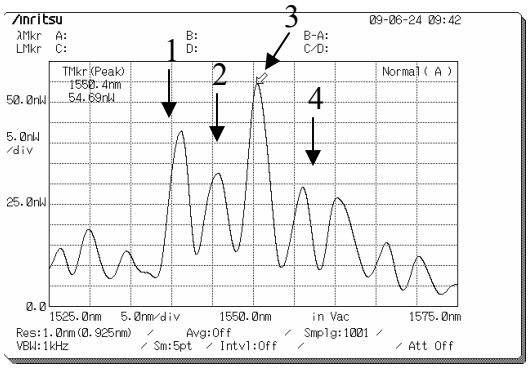

Figure 3-30: The fringe patterns of a sensor made of 75-µm sapphire fiber as the waveguide and a 136-µm thick sapphire wafer at room temperature.

The sensor was heated to 100°C and was kept at this temperature for 20 minutes; the resulting interference patterns are shown in Figure 3-31. During the heating process, it was observed that the relative intensity of each peak varies quite significantly. That is, some peaks may increase in intensity and other peaks decrease intensity. The degree of variation of peak intensity decreased when the temperature was stable at 100°C.

As shown in Figure 3-31, the relative intensity among peak 1 to 4 changed relative to that shown in Figure 3-30. Furthermore, the peak spacing between two adjacent peaks also changed. Here the spacing between peak 1 and peak 2 is 5.0 nm, and those between peak 2 and peak 3 and peak 3 and peak 4 are 4.6 nm and 5.4 nm, respectively. As a result of the temperature increase, the spacing between peak 1 and peak 2 *increases* 0.6 nm, while the spacing between peak 2 and peak 3 *decreases* 0.3 nm and the peak distance between peak 3 and peak 4 also *decreases* 0.3 nm. The average peak spacing is still 5.0 nm, the same as the case at room temperature. In an ideal system where no modal noise exists, the spacing between each pair of adjacent peaks should either *all increase* or *all decrease* in response to temperature change. The current testing system with modal noise creates difficulty in using the peak spacing to interpret the spectrum response.

On the other hand, another possible method to interpret the response is by the amount of peak shift as a result of temperature change. Here all four peaks shift to the right when the temperature is increased to 100°C. By comparing the peak locations in Figure 3-30 and Figure 3-31, peak 1 shifts to the right for 0.6 nm, peak 2 for 1.2 nm, peak 3 for 0.9 nm, and peak 4 for 0.6 nm. Therefore, the amount of shift towards longer wavelength varies from 0.6 nm to 0.9 nm among the 4 peaks. This is also most likely caused by the

modulation of peak locations by modal noise. This also makes it difficult to interpretate the interference pattern by tracking the amount of peak shift.

The influence of the modal noise can be greatly minimized, if not completely eliminated, through the use of multimode fibers exclusively in the sensor system, in addition to the use of a spectrometer designed for use with multimode fibers. Towards this end, a spectrometer optimized for use of multimode fiber has been obtained, and further evaluation of the sapphire temperature sensor is continuing. An all multimode fiber system is current under fabrication to address the modal noise problem.

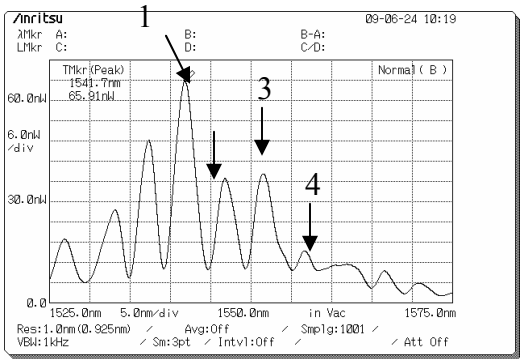

Figure 3-31: The fringe patterns of a sensor made of 75-µm sapphire fiber as the waveguide and a 136-µm thick sapphire wafer at 100°C.

A. Appendix A

In this Appendix, the original cross-sectional pictures and the average responses of the rest of the 17 samples are listed from Figure A-2 to Figure A-18 follow (the cross-sectional pictures for Sample 1 are presented in Section 3.1.1.5).

A-2: Sample 2

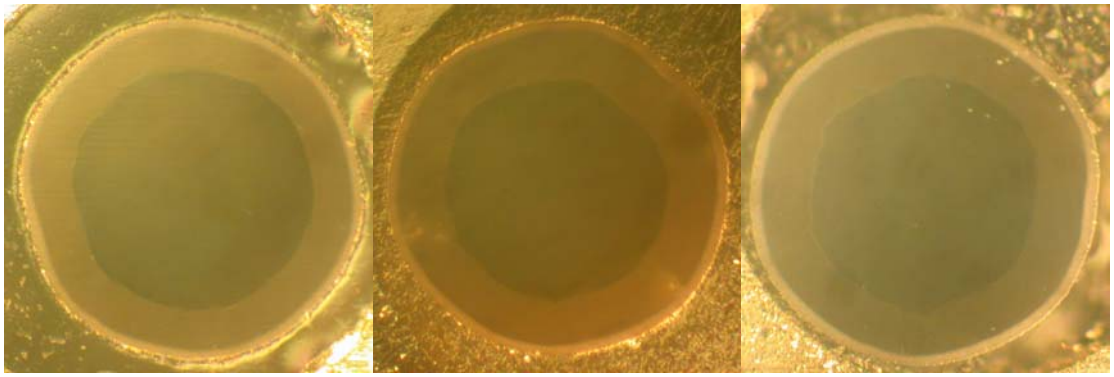

(a) cross-1 (top) (b) cross-3 (middle) (c) cross-2 (bottom)

Figure A-2 (a) to (c): the 3 cross sections polished and analyzed for sample 2, and (d): the results of all 13 responses for sample 2.

	G1 (um)	G2 (um)	G3 (um)	G4 (um)	G5 (um)	G6 (um)	M1 (mm)	M2 (um^2)	M3 (um)	M4 (no unit)	O1 (no unit)	O2 (no unit)	O3 (dB)
2	89.9	22.1	3.9	1.6	134.3	0.81	0.71	0.0	0.0	0.00	0.40	0.046	8.4

Table A-2: The results of all 13 responses for sample 2

A-3: Sample 3

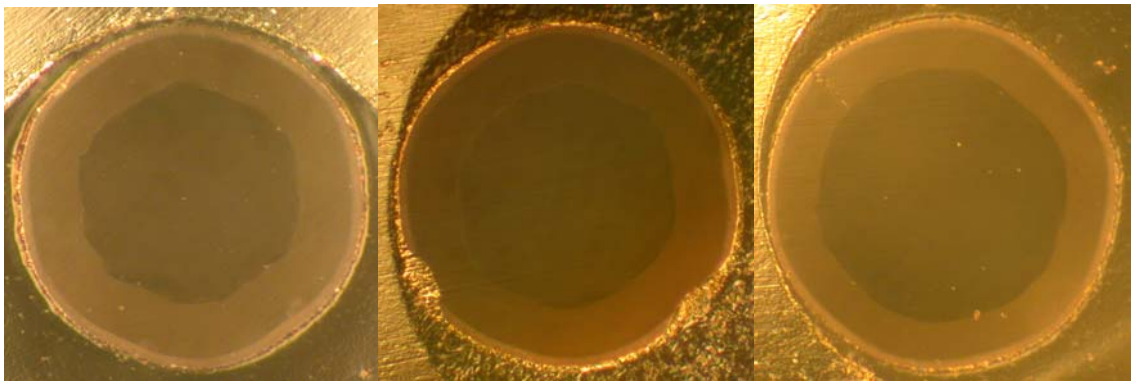

(a) cross-1 (top) (b) cross-3 (middle) (c) cross-2 (bottom)

Figure A-3 (a) to (c): the 3 cross sections polished and analyzed for sample 3, and (d): the results of all 13 responses for sample 3.

	G1 (um)	G2 (um)	G3 (um)	G4 (um)	G5 (um)	G6 (um)	M1 (mm)	M2 (um^2)	M3 (um)	M4 (no unit)	O1 (no unit)	O2 (no unit)	O3 (dB)
3	86.8	21.4	3.4	2.1	131.1	0.67	0.84	3.9	6.0	0.33	0.56	0.055	7.2

Table A-3: The results of all 13 responses for sample 3

A-4: Sample 4

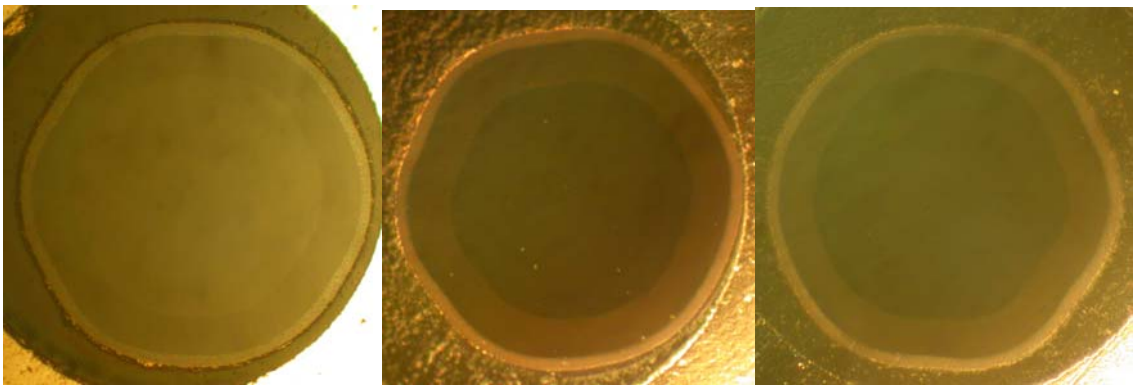

(a) cross-1 (top) (b) cross-3 (middle) (c) cross-2 (bottom)

Figure A-4 (a) to (c): the 3 cross sections polished and analyzed for sample 4, and (d): the results of all 13 responses for sample 4.

	G1 (um)	G2 (um)	G3 (um)	G4 (um)	G5 (um)	G6 (um)	M1 (mm)	M2 (um^2)	M3 (um)	M4 (no unit)	O1 (no unit)	O2 (no unit)	O3 (dB)
4	94.4	20.1	4.6	1.5	134.4	1.22	0.88	0.0	0.0	0.00	0.24	0.068	3.1

Table A-4: The results of all 13 responses for sample 4

A-5: Sample 5

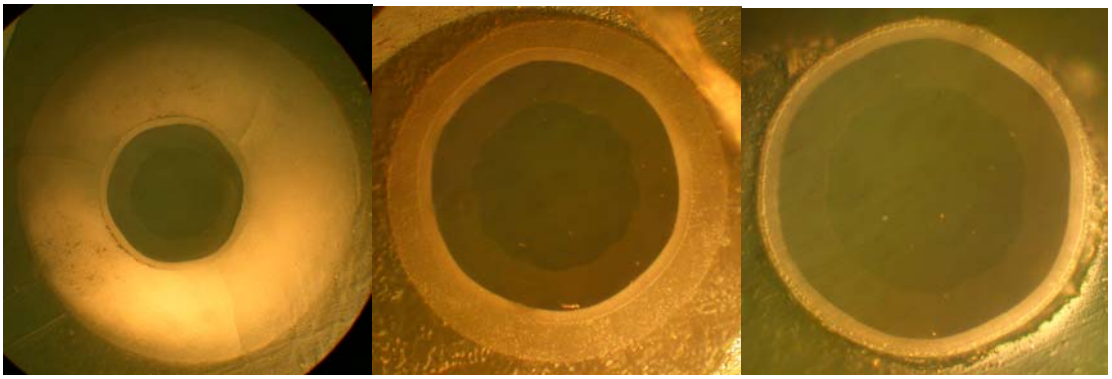

(a) cross-1 (top) (b) cross-3 (middle) (c) cross-2 (bottom)

Figure A-5 (a) to (c): the 3 cross sections polished and analyzed for sample 5_{R1}

	G1 (um)	G2 (um)	G3 (um)	G4 (um)	G5 (um)	G6 (um)	M1 (mm)	M2 (um^2)	M3 (um)	M4 (no unit)	O1 (no unit)	O2 (no unit)	O3 (dB)
5 (R1)	79.4	24.7	5.8	33.0	194.1	0.76	0.73	0.0	0.0	0.00	0.59	0.059	4.5

Table A-5: The results of all 13 responses for sample 5_{R1} (R1 indicates that the results are from a repeated sample prepared using the same conditions)

It is to be noted that sample 5_{R1} is the first sample showing a significant "carrot" shape. The skin thickness, G4, of the cross section at the top of the fiber shown in Figure A-5 (a) is 82.5µm. The thickness decreases to 13.9µm at the middle of fiber, as shown in Figure A-5 (b), and to 2.5µm at the bottom of fiber as shown in Figure A-5 (c). The reported valued of G4 in Figure A-5 (d), 33.0µm, is the average of these 3 values.

A-6: Sample 6

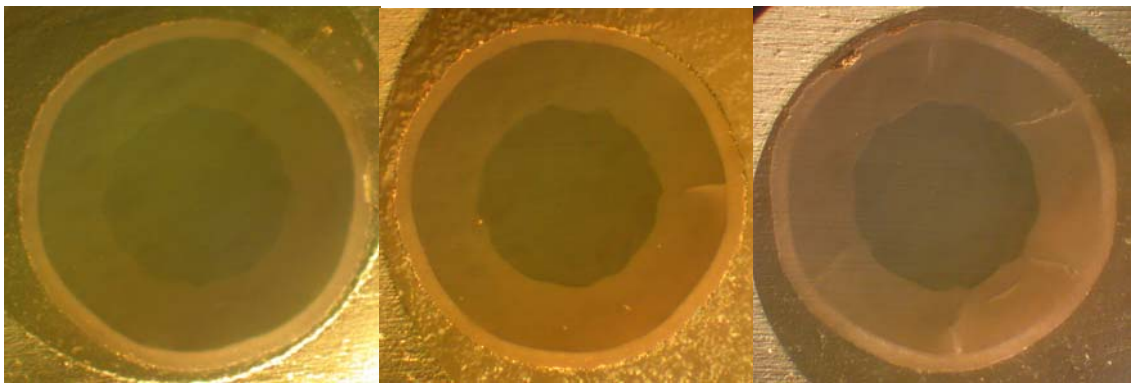

(a) cross-1 (top) (b) cross-3 (middle) (c) cross-2 (bottom)

Figure A-6 (a) to (c): the 3 cross sections polished and analyzed for sample 6_{R1}

	G1 (um)	G2 (um)	G3 (um)	G4 (um)	G5 (um)	G6 (um)	M1 (mm)	M2 (um^2)	M3 (um)	M4	O1	O2	O3 (dB)
6 (R1)	71.7	32.9	6.2	1.3	138.4	0.90	0.41	28.4	24.1	2.00	1.30	0.052	5.1

Table A-6: The results of all 13 responses for sample 6_{R1} (R1 indicates that the results are from a repeated sample prepared using the same conditions)

A-7: Sample 7

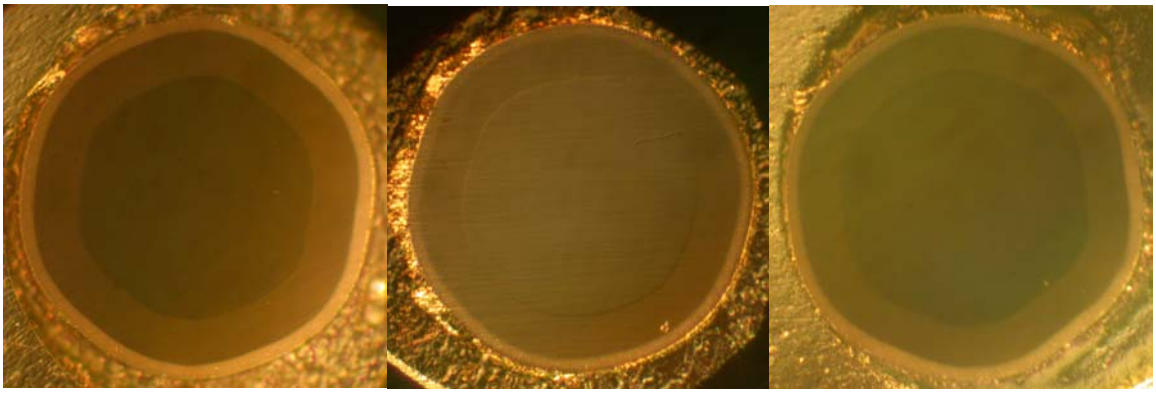

(a) cross-1 (top) (b) cross-3 (middle) (c) cross-2 (bottom)

Figure A-7 (a) to (c): the 3 cross sections polished and analyzed for sample 7

	G1 (um)	G2 (um)	G3 (um)	G4 (um)	G5 (um)	G6 (um)	M1 (mm)	M2 (um^2)	M3 (um)	M4	O1	O2	O3 (dB)
7	92.8	21.6	4.9	2.5	138.9	0.82	0.83	0.0	0.0	0.00	0.02	0.063	4.9

Table A-7: The results of all 13 responses for sample 7

A-8: Sample 8

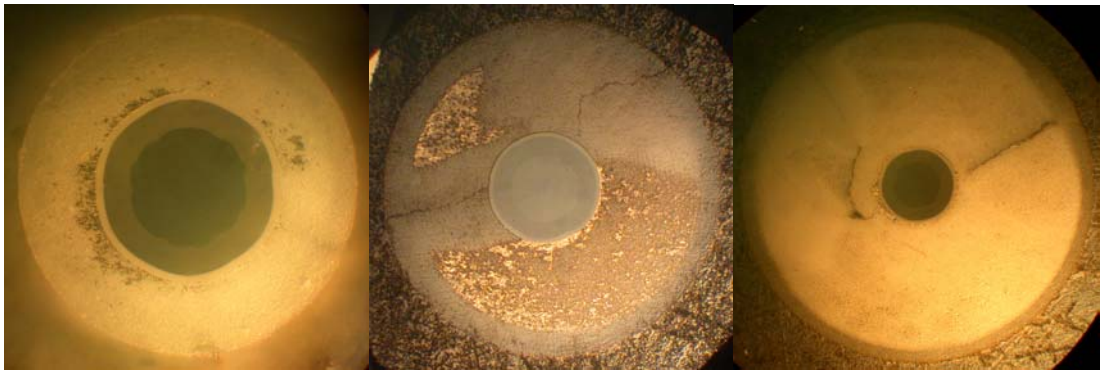

(a) cross-1 (top) (b) cross-3 (middle) (c) cross-2 (bottom)

Figure A-8 (a) to (c): the 3 cross sections polished and analyzed for sample 8_{R1}

	G1 (um)	G2 (um)	G3 (um)	G4 (um)	G5 (um)	G6 (um)	M1 (mm)	M2 (um^2)	M3 (um)	M4	O1	O2	O3 (dB)
8 (R1)	84.7	27.4	5.8	150.3	442.1	1.18	0.78	0.0	0.0	0.00	1.13	0.096	24

Table A-8: The results of all 13 responses for sample 8_{R1}

A-9: Sample A-9

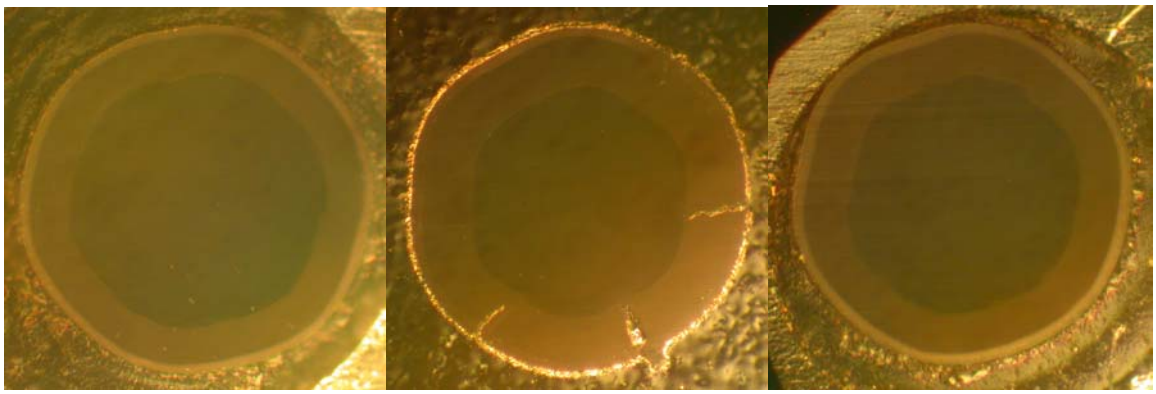

(a) cross-1 (top) (b) cross-3 (middle) (c) cross-2 (bottom)

Figure A-9 (a) to (c): the 3 cross sections polished and analyzed for sample 9_{R1}

	G1 (um)	G2 (um)	G3 (um)	G4 (um)	G5 (um)	G6 (um)	M1 (mm)	M2 (um^2)	M3 (um)	M4	O1	O2	O3 (dB)
9 (R1)	93.5	21.1	4.0	1.5	137.1	0.92	0.46	50.5	8.5	1.00	0.59	0.087	5.2

Table A-9: The results of all 13 responses for sample 9_{R1}

A-10: Sample 10

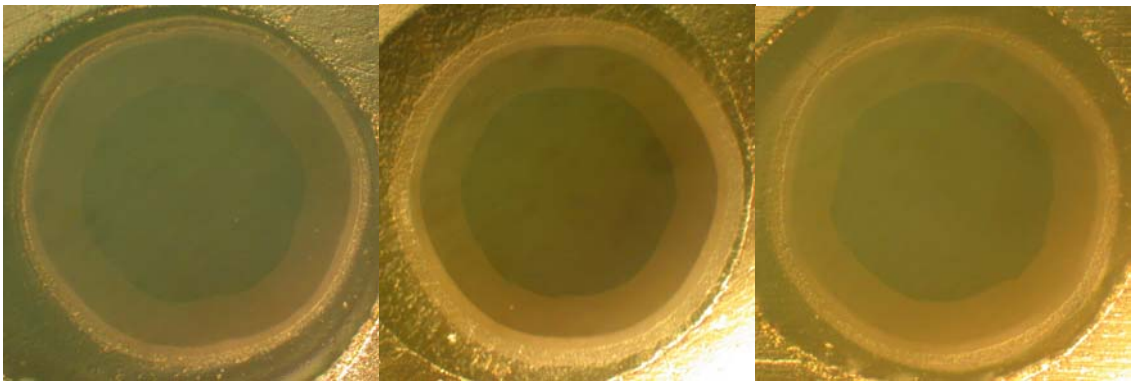

(a) cross-1 (top) (b) cross-3 (middle) (c) cross-2 (bottom)

Figure A-10 (a) to (c): the 3 cross sections polished and analyzed for sample 10

	G1 (um)	G2 (um)	G3 (um)	G4 (um)	G5 (um)	G6 (um)	M1 (mm)	M2 (um^2)	M3 (um)	M4	O1	O2	O3 (dB)
10	90.4	22.5	4.4	5.5	140.2	0.60	0.67	0.0	0.0	0.00	0.41	0.052	2.5

Table 10: The results of all 13 responses for sample 10

A-11: Sample 11

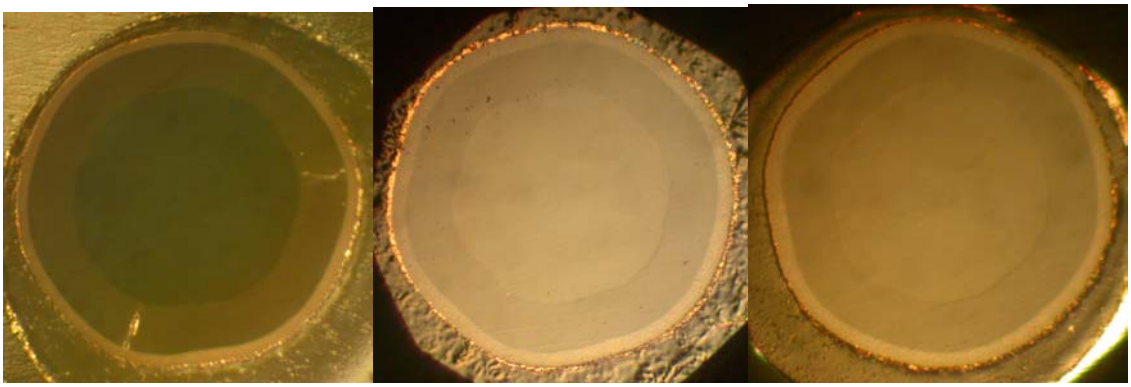

(a) cross-1 (top) (b) cross-3 (middle) (c) cross-2 (bottom)

Figure A-11 (a) to (c): the 3 cross sections polished and analyzed for sample 11 $_{R1}$

	G1 (um)	G2 (um)	G3 (um)	G4 (um)	G5 (um)	G6 (um)	M1 (mm)	M2 (um^2)	M3 (um)	M4	O1	O2	O3 (dB)
11 (R1)	89.3	25.2	5.5	2.1	141.1	0.50	0.59	17.6	6.7	0.67	0.44	0.061	7.2

Table A-11. The results of all 13 responses for sample 11 $_{R1}$

A-12: Sample 12

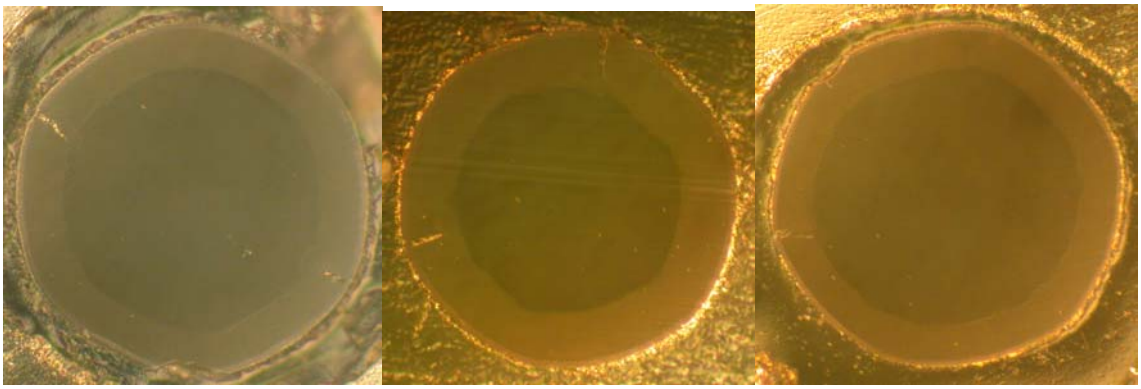

(a) cross-1 (top) (b) cross-3 (middle) (c) cross-2 (bottom)

Figure A-12 (a) to (c): the 3 cross sections polished and analyzed for sample 12

	G1 (um)	G2 (um)	G3 (um)	G4 (um)	G5 (um)	G6 (um)	M1 (mm)	M2 (um^2)	M3 (um)	M4	O1	O2	O3 (dB)
12	97.6	19.2	2.6	2.4	135.7	0.61	0.73	35.6	18.9	1.67	0.70	0.089	10.5

Table A-12: The results of all 13 responses for sample 12

A-13: Sample 13

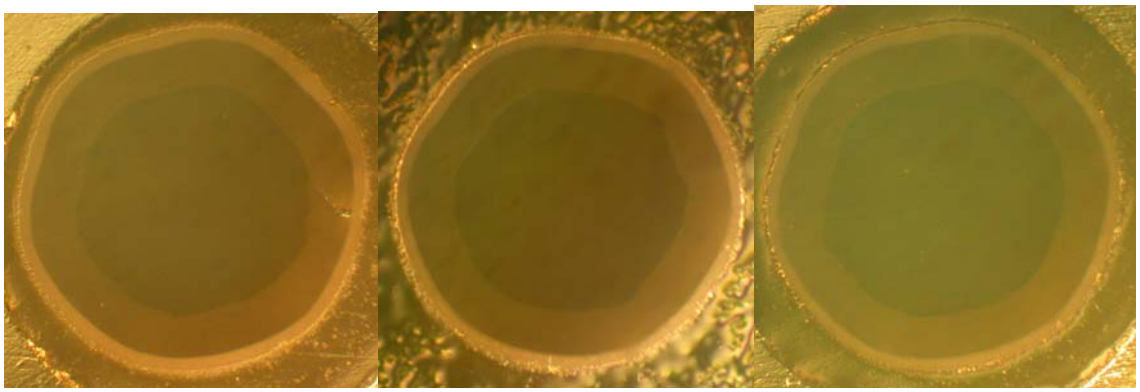

(a) cross-1 (top) (b) cross-3 (middle) (c) cross-2 (bottom)

Figure A-13 (a) to (c): the 3 cross sections polished and analyzed for sample 13

	G1 (um)	G2 (um)	G3 (um)	G4 (um)	G5 (um)	G6 (um)	M1 (mm)	M2 (um^2)	M3 (um)	M4	O1	O2	O3 (dB)
13	92.4	22.6	4.9	2.6	137.8	0.93	1.08	9.3	7.1	0.33	0.65	0.152	5.3

Table A-13: The results of all 13 responses for sample 13

A-14: Sample 14

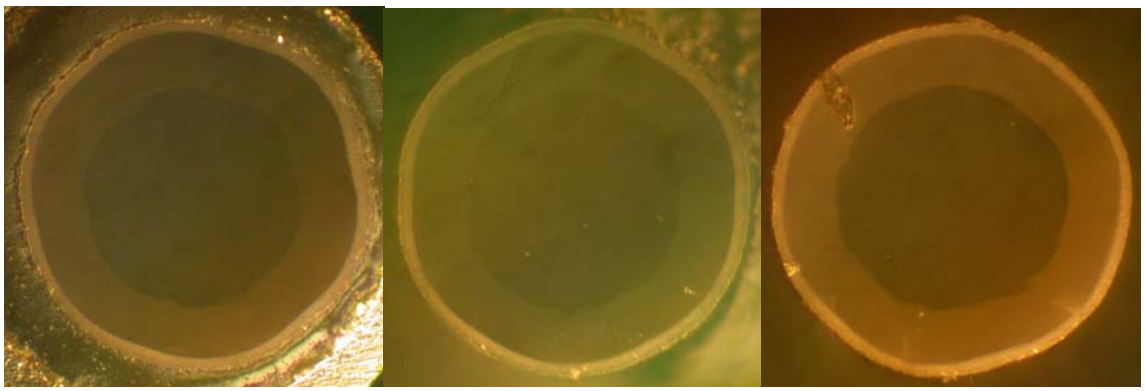

(a) cross-1 (top) (b) cross-3 (middle) (c) cross-2 (bottom)

Figure A-14 (a) to (c): the 3 cross sections polished and analyzed for sample 14

	G1 (um)	G2 (um)	G3 (um)	G4 (um)	G5 (um)	G6 (um)	M1 (mm)	M2 (um^2)	M3 (um)	M4	O1	O2	O3 (dB)
14	87.2	25.8	4.6	1.4	138.6	0.72	0.65	108.3	25.9	1.33	0.73	0.107	12

Table A-14: The results of all 13 responses for sample 14

A-15: Sample 15

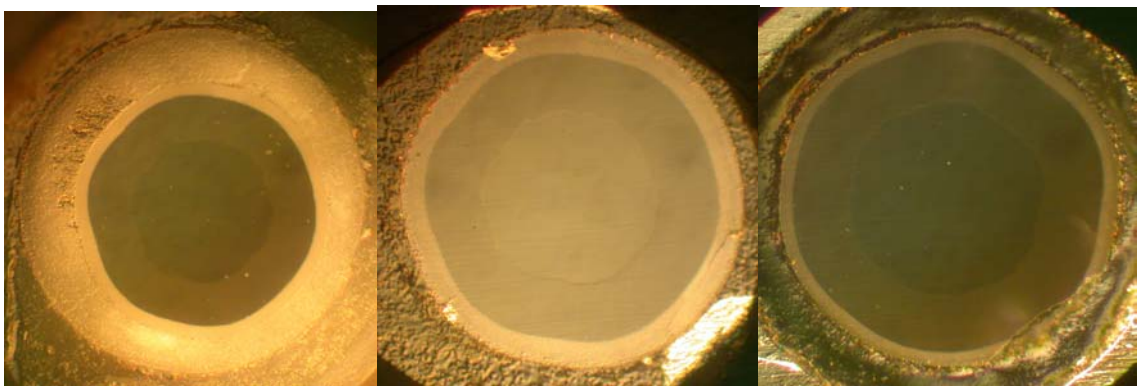

(a) cross-1 (top) (b) cross-3 (middle) (c) cross-2 (bottom)

Figure A-15 (a) to (c): the 3 cross sections polished and analyzed for sample 15_{R1}

	G1 (um)	G2 (um)	G3 (um)	G4 (um)	G5 (um)	G6 (um)	M1 (mm)	M2 (um^2)	M3 (um)	M4	O1	O2	O3 (dB)
15 (R1)	80.4	33.4	8.3	10.5	165.5	0.93	0.54	0.0	0.0	0.00	0.99	0.052	3.9

Table A-15: The results of all 13 responses for sample 15_{R1}

A-16: Sample 16

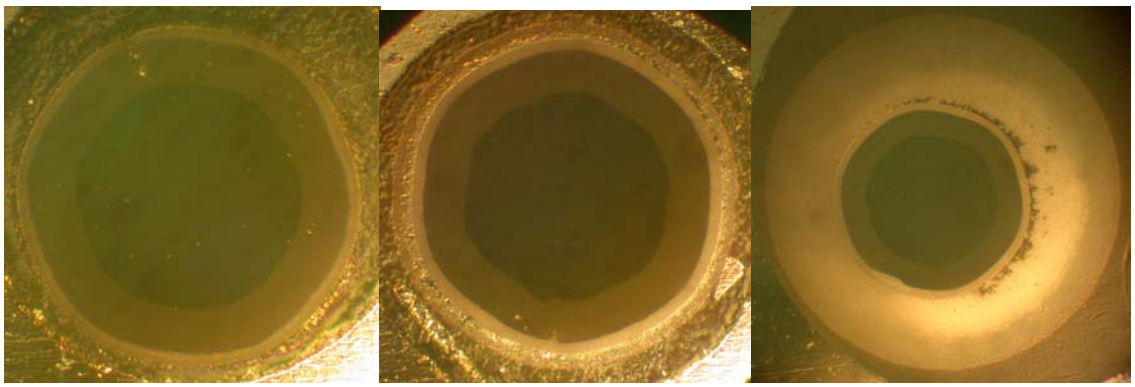

(a) cross-1 (top) (b) cross-3 (middle) (c) cross-2 (bottom)

Figure A-16 (a) to (c): the 3 cross sections polished and analyzed for sample 16

	G1 (um)	G2 (um)	G3 (um)	G4 (um)	G5 (um)	G6 (um)	M1 (mm)	M2 (um^2)	M3 (um)	M4	O1	O2	O3 (dB)
16	86.6	22.1	4.6	21.3	172.8	0.66	0.93	18.1	7.2	0.67	0.36	0.065	1.4

Table A-16: The results of all 13 responses for sample 16

A-17: Sample 17

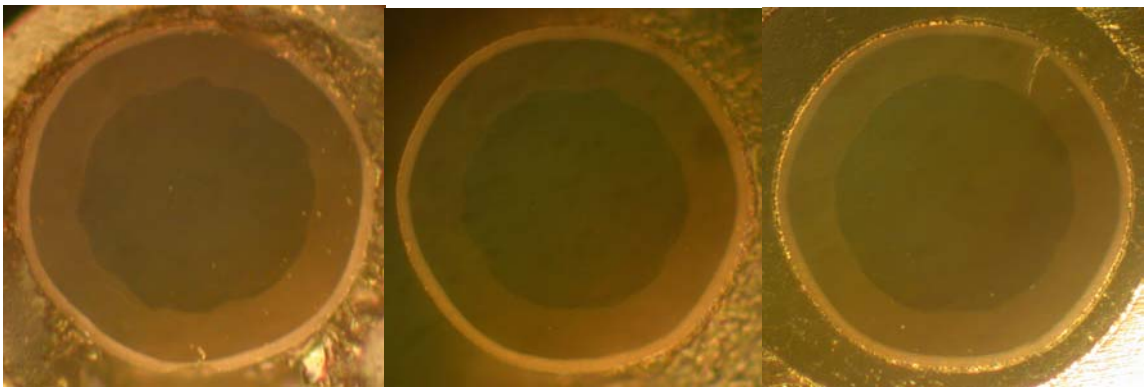

(a) cross-1 (top) (b) cross-3 (middle) (c) cross-2 (bottom)

Figure A-17 (a) to (c): the 3 cross sections polished and analyzed for sample 17

	G1 (um)	G2 (um)	G3 (um)	G4 (um)	G5 (um)	G6 (um)	M1 (mm)	M2 (um^2)	M3 (um)	M4	O1	O2	O3 (dB)
17	88.5	23.0	4.5	1.5	134.2	0.77	0.81	12.7	7.3	0.33	1.06	0.107	11.3

Table A-17: The results of all 13 responses for sample 17

A-18: Sample 18

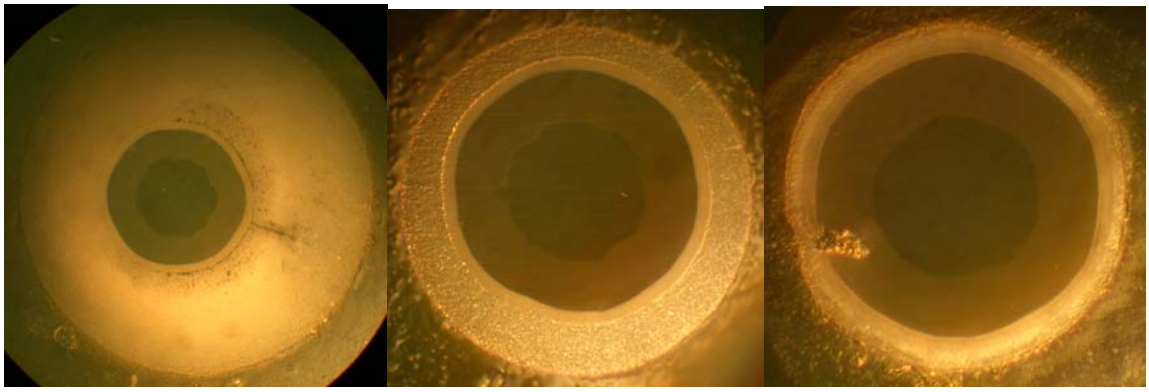

(a) cross-1 (top) (b) cross-3 (middle) (c) cross-2 (bottom)

Figure A-18 (a) to (c): the 3 cross sections polished and analyzed for sample 18_{R1}

	G1 (um)	G2 (um)	G3 (um)	G4 (um)	G5 (um)	G6 (um)	M1 (mm)	M2 (um^2)	M3 (um)	M4	O1	O2	O3 (dB)
18 (R1)	67.5	31.1	6.3	37.8	206.1	0.59	0.64	0.0	0.0	0.00	1.88	0.044	5.3

Table A-18: The results of all 13 responses for sample 18_{R1}

All the response data obtained for all 18 samples are listed in Table 3-7 in the main body of the report. These data are fed into the Taguchi software for analysis.

A. Appendix B

In this Appendix, the results of the Taguchi analysis of eleven of the twelve responses are follow. The results of the analysis of response G1, Core Diameter, are presented in Section 3.1.1.6.1.

G2 - Overall Cladding Thickness

The following is the analysis of the sapphire fiber overall cladding thickness data generated in the 18 samples that were measured. The quality characteristic used was "smaller is better". Table G2-1 shows the factors and levels and the averages of level 3 minus level 1.

Table G2-1

Column # / Factors	Level 1	Level 2	Level 3	L3 - L1
1 Nano MgO amount	23.633	24.988		n/a
2 Dipping Speed	21.966	26.583	24.383	2.416
3 Firing Profile	21.716	24.7	26.516	4.799
4 MgO/Spinel ratio	24.033	23.55	25.35	1.317
5 First Stage Ball	26.333	24.05	22.549	-3.784
6 Fish oil amount	24.416	23.783	24.733	.317
7 PVP type (K)	22.383	25.916	24.633	2.25
8 PVP amount	26.75	24.333	21.85	-4.9

Table G2-2 shows the ANOVA table for the analysis of the factor influences. It appears that almost all the factors are significant at the 99% level.

Table G2-2

Col # / Factor	DOF (f)	Sum of Sqrs. (S)	Variance (V)	F - Ratio (F)	Pure Sum (S')	Percent P(%)
1 Nano MgO amount	1	8.27	8.27	11.825	7.571	2.431
2 Dipping Speed	2	63.987	31.993	45.744	62.588	20.103
3 Firing Profile	2	70.482	35.241	50.387	69.083	22.189
4 MgO/Spinel ratio	2	10.414	5.207	7.445	9.016	2.895
5 First Stage Ball	2	43.554	21.777	31.136	42.155	13.54
6 Fish oil amount	2	2.807	1.403	2.006	1.408	.452
7 PVP type (K)	2	38.387	19.193	27.442	36.988	11.88
8 PVP amount	2	72.034	36.017	51.497	70.635	22.687
Other/Error	2	1.397	.698			3.823

Table G2-3 shows the results of the ANOVA analysis. As seen in this table, the confidence levels of all the factors except for three are greater than 99 %.

Table G2-3

Col # / Factor	DOF (f)	Sum of Sqrs. (S)	Variance (V)	F - Ratio (F)	Pure Sum (S')	Percent P(%)
1 Nano MgO amount	(1)	(8.27)		POOLED	(CL=98.98%)	
2 Dipping Speed	2	63.987	31.993	45.744	62.588	20.103
3 Firing Profile	2	70.482	35.241	50.387	69.083	22.189
4 MgO/Spinel ratio	(2)	(10.414)		POOLED	(CL=88.43%)	
5 First Stage Ball	2	43.554	21.777	31.136	42.155	13.54
6 Fish oil amount	(2)	(2.807)		POOLED	(CL=75.51%)	
7 PVP type (K)	2	38.387	19.193	27.442	36.988	11.88
8 PVP amount	2	72.034	36.017	51.497	70.635	22.687
Other/Error	7	22.888	3.27			9.601
Total:	17	311.337				100.00%

Figure G2 shows the plots of the effects of each of the factors on the measured response.

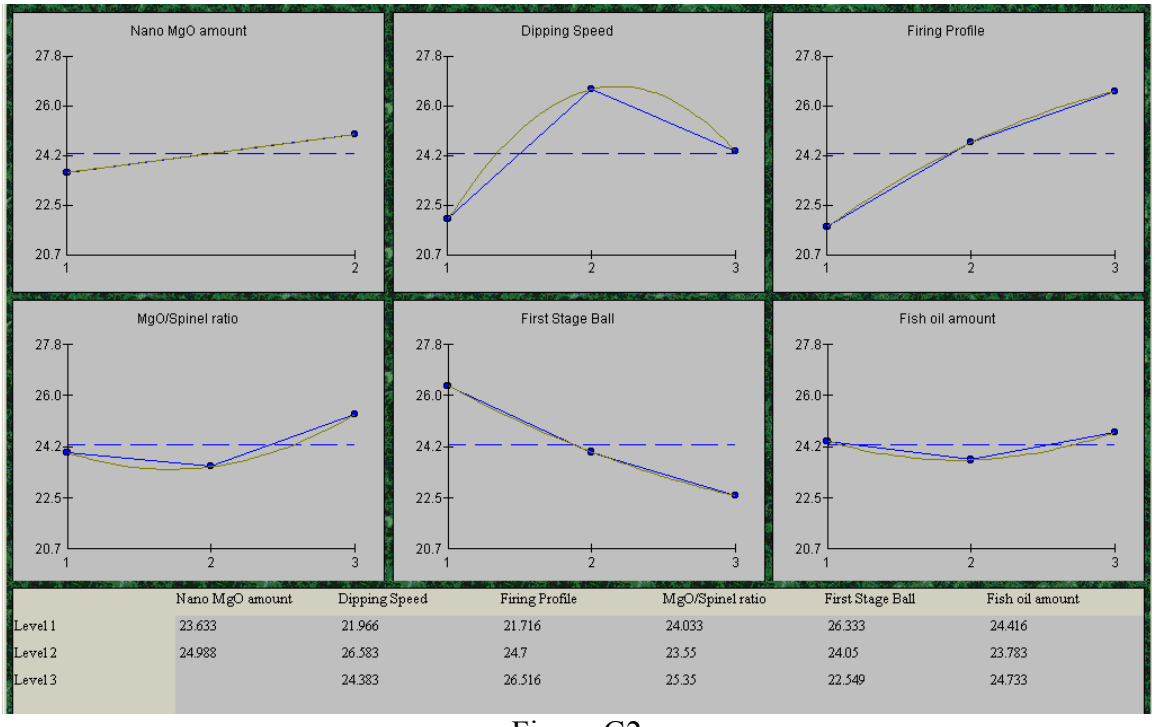

Figure G2

Table G2-4 shows the expected optimal performance for the factors determined as significant (with a confidence level greater than 99%).

Table G2-4

Column # / Factor	Level Description	Level	Contribution
2 Dipping Speed	.09	1	-2.345
3 Firing Profile	1550	1	-2.595
5 First Stage Ball	12	3	-1.762
7 PVP type (K)	10	1	-1.928
8 PVP amount	0.6	3	-2.462

Total Contribution From All Factors...	-11.093
Current Grand Average Of Performance...	24.311
Expected Result At Optimum Condition...	13.219

If we assumed that all the factors were significant the optimal levels would be as those listed in Table G2-5 below.

Table G2-5

Column # / Factor	Level Description	Level	Contribution
1 Nano MgO amount	10	1	-.678
2 Dipping Speed	.09	1	-2.345
3 Firing Profile	1550	1	-2.595
4 MgO/Spinel ratio	9:1	2	-.762
5 First Stage Ball	12	3	-1.762
6 Fish oil amount	50	2	-.528
7 PVP type (K)	10	1	-1.928
8 PVP amount	0.6	3	-2.462

This gives the optimal levels as predicted by the data, but as stated before most of the factors are significant at the 99% level.

G3 - Outer Cladding Thickness

The following is the analysis of the sapphire fiber outer cladding thickness data generated in the 18 samples that were measured. The quality characteristic used was “smaller is better”. Table G3-1 shows the factors and levels and the averages of level 3 minus level 1.

Table G3-1

Column # / Factors	Level 1	Level 2	Level 3	L3 - L1
1 Nano MgO amount	4.856	4.822		n/a
2 Dipping Speed	4.151	5.349	5.016	.865
3 Firing Profile	4.366	5.016	5.134	.768
4 MgO/Spinel ratio	5.333	4.35	4.835	-.499
5 First Stage Ball	5.433	4.966	4.118	-1.315
6 Fish oil amount	4.466	4.633	5.418	.951
7 PVP type (K)	4.45	5.366	4.701	.25
8 PVP amount	5.95	4.466	4.101	-1.85

Table G3-2 shows the ANOVA table for the analysis of the factor influences. It appears that almost all the factors are significant at the 90% level.

Table G3-2

Col # / Factor	DOF (f)	Sum of Sqrs. (S)	Variance (V)	F - Ratio (F)	Pure Sum (S')	Percent P(%)
1 Nano MgO amount	1	.005	.005	.038	0	0
2 Dipping Speed	2	4.59	2.295	16.436	4.311	13.284
3 Firing Profile	2	2.053	1.026	7.353	1.774	5.467
4 MgO/Spinel ratio	2	2.901	1.45	10.387	2.621	8.078
5 First Stage Ball	2	5.333	2.666	19.095	5.054	15.572
6 Fish oil amount	2	3.099	1.549	11.096	2.82	8.689
7 PVP type (K)	2	2.691	1.345	9.637	2.412	7.433
8 PVP amount	2	11.499	5.749	41.174	11.22	34.573
Other/Error	2	.279	.139			6.904
Total:	17	32.454				100.00%

Table G3-3 shows the results of the ANOVA analysis. As seen in this table, the confidence levels of all the factors except the first three are greater than 99 %.

Table G3-3

Col # / Factor	DOF (f)	Sum of Sqrs. (S)	Variance (V)	F - Ratio (F)	Pure Sum (S')	Percent P(%)
1 Nano MgO amount	(1)	(.005)		POOLED	(CL= *NC*)	
2 Dipping Speed	(2)	(4.59)		POOLED	(CL=97.58%	
3 Firing Profile	(2)	(2.053)		POOLED	(CL=96.86%	
4 MgO/Spinel ratio	2	2.901	1.45	10.387	2.621	8.078
5 First Stage Ball	2	5.333	2.666	19.095	5.054	15.572
6 Fish oil amount	2	3.099	1.549	11.096	2.82	8.689
7 PVP type (K)	2	2.691	1.345	9.637	2.412	7.433
8 PVP amount	2	11.499	5.749	41.174	11.22	34.573
Other/Error	7	6.927	.989			25.655
Total:	17	32.454				100.00%

Figure G3 shows the plots of the effects of each of the factors on the measured response.

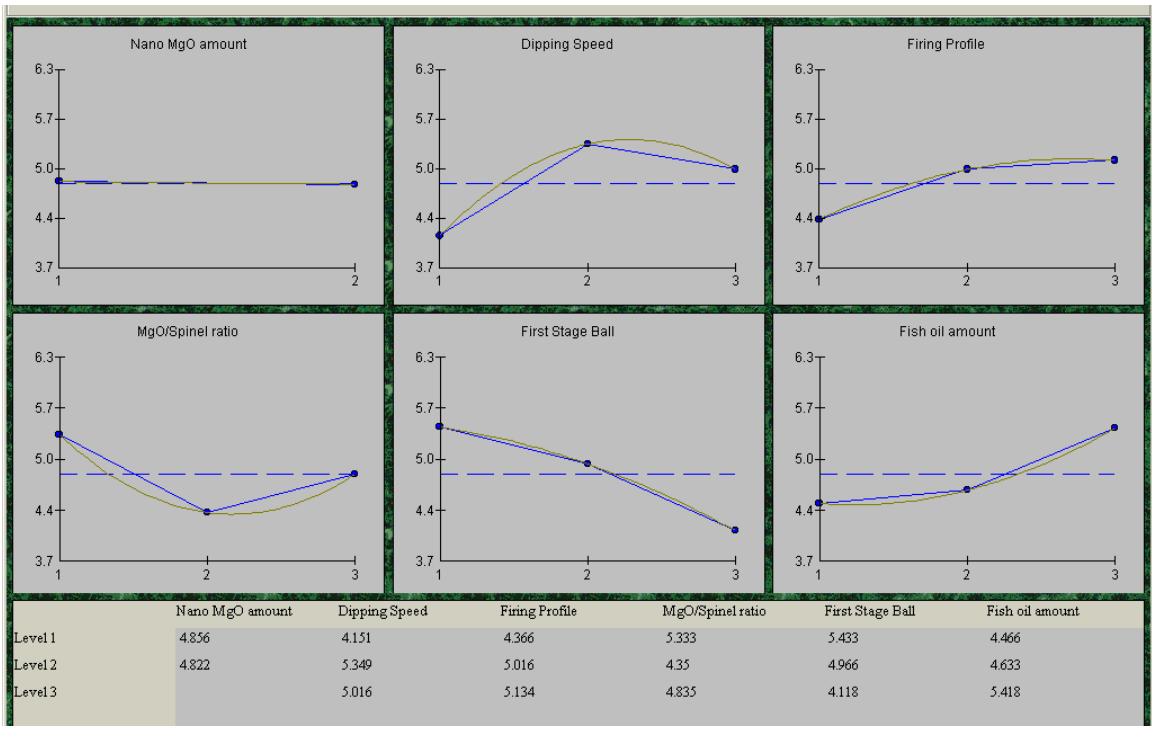

	Nano MgO amount	Dipping Speed	Firing Profile	MgO/Spinel ratio	First Stage Ball	Fish oil amount
Level 1	4.856	4.151	4.366	5.333	5.433	4.466
Level 2	4.822	5.349	5.016	4.35	4.966	4.633
Level 3		5.016	5.134	4.835	4.118	5.418

Figure G3

Table G3-4 shows the expected optimal performance for the factors determined as significant (with a confidence level greater than 99%).

Table G3-4

Column # / Factor	Level Description	Level	Contribution
4 MgO/Spinel ratio	9:1	2	-.49
5 First Stage Ball	12	3	-.722
6 Fish oil amount	25	1	-.373
7 PVP type (K)	10	1	-.39
8 PVP amount	0.6	3	-.738

Total Contribution From All Factors...	-2.714
Current Grand Average Of Performance...	4.839
Expected Result At Optimum Condition...	2.126

If we assumed that all the factors were significant the optimal levels would be those listed in Table G3-5.

Table G3-5

Column # / Factor	Level Description	Level	Contribution
1 Nano MgO amount	20	2	-.018
2 Dipping Speed	.09	1	-.688
3 Firing Profile	1550	1	-.473
4 MgO/Spinel ratio	9:1	2	-.49
5 First Stage Ball	12	3	-.722
6 Fish oil amount	25	1	-.373
7 PVP type (K)	10	1	-.39
8 PVP amount	0.6	3	-.738

This gives the optimal levels as predicted by the data, but as stated before most of the factors are significant at the 99% level.

G4 - Skin Thickness

The following is the analysis of the skin thickness data generated in the 18 samples that were measured. The quality characteristic used was “smaller is better”. Table G4-1 shows the factors and levels and the averages of level 3 minus level 1.

Table G4-1

Column # / Factors	Level 1	Level 2	Level 3	L3 - L1
1 Nano MgO amount	21.742	9.455		n/a
2 Dipping Speed	2.6	8.383	35.813	33.213
3 Firing Profile	5.883	31.649	9.263	3.379
4 MgO/Spinel ratio	3.163	13.316	30.316	27.152
5 First Stage Ball	7.833	31.266	7.696	-.138
6 Fish oil amount	26.666	8.213	11.916	-14.75
7 PVP type (K)	10.246	3.816	32.733	22.486
8 PVP amount	39.833	5.063	1.899	-37.934

Table G4-2 shows the ANOVA table for the analysis of the factor influences. It appears that two of the factors are significant at the 90% level.

Table G4-2

Col # / Factor	DOF (f)	Sum of Sqrs. (S)	Variance (V)	F - Ratio (F)	Pure Sum (S')	Percent P(%)
1 Nano MgO amount	1	679.329	679.329	1.575	248.246	1.161
2 Dipping Speed	2	3777.955	1888.977	4.381	2915.788	13.646
3 Firing Profile	2	2353.016	1176.508	2.729	1490.849	6.977
4 MgO/Spinel ratio	2	2258.786	1129.393	2.619	1396.619	6.536
5 First Stage Ball	2	2209.369	1104.684	2.562	1347.203	6.305
6 Fish oil amount	2	1143.605	571.802	1.326	281.438	1.317
7 PVP type (K)	2	2766.338	1383.169	3.208	1904.172	8.912
8 PVP amount	2	5315.795	2657.897	6.165	4453.629	20.844
Other/Error	2	862.166	431.083			34.302
Total:	17	21366.365				100.00%

Table G4-3 shows the results of the ANOVA analysis. As seen in this table, the confidence levels of all the factors except for two are less than 90%.

Table G4-3

Col # / Factor	DOF (f)	Sum of Sqrs. (S)	Variance (V)	F - Ratio (F)	Pure Sum (S')	Percent P(%)
1 Nano MgO amount	(1)	(679.329)		POOLED	(CL=71.15%)	
2 Dipping Speed	(2)	(3777.955)		POOLED	(CL=87.42%)	
3 Firing Profile	(2)	(2353.016)		POOLED	(CL=84.56%)	
4 MgO/Spinel ratio	(2)	(2258.786)		POOLED	(CL=86.19%)	
5 First Stage Ball	(2)	(2209.369)		POOLED	(CL=87.16%)	
6 Fish oil amount	(2)	(1143.605)		POOLED	(CL=69.92%)	
7 PVP type (K)	2	2766.338	1383.169	3.208	1904.172	8.912
8 PVP amount	2	5315.795	2657.897	6.165	4453.629	20.844
Other/Error	13	13284.226	1021.863			70.244
Total:	17	21366.365				100.00%

Figure G4 shows the plots of the effects of each of the factors on the measured response.

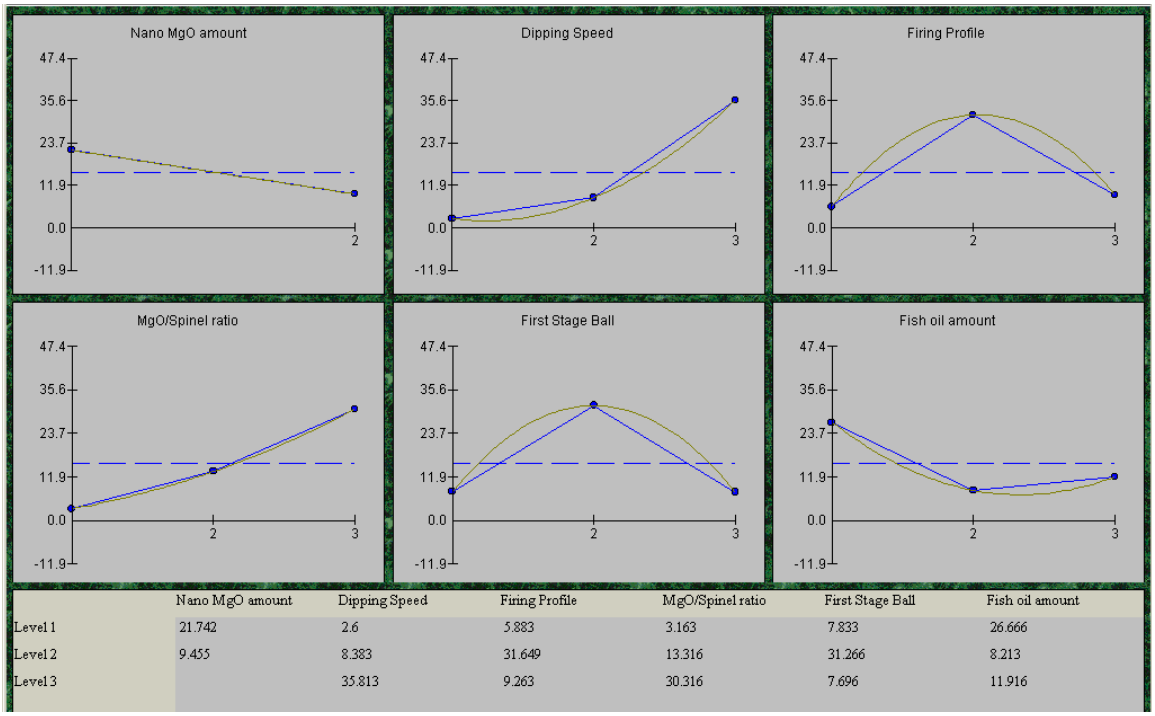

	Nano MgO amount	Dipping Speed	Firing Profile	MgO/Spinel ratio	First Stage Ball	Fish oil amount
Level 1	21.742	2.6	5.883	3.163	7.833	26.666
Level 2	9.455	8.383	31.649	13.316	31.266	8.213
Level 3		35.813	9.263	30.316	7.696	11.916

Figure G4

Table G4-4 shows the expected optimal performance for the factors determined as significant (with a confidence level greater than 90%).

Table G4-4

Column # / Factor	Level Description	Level	Contribution
7 PVP type (K)	90% 10K	2	-11.783
8 PVP amount	0.6	3	-13.699

Total Contribution From All Factors...	-25.482
Current Grand Average Of Performance...	15.598
Expected Result At Optimum Condition...	-9.884

If we assumed that all the factors were significant the optimal levels would be as those listed in Table G4-5.

Table G4-5

Column # / Factor	Level Description	Level	Contribution
1 Nano MgO amount	20	2	-6.144
2 Dipping Speed	.09	1	-12.999
3 Firing Profile	1550	1	-9.716
4 MgO/Spinel ratio	6:1	1	-12.436
5 First Stage Ball	12	3	-7.903
6 Fish oil amount	50	2	-7.386
7 PVP type (K)	90% 10K	2	-11.783
8 PVP amount	0.6	3	-13.699

This gives the optimal levels as predicted by the data, but as stated before all but two of the factors are not significant at the 90% level.

G5 - Overall fiber diameter

The following is the analysis of the sapphire fiber overall fiber diameter data generated in the 18 samples that were measured. The quality characteristic used was “smaller is better”. Table G5-1 shows the factors and levels and the averages of level 3 minus level 1.

Table G5-1

Column # / Factors	Level 1	Level 2	Level 3	L3 - L1
1 Nano MgO amount	176.411	152.444		n/a
2 Dipping Speed	136.616	151.466	205.199	68.582
3 Firing Profile	143.566	197.399	152.316	8.75
4 MgO/Spinel ratio	141.6	157.816	193.866	52.266
5 First Stage Ball	150.066	197.466	145.75	-4.317
6 Fish oil amount	187.583	148.449	157.25	-30.333
7 PVP type (K)	152.6	141.916	198.766	46.165
8 PVP amount	214.216	143.583	135.483	-78.734

Table G5-2 shows the ANOVA table for the analysis of the factor influences. It appears that almost all the factors are not significant at the 90% level.

Table G5-2

Col # / Factor	DOF (f)	Sum of Sqrs. (S)	Variance (V)	F - Ratio (F)	Pure Sum (S')	Percent P(%)
1 Nano MgO amount	1	2584.763	2584.763	1.134	305.889	.34
2 Dipping Speed	2	15622.936	7811.468	3.427	11065.187	12.326
3 Firing Profile	2	10014.131	5007.065	2.197	5456.382	6.078
4 MgO/Spinel ratio	2	8588.814	4294.407	1.884	4031.065	4.49
5 First Stage Ball	2	9880.022	4940.011	2.167	5322.274	5.928
6 Fish oil amount	2	5057.911	2528.955	1.109	500.163	.557
7 PVP type (K)	2	10954.835	5477.417	2.403	6397.087	7.126
8 PVP amount	2	22507.176	11253.588	4.938	17949.428	19.995
Other/Error	2	4557.748	2278.874			43.16
Total:	17	89768.34				100.00%

Table G5-3 shows the results of the ANOVA analysis. As seen in this table, the confidence levels of all the factors except PVP amount are less than 90 %.

Table G5-3

Col # / Factor	DOF (f)	Sum of Sqrs. (S)	Variance (V)	F - Ratio (F)	Pure Sum (S')	Percent P(%)
1 Nano MgO amount	(1)	(2584.763)		P O O L E D	(CL=64.36%)	
2 Dipping Speed	(2)	(15622.936)		P O O L E D	(CL=83.56%)	
3 Firing Profile	(2)	(10014.131)		P O O L E D	(CL=79.74%)	
4 MgO/Spinel ratio	(2)	(8588.814)		P O O L E D	(CL=78.26%)	
5 First Stage Ball	(2)	(9880.022)		P O O L E D	(CL=83.31%)	
6 Fish oil amount	(2)	(5057.911)		P O O L E D	(CL=63.77%)	
7 PVP type (K)	(2)	(10954.835)		P O O L E D	(CL=87.36%)	
8 PVP amount	2	22507.176	11253.588	4.938	17949.428	19.995
Other/Error	15	67261.16	4484.077			80.005
Total:	17	89768.34				100.00%

Figure G5 shows the plots of the effects of each of the factors on the measured response.

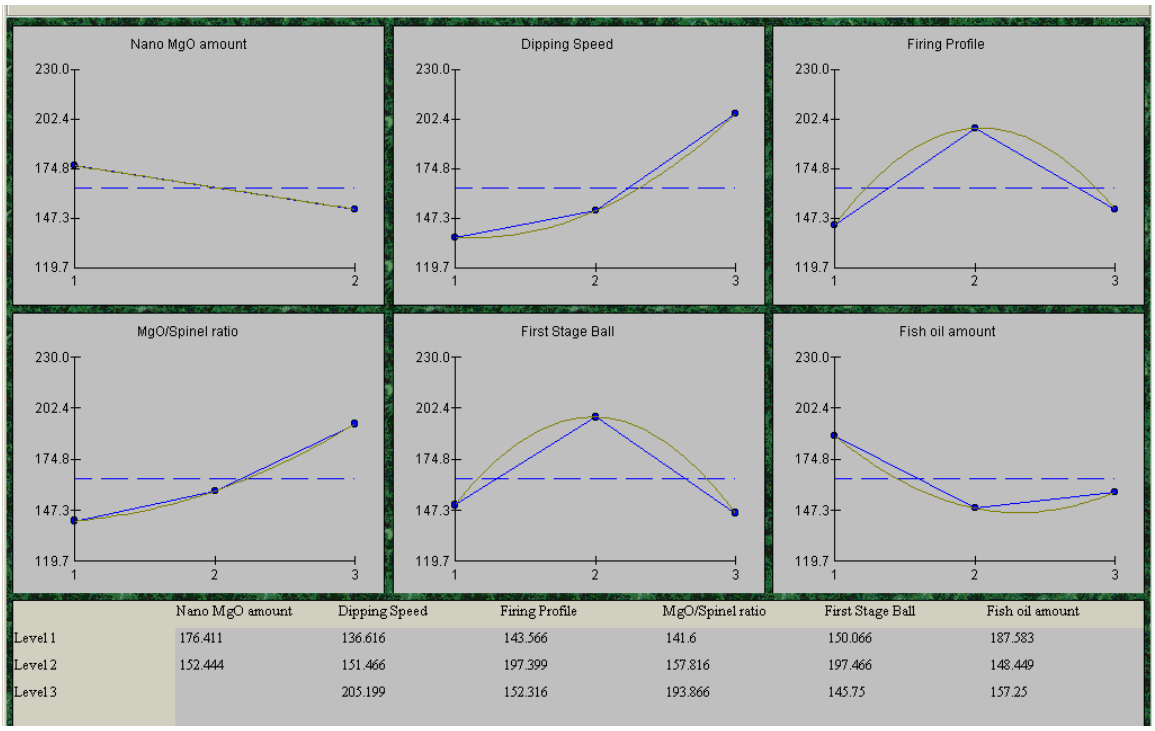

	Nano MgO amount	Dipping Speed	Firing Profile	MgO/Spinel ratio	First Stage Ball	Fish oil amount
Level 1	176.411	136.616	143.566	141.6	150.066	187.583
Level 2	152.444	151.466	197.399	157.816	197.466	148.449
Level 3		205.199	152.316	193.866	145.75	157.25

Figure G5

Table G5-4 shows the expected optimal performance for the factors determined as significant (with a confidence level greater than 90%).

Table G5-4

Column # / Factor	Level Description	Level	Contribution
8 PVP amount	0.6	3	-28.945

Total Contribution From All Factors...	-28.946
Current Grand Average Of Performance...	164.427
Expected Result At Optimum Condition...	135.482

If we assumed that all the factors were significant the optimal levels would be as shown in Table G5-5.

Table G5-5

Column # / Factor	Level Description	Level	Contribution
1 Nano MgO amount	20	2	-11.984
2 Dipping Speed	.09	1	-27.812
3 Firing Profile	1550	1	-20.862
4 MgO/Spinel ratio	6:1	1	-22.828
5 First Stage Ball	12	3	-18.678
6 Fish oil amount	50	2	-15.978
7 PVP type (K)	90% 10K	2	-22.512
8 PVP amount	0.6	3	-28.945

This gives the optimal levels as predicted by the data, but as stated before all of the factors except one are not significant at the 90% level.

G6 – Concentricity - Inter Center Distance

The following is the analysis of the sapphire interface center distance data generated in the 18 samples that were measured. The quality characteristic used was “smaller is better”. Table G6-1 shows the factors and levels and the averages of level 3 minus level 1.

Table G6-1

Column # / Factors	Level 1	Level 2	Level 3	L3 - L1
1 Nano MgO amount	11.003	.701		n/a
2 Dipping Speed	.643	.91	16.003	15.36
3 Firing Profile	.816	.789	15.949	15.132
4 MgO/Spinel ratio	16.014	.753	.788	-15.226
5 First Stage Ball	.699	.901	15.954	15.255
6 Fish oil amount	.843	15.989	.723	-.12
7 PVP type (K)	15.903	.805	.848	-15.056
8 PVP amount	.788	15.966	.801	.013

Table G6-2 shows the ANOVA table for the analysis of the factor influences. It appears that all the factors are not significant at the 70% level.

Table G6-2

Col # / Factor	DOF (f)	Sum of Sqrs. (S)	Variance (V)	F - Ratio (F)	Pure Sum (S')	Percent P(%)
1 Nano MgO amount	1	477.61	477.61	1.024	11.365	.144
2 Dipping Speed	2	927.618	463.809	.994	0	0
3 Firing Profile	2	917.688	458.844	.984	0	0
4 MgO/Spinel ratio	2	929.542	464.771	.996	0	0
5 First Stage Ball	2	918.716	459.358	.985	0	0
6 Fish oil amount	2	925.013	462.506	.991	0	0
7 PVP type (K)	2	909.229	454.614	.975	0	0
8 PVP amount	2	920.718	460.359	.987	0	0
Other/Error	2	932.489	466.244			99.856
Total:	17	7858.628				100.00%

Table G6-3 shows the results of the ANOVA analysis. As seen in this table, the confidence levels of all the factors except for one are less than 60%.

Table G6-3

Col # / Factor	DOF (f)	Sum of Sqrs. (S)	Variance (V)	F - Ratio (F)	Pure Sum (S')	Percent P(%)
1 Nano MgO amount	(1)	(477.61)		POOLED	(CL=62.1%)	
2 Dipping Speed	(2)	(927.618)		POOLED	(CL= *NC*)	
3 Firing Profile	(2)	(917.688)		POOLED	(CL= *NC*)	
4 MgO/Spinel ratio	(2)	(929.542)		POOLED	(CL= *NC*)	
5 First Stage Ball	(2)	(918.716)		POOLED	(CL= *NC*)	
6 Fish oil amount	(2)	(925.013)		POOLED	(CL= *NC*)	
7 PVP type (K)	(2)	(909.229)		POOLED	(CL= *NC*)	
8 PVP amount	(2)	(920.718)		POOLED	(CL= *NC*)	
Other/Error	17	7858.623	462.272			100
Total:	17	7858.628				100.00%

Figure G6 shows the plots of the effects of each of the factors on the measured response.

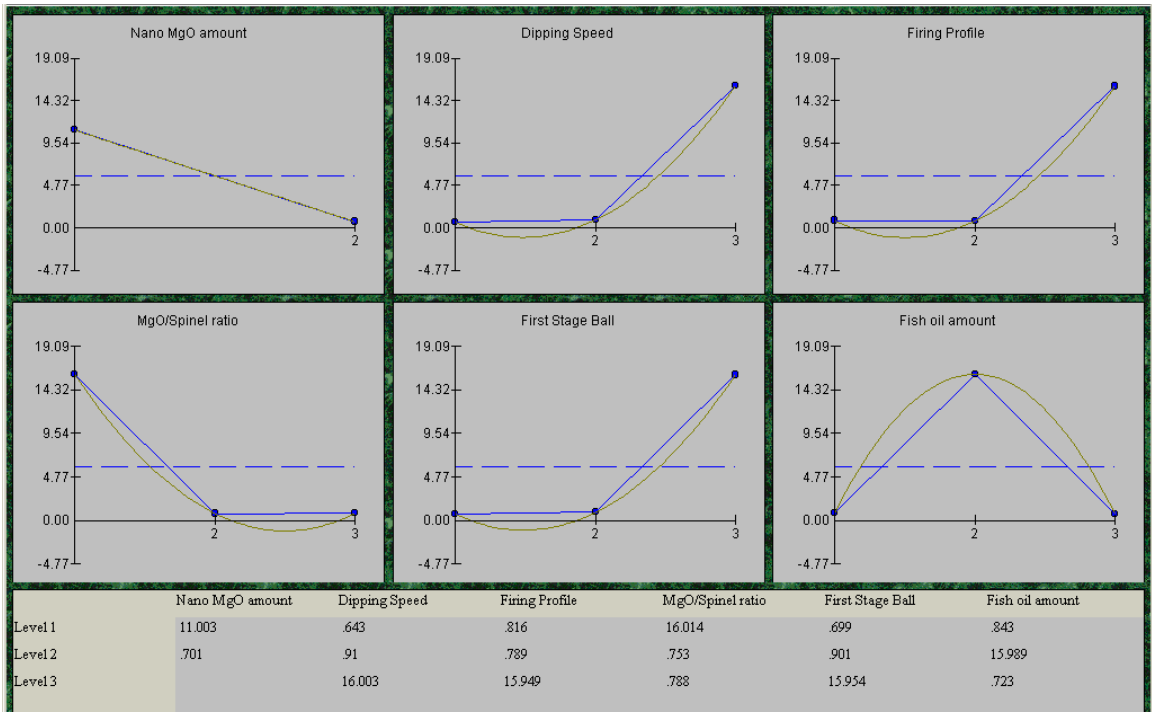

Figure G6

Table G6-4 shows the expected optimal performance for the factors determined as significant (with a confidence level greater than 60%).

Table G6-4

Column # / Factor	Level Description	Level	Contribution
1 Nano MgO amount	20	2	-5.152

Total Contribution From All Factors...	-5.153
Current Grand Average Of Performance...	5.852
Expected Result At Optimum Condition...	.7

If we assumed that all the factors were significant the optimal levels should be as those shown in Table G6-5.

Table G6-5

Column # / Factor	Level Description	Level	Contribution
1 Nano MgO amount	20	2	-5.152
2 Dipping Speed	.09	1	-5.209
3 Firing Profile	1575	2	-5.063
4 MgO/Spinel ratio	9:1	2	-5.099
5 First Stage Ball	3	1	-5.153
6 Fish oil amount	75	3	-5.129
7 PVP type (K)	90% 10K	2	-5.048
8 PVP amount	0.4	1	-5.064

This gives the optimal levels as predicted by the data, but as stated before most of the factors are not significant at the 70% level.

M1: Bend Analysis

The following is the analysis of bend data generated in the 18 samples that were measured. The quality characteristic used was “bigger is better”.

Table M1-1 shows the results of the anova analysis. As seen in this table, the confidence levels of all the factors but one – firing profile – are less than 90 %. Therefore, based on the amount of scatter in the data, only the effect of the firing profile seems significant when approaching 90%. More data would be needed to improve the estimates of these effects.

Table M1-1

Col # / Factor	DOF (f)	Sum of Sqrs. (S)	Variance (V)	F - Ratio (F)	Pure Sum (S')	Percent P(%)
1 Nano MgO amount	(1)	(.003)		POOLED	(CL= *NC*)	
2 Dipping Speed	(2)	(.002)		POOLED	(CL= *NC*)	
3 Firing Profile	2	.193	.096	4.973	.154	33.294
4 MgO/Spinel ratio	(2)	(.04)		POOLED	(CL=58.54%)	
5 First Stage Ball	(2)	(.056)		POOLED	(CL=70.42%)	
6 Fish oil amount	(2)	(.028)		POOLED	(CL= *NC*)	
7 PVP type (K)	(2)	(.06)		POOLED	(CL=75.14%)	
8 PVP amount	(2)	(.039)		POOLED	(CL=61.47%)	
Other/Error	15	.266	.018			66.706
Total:	17	.465				100.00%

The optimal level for firing profile is level 1.

Table M1-2

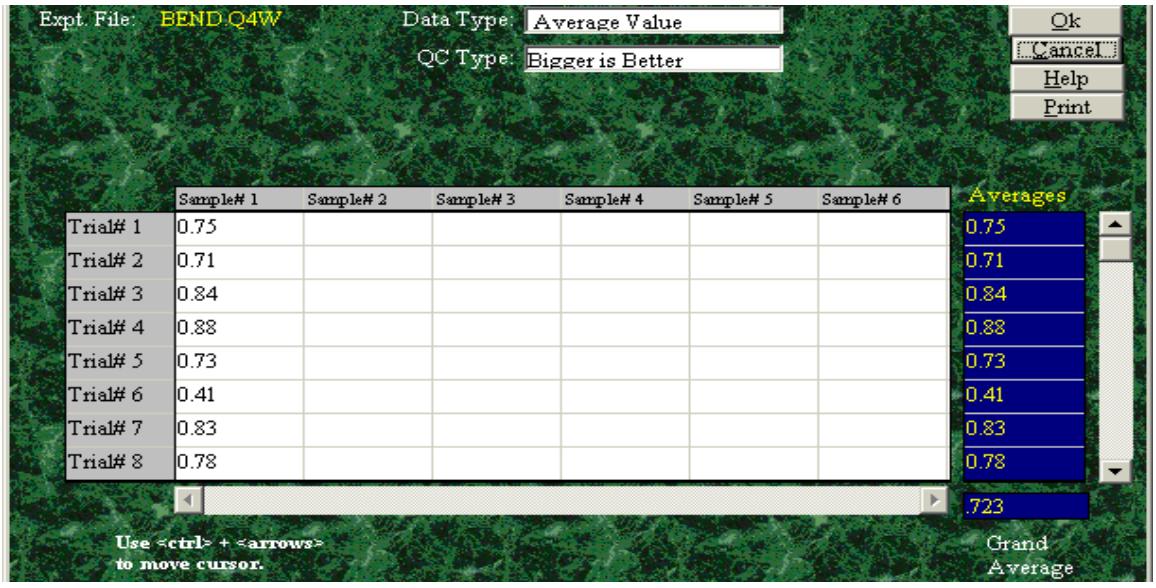

Table M1-3

Column # / Factor	Level Description	Level	Contribution
3 Firing Profile	1550	1	.132

Total Contribution From All Factors...	.132
Current Grand Average Of Performance...	.723
Expected Result At Optimum Condition...	.855

Table M1-4

Expt. File: BEND.Q4W Data Type: Average Values QC Type: Bigger is Better Print Ok Help Cancel

Column # / Factors	Level 1	Level 2	Level 3	L2 - L1
1 Nano MgO amount	.709	.737		.028
2 Dipping Speed	.714	.714	.741	0
3 Firing Profile	.856	.711	.603	-.146
4 MgO/Spinel ratio	.671	.786	.713	.114
5 First Stage Ball	.644	.761	.765	.116
6 Fish oil amount	.759	.668	.743	-.091
7 PVP type (K)	.708	.661	.801	-.047
8 PVP amount	.685	.696	.789	.01

Noise Effects Interactions Plot Multi Plot Anova

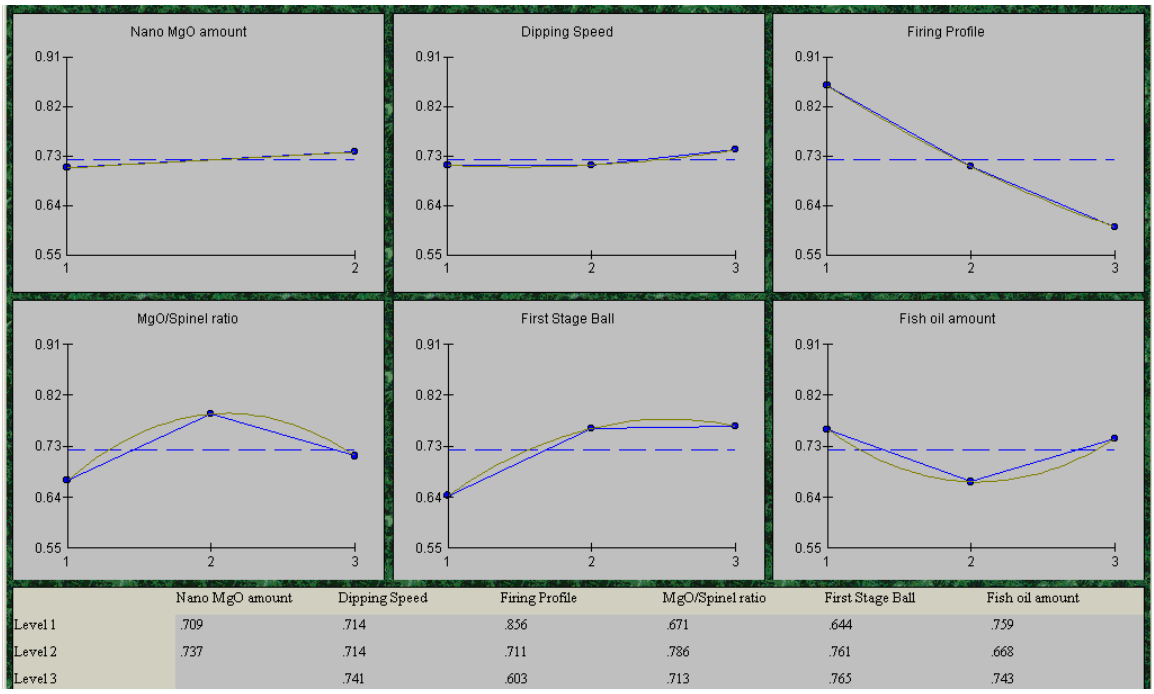

	Nano MgO amount	Dipping Speed	Firing Profile	MgO/Spinel ratio	First Stage Ball	Fish oil amount
Level 1	.709	.714	.856	.671	.644	.759
Level 2	.737	.714	.711	.786	.761	.668
Level 3		.741	.603	.713	.765	.743

Figure M1-1

M2 - Total Area of Crack

The following is the analysis of the sapphire crack parameter (total area of crack) data generated in the 18 samples that were measured. The quality characteristic used was "smaller is better". Table M2-1 shows the factors and levels and the averages of level 3 minus level 1.

Table M2-1

Column # / Factors	Level 1	Level 2	Level 3	L3 - L1
1 Nano MgO amount	10.055	22.4		n/a
2 Dipping Speed	10.8	24.333	13.55	2.75
3 Firing Profile	5.85	23.1	19.733	13.883
4 MgO/Spinel ratio	14.75	7.483	26.45	11.699
5 First Stage Ball	27	8.95	12.733	-14.267
6 Fish oil amount	15.616	26.466	6.6	-9.017
7 PVP type (K)	36.7	6.85	5.133	-31.568
8 PVP amount	1.283	20.649	26.75	25.467

Table M2-2 shows the ANOVA table for the analysis of the factor influences. It appears that almost all the factors are not significant at the 90% level.

Table M2-2

Col # / Factor	DOF (f)	Sum of Sqrs. (S)	Variance (V)	F - Ratio (F)	Pure Sum (S')	Percent P(%)
1 Nano MgO amount	1	685.734	685.734	1.38	188.993	1.503
2 Dipping Speed	2	613.987	306.993	.618	0	0
3 Firing Profile	2	1003.288	501.644	1.009	9.806	.078
4 MgO/Spinel ratio	2	1098.857	549.428	1.106	105.376	.838
5 First Stage Ball	2	1087.307	543.653	1.094	93.825	.746
6 Fish oil amount	2	1187.414	593.707	1.195	193.933	1.542
7 PVP type (K)	2	3780.846	1890.423	3.805	2787.365	22.17
8 PVP amount	2	2121.656	1060.828	2.135	1128.174	8.973
Other/Error	2	993.481	496.74			64.15
Total:	17	12572.574				100.00%

Table M2-3 shows the results of the ANOVA analysis. As seen in this table, the confidence levels of all the factors except PVP type are less than 90 %.

Table M2-3

Col # / Factor	DOF (f)	Sum of Sqrs. (S)	Variance (V)	F - Ratio (F)	Pure Sum (S')	Percent P(%)
1 Nano MgO amount	(1)	(685.734)		POOLED	(CL=68.51%	
2 Dipping Speed	(2)	(613.987)		POOLED	(CL= *NC*)	
3 Firing Profile	(2)	(1003.288)		POOLED	(CL=57.52%	
4 MgO/Spinel ratio	(2)	(1098.857)		POOLED	(CL=62.13%	
5 First Stage Ball	(2)	(1087.307)		POOLED	(CL=62.84%	
6 Fish oil amount	(2)	(1187.414)		POOLED	(CL=66.48%	
7 PVP type (K)	2	3780.846	1890.423	3.805	2787.365	22.17
8 PVP amount	(2)	(2121.656)		POOLED	(CL=84.55%	
Other/Error	15	8791.724	586.115			77.83
Total:	17	12572.574				100.00%

Figure M2 shows the plots of the effects of each of the factors on the measured response.

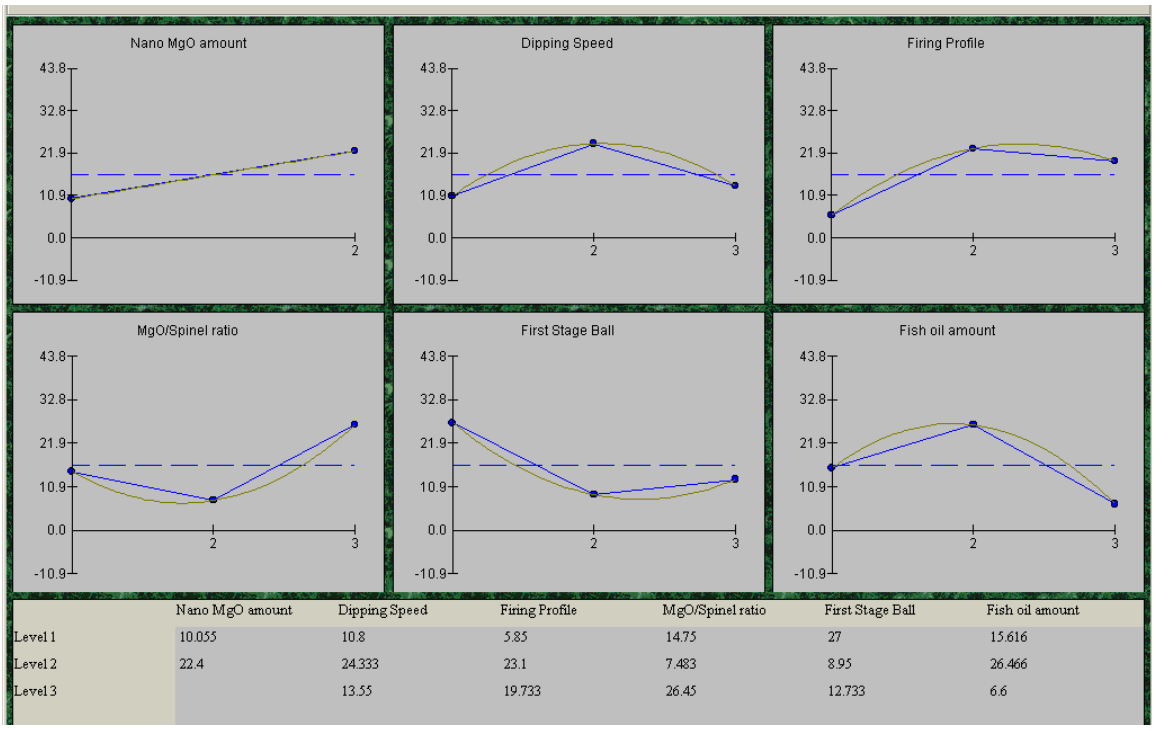

	Nano MgO amount	Dipping Speed	Firing Profile	MgO/Spinel ratio	First Stage Ball	Fish oil amount
Level 1	10.055	10.8	5.85	14.75	27	15.616
Level 2	22.4	24.333	23.1	7.483	8.95	26.466
Level 3		13.55	19.733	26.45	12.733	6.6

Figure M2

Table M2-4 shows the expected optimal performance for the factors determined as significant (with a confidence level greater than 90%).

Table M2-4

Column # / Factor	Level Description	Level	Contribution
7 PVP type (K)	80% 10K	3	-11.095

If we assumed that all the factors were significant the optimal levels would be as those shown in Table M2-5.

Table M2-5

Column # / Factor	Level Description	Level	Contribution
1 Nano MgO amount	10	1	-6.173
2 Dipping Speed	.09	1	-5.428
3 Firing Profile	1550	1	-10.378
4 MgO/Spinel ratio	9:1	2	-8.745
5 First Stage Ball	6	2	-7.278
6 Fish oil amount	75	3	-9.628
7 PVP type (K)	80% 10K	3	-11.095
8 PVP amount	0.4	1	-14.945

This gives the optimal levels as predicted by the data, but as stated before most of the factors are not significant at the 90% level.

M3 – Length of the Longest Crack

The following is the analysis of the length of the longest crack data generated in the 18 samples that were measured. The quality characteristic used was "smaller is better". Table M3-1 shows the factors and levels and the averages of level 3 minus level 1.

Table M3-1

Column # / Factors	Level 1	Level 2	Level 3	L3 - L1
1 Nano MgO amount	5.644	8.122		n/a
2 Dipping Speed	7.3	9.516	3.833	-3.467
3 Firing Profile	4.416	6.65	9.583	5.166
4 MgO/Spinel ratio	5.783	4.333	10.533	4.749
5 First Stage Ball	11.483	4.35	4.816	-6.668
6 Fish oil amount	11.6	5.733	3.316	-8.284
7 PVP type (K)	12.116	5.233	3.3	-8.816
8 PVP amount	2.033	8.933	9.683	7.649

Table M3-2 shows the ANOVA table for the analysis of the factor influences. It appears that almost all the factors are significant at the 90% level.

Table M3-2

Col # / Factor	DOF (f)	Sum of Sqrs. (S)	Variance (V)	F - Ratio (F)	Pure Sum (S')	Percent P(%)
1 Nano MgO amount	1	27.627	27.627	78.805	27.276	2.247
2 Dipping Speed	2	98.463	49.231	140.43	97.762	8.056
3 Firing Profile	2	80.573	40.286	114.915	79.872	6.581
4 MgO/Spinel ratio	2	126.209	63.104	180.003	125.508	10.342
5 First Stage Ball	2	191.093	95.546	272.542	190.392	15.689
6 Fish oil amount	2	217.743	108.871	310.551	217.042	17.885
7 PVP type (K)	2	257.703	128.851	367.542	257.001	21.178
8 PVP amount	2	213.389	106.694	304.341	212.688	17.526
Other/Error	2	.701	.35			.496
Total:	17	1213.504				100.00%

Table M3-3 shows the results of the ANOVA analysis. As seen in this table, the confidence levels of all the factors are greater than 90 %.

Table M3-3

Col # / Factor	DOF (f)	Sum of Sqrs. (S)	Variance (V)	F - Ratio (F)	Pure Sum (S')	Percent P(%)
1 Nano MgO amount	(1)	(27.627)		POOLED	(CL=98.9%)	
2 Dipping Speed	(2)	(98.463)		POOLED	(CL=99.76%	
3 Firing Profile	2	80.573	40.286	114.915	79.872	6.581
4 MgO/Spinel ratio	2	126.209	63.104	180.003	125.508	10.342
5 First Stage Ball	2	191.093	95.546	272.542	190.392	15.689
6 Fish oil amount	2	217.743	108.871	310.551	217.042	17.885
7 PVP type (K)	2	257.703	128.851	367.542	257.001	21.178
8 PVP amount	2	213.389	106.694	304.341	212.688	17.526
Other/Error	5	126.791	25.358			10.799
Total:	17	1213.504				100.00%

Figure M3 shows the plots of the effects of each of the factors on the measured response.

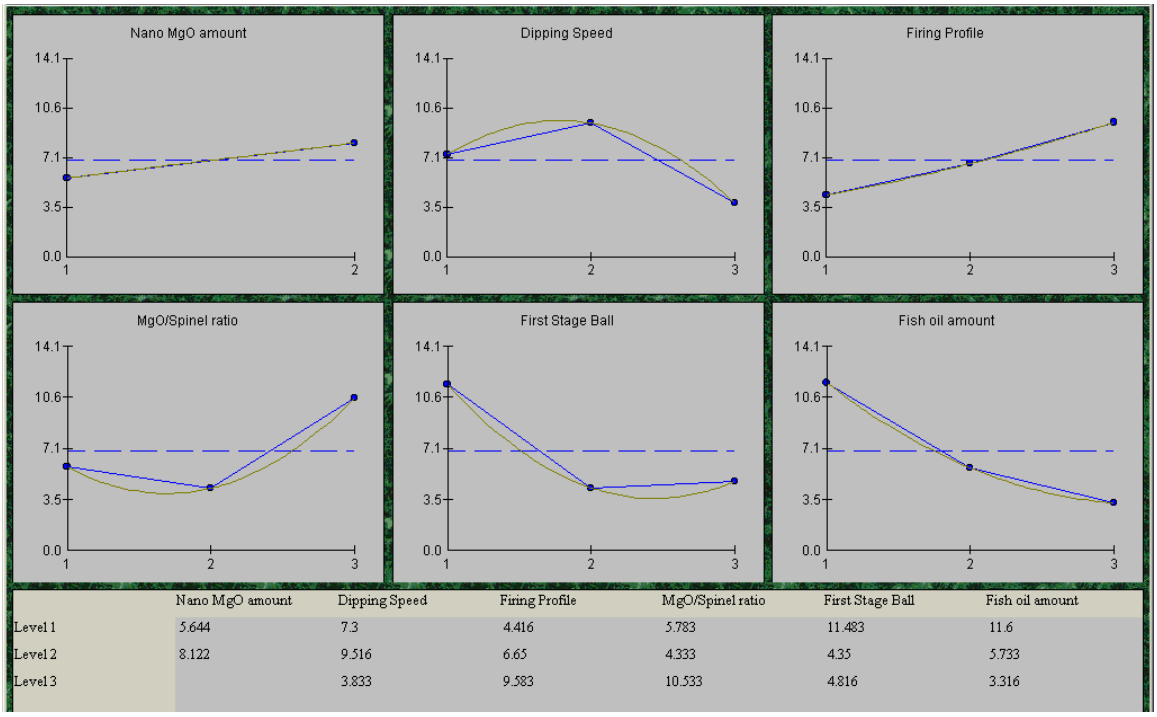

	Nano MgO amount	Dipping Speed	Firing Profile	MgO/Spinel ratio	First Stage Ball	Fish oil amount
Level 1	5.644	7.3	4.416	5.783	11.483	11.6
Level 2	8.122	9.516	6.65	4.333	4.35	5.733
Level 3		3.833	9.583	10.533	4.816	3.316

Figure M3

Table M3-4 shows the expected optimal performance for the factors determined as significant (with a confidence level greater than 99.5%.

Table M3-4

Column # / Factor	Level Description	Level	Contribution
3 Firing Profile	1550	1	-2.467
4 MgO/Spinel ratio	9:1	2	-2.55
5 First Stage Ball	6	2	-2.534
6 Fish oil amount	75	3	-3.567
7 PVP type (K)	80% 10K	3	-3.584
8 PVP amount	0.4	1	-4.85

Total Contribution From All Factors...	-19.552
Current Grand Average Of Performance...	6.883
Expected Result At Optimum Condition...	-12.669

If we assumed that all the factors were significant the optimal levels would be as those shown in Table M3-5.

Table M3-5

Column # / Factor	Level Description	Level	Contribution
1 Nano MgO amount	10	1	-1.239
2 Dipping Speed	.120	3	-3.05
3 Firing Profile	1550	1	-2.467
4 MgO/Spinel ratio	9:1	2	-2.55
5 First Stage Ball	6	2	-2.534
6 Fish oil amount	75	3	-3.567
7 PVP type (K)	80% 10K	3	-3.584
8 PVP amount	0.4	1	-4.85

This gives the optimal levels as predicted by the data.

M4 - Number of Cracks

The following is the analysis of the sapphire number of cracks data generated in the 18 samples that were measured. The quality characteristic used was "smaller is better". Table M4-1 shows the factors and levels and the averages of level 3 minus level 1.

Table M4-1

Column # / Factors	Level 1	Level 2	Level 3	L3 - L1
1 Nano MgO amount	.444	.555		n/a
2 Dipping Speed	.566	.6	.333	-.233
3 Firing Profile	.283	.383	.833	.549
4 MgO/Spinel ratio	.45	.333	.716	.265
5 First Stage Ball	.783	.4	.316	-.468
6 Fish oil amount	.833	.383	.283	-.55
7 PVP type (K)	.9	.383	.216	-.685
8 PVP amount	.116	.783	.6	.483

Table M4-2 shows the ANOVA table for the analysis of the factor influences. It appears that the firing profile and fish oil amount are the only significant factors affecting the attenuation from the data generated.

Table M4-2

Col # / Factor	DOF (f)	Sum of Sqrs. (S)	Variance (V)	F - Ratio (F)	Pure Sum (S')	Percent P(%)
1 Nano MgO amount	1	.055	.055	.373	0	0
2 Dipping Speed	2	.253	.126	.85	0	0
3 Firing Profile	2	1.03	.515	3.458	.732	10.736
4 MgO/Spinel ratio	2	.463	.231	1.555	.165	2.427
5 First Stage Ball	2	.743	.371	2.496	.445	6.533
6 Fish oil amount	2	1.029	.514	3.458	.732	10.736
7 PVP type (K)	2	1.523	.761	5.115	1.225	17.969
8 PVP amount	2	1.423	.711	4.779	1.125	16.503
Other/Error	2	.296	.148			35.096
Total:	17	6.819				100.00%

Table M4-3 shows the results of the ANOVA analysis. As seen in this table, the confidence levels of all of the last three factors are greater than 90 %.

Table M4-3

Col # / Factor	DOF (f)	Sum of Sqrs. (S)	Variance (V)	F - Ratio (F)	Pure Sum (S')	Percent P(%)
1 Nano MgO amount	(1)	(.055)		POOLED	(CL= *NC*)	
2 Dipping Speed	(2)	(.253)		POOLED	(CL= *NC*)	
3 Firing Profile	(2)	(1.03)		POOLED	(CL=88.91%)	
4 MgO/Spinel ratio	(2)	(.463)		POOLED	(CL=72.81%)	
5 First Stage Ball	(2)	(.743)		POOLED	(CL=86.6%)	
6 Fish oil amount	2	1.029	.514	3.458	.732	10.736
7 PVP type (K)	2	1.523	.761	5.115	1.225	17.969
8 PVP amount	2	1.423	.711	4.779	1.125	16.503
Other/Error	11	2.84	.258			54.792
Total:	17	6.819				100.00%

Figure M4 shows the plots of the effects of each of the factors on the measured response.

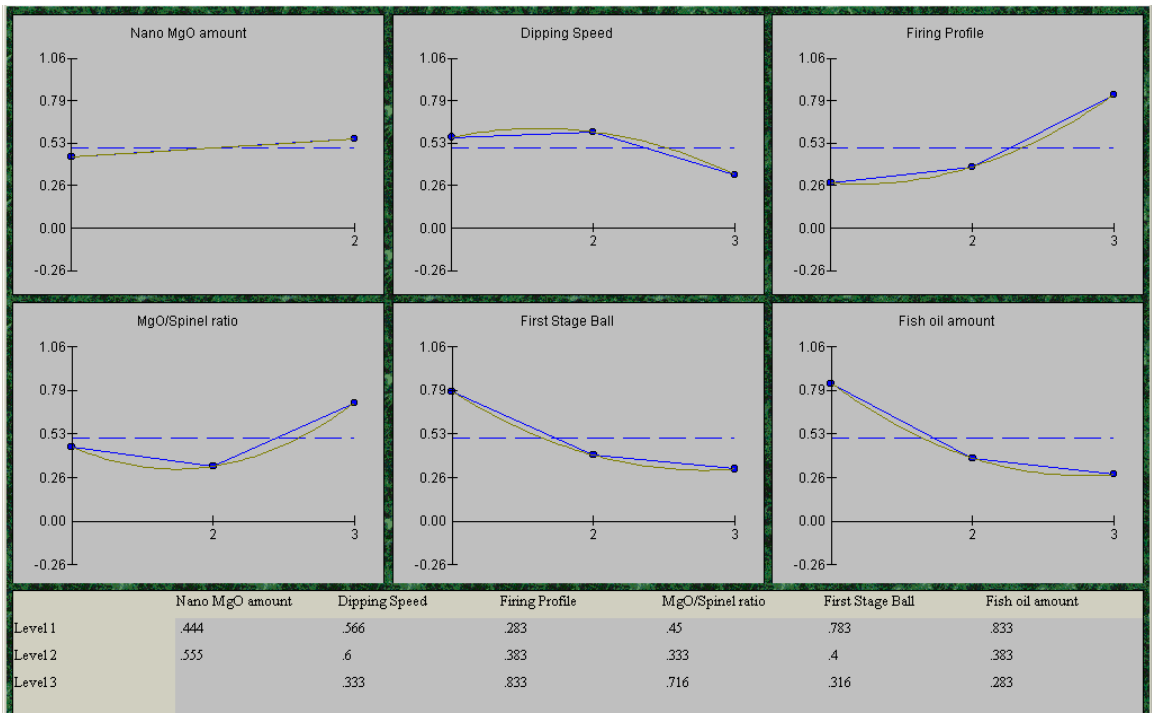

	Nano MgO amount	Dipping Speed	Firing Profile	MgO/Spinel ratio	First Stage Ball	Fish oil amount
Level 1	.444	.566	.283	.45	.783	.833
Level 2	.555	.6	.383	.333	.4	.383
Level 3		.333	.833	.716	.316	.283

Figure M-4

Table M4-4 shows the expected optimal performance for PVP type, PVP amount and fish oil amount being determined as significant (with a confidence level less than 90).

Table M4-4

Column # / Factor	Level Description	Level	Contribution
6 Fish oil amount	75	3	-.217
7 PVP type (K)	80% 10K	3	-.284
8 PVP amount	0.4	1	-.384

Total Contribution From All Factors...	-.886
Current Grand Average Of Performance...	.5
Expected Result At Optimum Condition...	-.386

If we assumed that all the factors were significant the optimal levels would be as those shown in Table M4-5.

Table M4-5

Column # / Factor	Level Description	Level	Contribution
1 Nano MgO amount	10	1	-.056
2 Dipping Speed	.120	3	-.167
3 Firing Profile	1550	1	-.217
4 MgO/Spinel ratio	9:1	2	-.167
5 First Stage Ball	12	3	-.184
6 Fish oil amount	75	3	-.217
7 PVP type (K)	80% 10K	3	-.284
8 PVP amount	0.4	1	-.384

O1: Core/Cladding Interface Roughness Analysis

The following is the analysis of the interface roughness data generated in the 18 samples that were measured. The quality characteristic used was "smaller is better".

Table O1-1 shows the results of the Anova analysis. As seen in this table, the confidence levels of all the factors but one – firing profile – are less than 90 %. Therefore, based on the amount of scatter in the data, only the effect of the firing profile seems significant when approaching 90%. More data would be needed to improve the estimates of these effects.

Table O1-1

Col # / Factor	DOF (f)	Sum of Sqrs. (S)	Variance (V)	F - Ratio (F)	Pure Sum (S')	Percent P(%)
1 Nano MgO amount	(1)	(.204)		POOLED	(CL=74.88%)	
2 Dipping Speed	(2)	(.38)		POOLED	(CL=69.57%)	
3 Firing Profile	2	1.255	.627	5.901	1.043	31.781
4 MgO/Spinel ratio	(2)	(.041)		POOLED	(CL= *NC*)	
5 First Stage Ball	(2)	(.111)		POOLED	(CL= *NC*)	
6 Fish oil amount	(2)	(.461)		POOLED	(CL=83.33%)	
7 PVP type (K)	(2)	(.177)		POOLED	(CL= *NC*)	
8 PVP amount	(2)	(.435)		POOLED	(CL=83.47%)	
Other/Error	15	2.021	.135			68.219
Total:	17	3.282				100.00%

The optimal level for firing profile is level 1.

Table O1-2

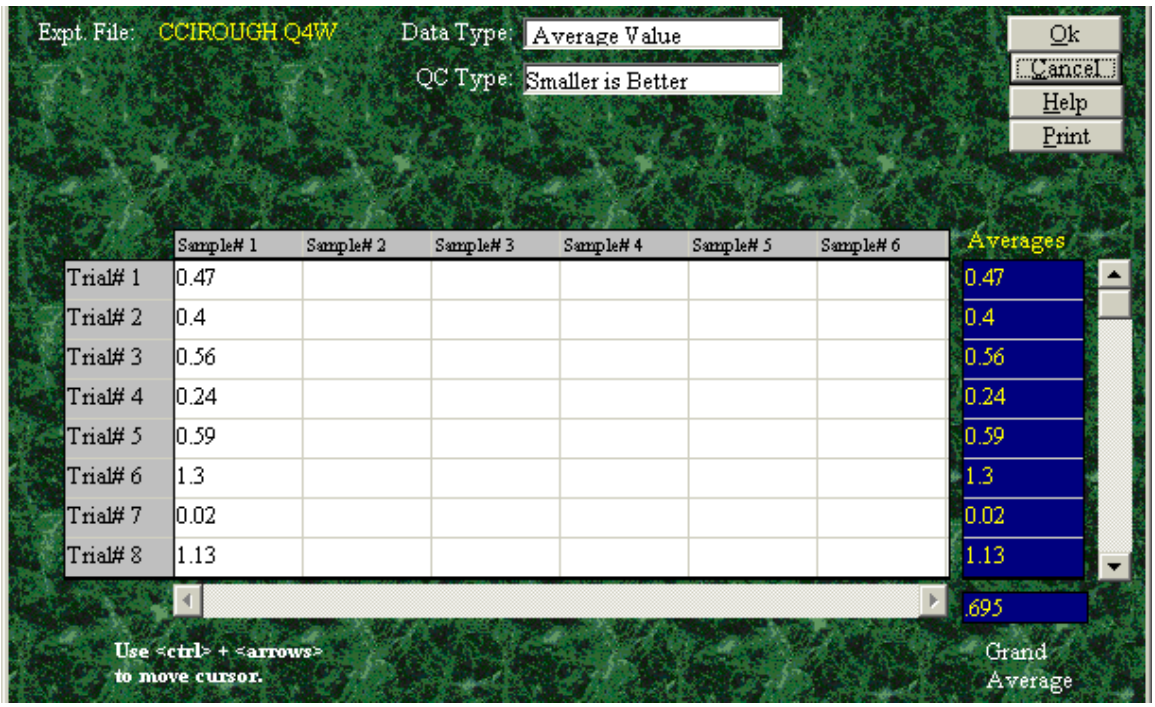

Table O1-3

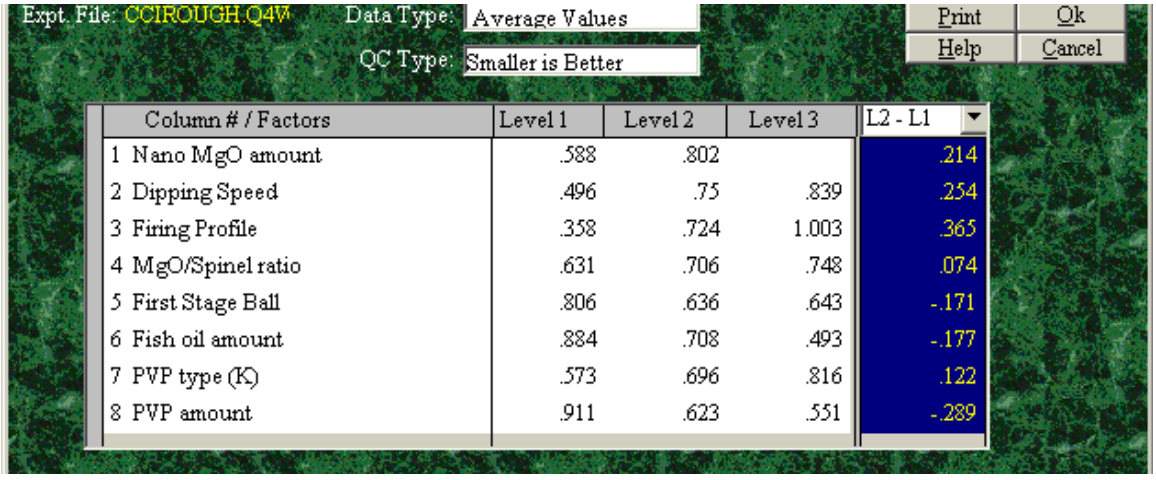

Table O1-4

Expt. File:CCIROUGH.Q4W Data Type: Average Value QC: Smaller is Better Print Ok Help Cancel

Column # / Factor	Level Description	Level	Contribution
3 Firing Profile	1550	1	-.338

Total Contribution From All Factors...	-.339
Current Grand Average Of Performance...	.695
Expected Result At Optimum Condition...	.357

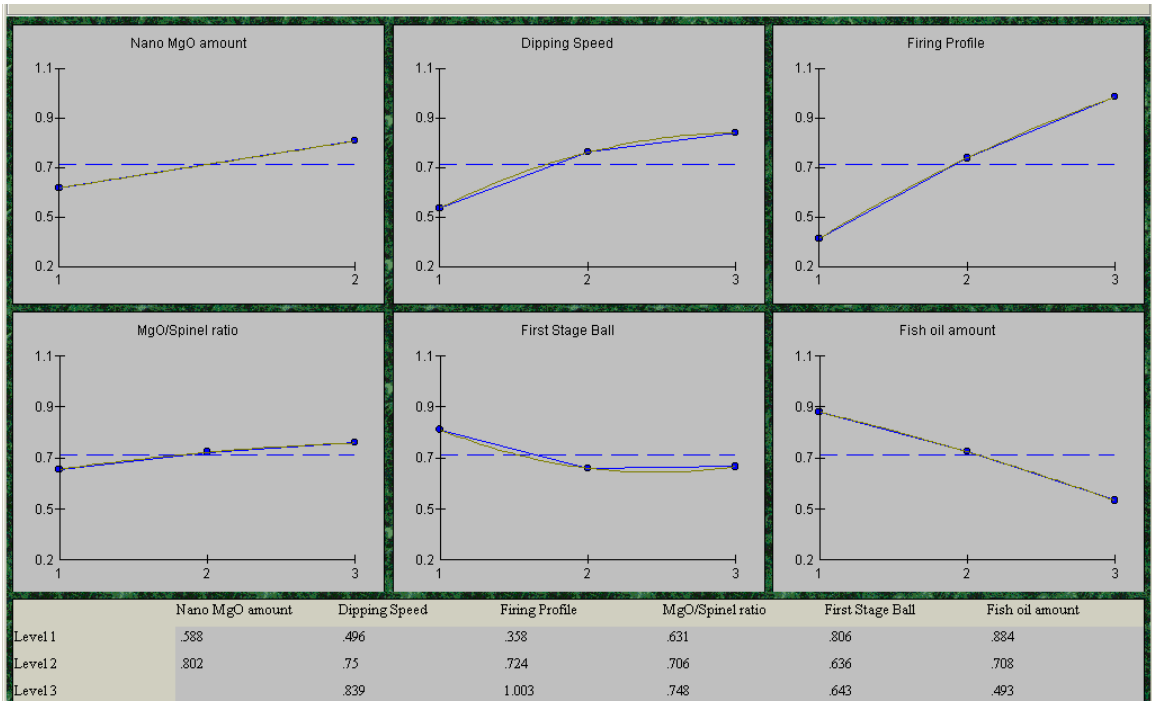

	Nano MgO amount	Dipping Speed	Firing Profile	MgO/Spinel ratio	First Stage Ball	Fish oil amount
Level 1	.588	.496	.358	.631	.806	.884
Level 2	.802	.75	.724	.706	.636	.708
Level 3		.839	1.003	.748	.643	.493

Figure O1-1

O2 - Numerical Aperture Measurement

The following is the analysis of the sapphire numerical aperture data generated in the 18 samples that were measured. The quality characteristic used was “smaller is better”. Table O2-1 shows the factors and levels and the averages of level 3 minus level 1.

Table O2-1

Column # / Factors	Level 1	Level 2	Level 3	L3 - L1
1 Nano MgO amount	.062	.081		n/a
2 Dipping Speed	.057	.081	.076	.018
3 Firing Profile	.073	.079	.063	-.01
4 MgO/Spinel ratio	.069	.075	.071	.001
5 First Stage Ball	.061	.069	.085	.024
6 Fish oil amount	.089	.067	.059	-.03
7 PVP type (K)	.074	.062	.079	.005
8 PVP amount	.057	.077	.081	.024

Table O2-2 shows the ANOVA table for the analysis of the factor influences. It appears that none of the factors has a very high percent contribution.

Table O2-2

.

Col # / Factor	DOF (f)	Sum of Sqrs. (S)	Variance (V)	F - Ratio (F)	Pure Sum (S')	Percent P(%)
1 Nano MgO amount	1	.001	.001	1.327	0	2.519
2 Dipping Speed	2	.002	.001	.911	0	0
3 Firing Profile	2	0	0	.366	0	0
4 MgO/Spinel ratio	2	0	0	.054	0	0
5 First Stage Ball	2	.001	0	.816	0	0
6 Fish oil amount	2	.002	.001	1.346	0	5.322
7 PVP type (K)	2	0	0	.439	0	0
8 PVP amount	2	.001	0	.907	0	0
Other/Error	2	.001	0			92.159
Total:	17	.014				100.00%

Table O2-3 shows the results of the ANOVA analysis. As seen in this table, the confidence levels of all the factors are less than 71%.

Table O2-3

Col # / Factor	DOF (f)	Sum of Sqrs. (S)	Variance (V)	F - Ratio (F)	Pure Sum (S')	Percent P(%)
1 Nano MgO amount	(1)	(.001)		POOLED	(CL=67.71%)	
2 Dipping Speed	(2)	(.002)		POOLED	(CL= *NC*)	
3 Firing Profile	(2)	(0)		POOLED	(CL= *NC*)	
4 MgO/Spinel ratio	(2)	(0)		POOLED	(CL= *NC*)	
5 First Stage Ball	(2)	(.001)		POOLED	(CL= *NC*)	
6 Fish oil amount	(2)	(.002)		POOLED	(CL=70.4%)	
7 PVP type (K)	(2)	(0)		POOLED	(CL= *NC*)	
8 PVP amount	(2)	(.001)		POOLED	(CL= *NC*)	
Other/Error	17	.008	0			100
Total:	17	.014				100.00%

Figure O2 shows the plots of the effects of each of the factors on the measured response.

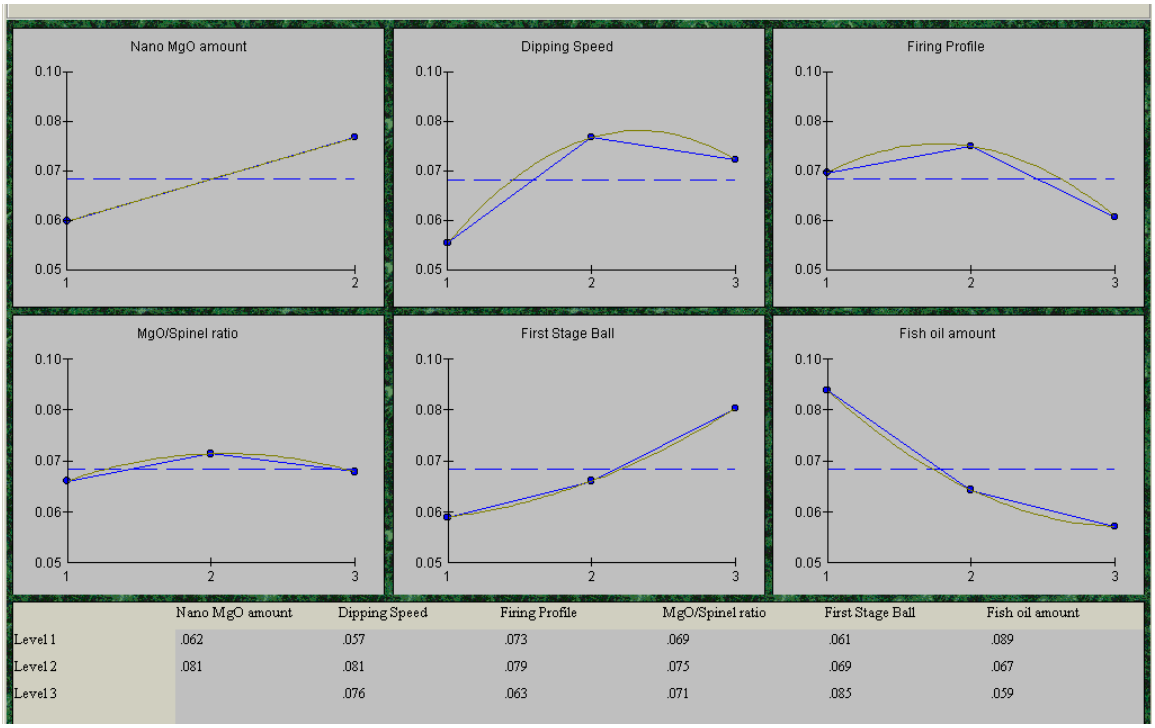

Figure O2

Table O2-4 shows the expected optimal performance for Nano MgO amount, PVP amount and fish oil amount being determined as significant (with a confidence level less than 70% - so a very large amount of variation in the data relative to the factor level change.

Table O2-4

Column # / Factor	Level Description	Level	Contribution
1 Nano MgO amount	10	1	-.01
6 Fish oil amount	75	3	-.013
8 PVP amount	0.4	1	-.015

Total Contribution From All Factors...	-.038
Current Grand Average Of Performance...	.071
Expected Result At Optimum Condition...	.033

Based on the very large scatter in the data, the confidence interval around the predicted average will be very large.

If we assumed that all the factors were significant the optimal levels would be as those shown in Table O2-5.

Table O2-5

Column # / Factor	Level Description	Level	Contribution
1 Nano MgO amount	10	1	-.01
2 Dipping Speed	.09	1	-.015
3 Firing Profile	1600	3	-.009
4 MgO/Spinel ratio	6:1	1	-.003
5 First Stage Ball	3	1	-.011
6 Fish oil amount	75	3	-.013
7 PVP type (K)	90% 10K	2	-.01
8 PVP amount	0.4	1	-.015

This gives the optimal levels as predicted by the data, but again due to the large scatter the factors mentioned above are not sufficiently high in significance to warrant inclusion in the optimal predictions.

O3 - Attenuation Measurement

The following is the analysis of the sapphire attenuation data generated in the 18 samples that were measured. The quality characteristic used was “smaller is better”.
Table O3-1 shows the factors and levels and the averages of level 3 minus level 1.

Table O3-1

Column # / Factors	Level 1	Level 2	Level 3	L3 - L1
1 Nano MgO amount	7.299	6.6		n/a
2 Dipping Speed	6.516	5.65	8.683	2.166
3 Firing Profile	3.416	11.233	6.2	2.784
4 MgO/Spinel ratio	5.666	6.483	8.699	3.032
5 First Stage Ball	6.299	8.55	6	-.3
6 Fish oil amount	9.916	6.083	4.849	-5.068
7 PVP type (K)	6.15	6.016	8.683	2.532
8 PVP amount	7.25	5.433	8.166	.916

Table O3-2 shows the ANOVA table for the analysis of the factor influences. It appears that the firing profile and fish oil amount are the only significant factors affecting the attenuation from the data generated.

Table O3-2

Col # / Factor	DOF (f)	Sum of Sqrs. (S)	Variance (V)	F - Ratio (F)	Pure Sum (S')	Percent P(%)
1 Nano MgO amount	1	2.205	2.205	.082	0	0
2 Dipping Speed	2	29.293	14.646	.549	0	0
3 Firing Profile	2	188.363	94.181	3.532	135.043	29.348
4 MgO/Spinel ratio	2	29.563	14.781	.554	0	0
5 First Stage Ball	2	23.31	11.655	.437	0	0
6 Fish oil amount	2	83.773	41.886	1.571	30.453	6.618
7 PVP type (K)	2	27.093	13.546	.508	0	0
8 PVP amount	2	23.223	11.611	.435	0	0
Other/Error	2	53.319	26.659			64.034
Total:	17	460.145				100.00%

Table O3-3 shows the results of the ANOVA analysis. As seen in this table, the confidence levels of all the factors are less than 90 %. Therefore, based on the amount of scatter in the data, only the effect of the firing profile seems significant when approaching 90%. More data would be needed to improve the estimates of these effects.

Table O3-3

Col # / Factor	DOF (f)	Sum of Sqrs. (S)	Variance (V)	F - Ratio (F)	Pure Sum (S')	Percent P(%)
1 Nano MgO amount	(1)	(2.205)		POOLED	(CL= *NC*)	
2 Dipping Speed	(2)	(29.293)		POOLED	(CL= *NC*)	
3 Firing Profile	(2)	(188.363)		POOLED	(CL=89.24%)	
4 MgO/Spinel ratio	(2)	(29.563)		POOLED	(CL= *NC*)	
5 First Stage Ball	(2)	(23.31)		POOLED	(CL= *NC*)	
6 Fish oil amount	(2)	(83.773)		POOLED	(CL=75.28%)	
7 PVP type (K)	(2)	(27.093)		POOLED	(CL= *NC*)	
8 PVP amount	(2)	(23.223)		POOLED	(CL= *NC*)	
Other/Error	17	460.142	27.067			100
Total:	17	460.145				100.00%

It should be noted that the attenuation measurement was developed quickly during the period where samples were being prepared. A rigorous analysis of the repeatability and reproducibility of the measurement procedure was decided against due to the extremely tight time constraints under which the project operated. The data indicate that there is a large amount of unexplained error present in the system and this may be due in part to the variation of the measurement process. Future work should focus on characterization of the variation from the measurement of the attenuation.

Figure O3 shows the plots of the effects of each of the factors on the measured attenuation.

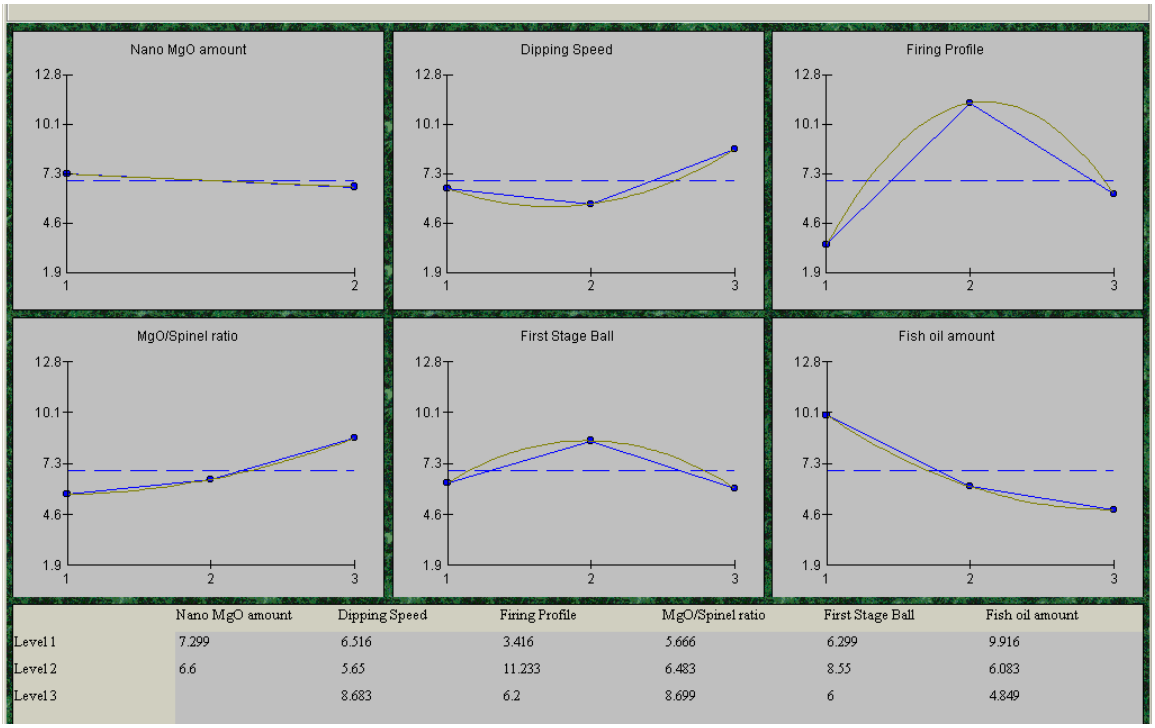

	Nano MgO amount	Dipping Speed	Firing Profile	MgO/Spinel ratio	First Stage Ball	Fish oil amount
Level 1	7.299	6.516	3.416	5.666	6.299	9.916
Level 2	6.6	5.65	11.233	6.483	8.55	6.083
Level 3		8.683	6.2	8.699	6	4.849

Figure O3

Table O3-4 shows the expected optimal performance for firing profile and fish oil amount being determined as significant.

Table O3-4

Column # / Factor	Level Description	Level	Contribution
3 Firing Profile	1550	1	-3.534
6 Fish oil amount	75	3	-2.101

Total Contribution From All Factors...	-5.635
Current Grand Average Of Performance...	6.95
Expected Result At Optimum Condition...	1.315

Based on the very large scatter in the data, the confidence interval around the predicted average will be very large.

If we assumed that all the factors were significant the optimal levels would be as those shown in Table O3-5.

Table O3-5

Column # / Factor	Level Description	Level
1 Nano MgO amount	20	2
2 Dipping Speed	.105	2
3 Firing Profile	1550	1
4 MgO/Spinel ratio	6:1	1
5 First Stage Ball	12	3
6 Fish oil amount	75	3
7 PVP type (K)	90% 10K	2
8 PVP amount	0.5	2

This gives the optimal levels as predicted by the data, but again due to the large scatter the factors other than the two mentioned above are not sufficiently high in significance to warrant inclusion in the optimal predictions.